ABSTRACT

Title of dissertation: EXPERIMENTAL AND NUMERICAL INVESTIGATION INTO THE EFFECTS OF PANEL CURVATURE ON THE HIGH VELOCITY BALLISTIC IMPACT RESPONSE OF ALUMINUM AND COMPOSITE PANELS

David Scott Stargel, Doctor of Philosophy, 2005

Dissertation directed by: Professor William L. Fourney
Professor Emeritus Robert J. Sanford
Department of Mechanical Engineering

Determining how a material responds to a ballistic impact is important for designing improved penetration-resistant structures. Historically, the majority of research into the effects of ballistic impact has been for flat geometries. However, in aerospace applications, the surfaces that would most likely be subjected to high velocity impacts, the fuselage and the wing sections, are not flat. A need therefore exists to systematically examine and understand the effect, if any, of panel curvature on the ballistic response of both aluminum and composite panels. For this dissertation, a hybrid combination of experimental testing and numerical modeling which was employed to examine the effects of panel curvature on the ballistic limit, the dynamic panel response, and the impact-induced damage in the target material is discussed. Panels of varying curvature were impacted by ½-inch diameter steel spheres for a range of impact velocities that bracketed the experimentally-determined ballistic limit. AS4-3501-6 graphite-epoxy composite panels with two varying curvatures, a 4.4-inch radius of

curvature and a 12-inch radius of curvature, and 2024-T3 aluminum panels with four varying curvatures, a 4.4-inch radius of curvature, an 8-inch radius of curvature, a 12-inch radius of curvature, and an infinite radius of curvature (flat plate), were tested. Non-linear finite element models consistently and reliably modeled the ballistic impact event, for both the flat and the curved panels, when the specified elastic modulus correctly captured the characteristics of the wave propagation behavior for the panel material being modeled. For the composite panels, dynamic deformation measurements and strain-gage-instrumented impact tests indicated that an effective elastic modulus on the order of the tensile modulus of the matrix material was more appropriate than a "rule-of-mixtures" effective modulus. The combined experimental-numerical results also identified a parabolic relationship between the panel curvature and the ballistic limit. More importantly, an optimal panel curvature with respect to maximizing the ballistic limit was shown for both the aluminum and the composite panels. Preliminary results from non-destructive and destructive post-impact evaluations suggest that the severity of impact damage may also vary with panel curvature.

EXPERIMENTAL AND NUMERICAL INVESTIGATION INTO THE EFFECTS OF PANEL CURVATURE ON THE HIGH VELOCITY BALLISTIC IMPACT RESPONSE OF ALUMINUM AND COMPOSITE PANELS

by

David Scott Stargel

Dissertation submitted to the Faculty of the Graduate School of the
University of Maryland, College Park in partial fulfillment
of the requirements for the degree of
Doctor of Philosophy
2005

Advisory Committee:

Professor William L. Fourney, Co-chair
Professor Robert J. Sanford, Co-chair
Professor Balakumar Balachandran
Dr. Robert J. Bonenberger, Jr.
Professor Bongtae Han
Dr. Jaime F. Cardenas-Garcia
Professor Darryll J. Pines

Acknowledgements

Words cannot adequately express the extent of my gratitude to the many individuals who have made this accomplishment possible. That being said, I would still like to acknowledge some key people who have gone above and beyond the call of duty.

To my advisors, Professor William L. Fourney and Professor Emeritus Robert J. Sanford, I thank you for your guidance, support, and patience over these many years.

To Dr. Ravinder Chona and Mr. John Bowlus, I cannot thank you enough for your mentorship and your Herculean efforts in making all of this possible.

And last, but certainly not least, my family. To my mother and father, your nurturing and upbringing have made me the person that I am. Thank you for always believing in me. To my wife, thank you for putting up with me over the course of this journey. Your love and support gave me the strength to finish. I love you.

Table of Contents

List of Tables

List of Figures

Chapter 1 Introduction

1.1 Motivation

Ballistic impact has been studied for more than two hundred years. While the early studies concentrated on isotropic and homogeneous metallic materials, more recent efforts have been dedicated to the study of anisotropic and non-homogeneous materials. Composite materials have steadily received more attention primarily due to the increased usage of these materials over the past twenty years in both military and commercial aircraft. The advantages of composite materials in terms of their lower weight, higher strength, higher stiffness, and the ability to tailor properties are the main drivers behind the increase in their use. Even though the more traditionally used metals are also susceptible to impact damage, damage in composite materials can be more extensive, more difficult to discern and, at lower impact velocities, the impact damage is often not visible to the naked eye. In the commercial arena, the biggest concern is damage due to low velocity impacts such as those caused by dropped tools or debris kicked up from the runway. These concerns are shared on the military side as well, but there is an added threat due to combat situations involving impact from enemy munitions. This type of impact, which is typified by high projectile velocities, is usually termed ballistic or terminal impact.

The vast majority of the previous research into the effects of ballistic impact has been performed on flat geometries. However, in aerospace applications, the surfaces that would most likely be subjected to a high velocity impact are the fuselage and the wing sections, neither of which are flat. Therefore, a need exists

to systematically examine and understand the effect, if any, of panel curvature on the ballistic response of both aluminum and composite panels. Comparison of the responses from flat and curved panels can help determine if experimental or numerical results obtained using flat panel testing can, in fact, be reliably used in place of experimentation on actual curved surfaces. A parallel goal is to develop a validated framework for efficient, economical, and reliable numerical simulation of the response of both flat and curved panels to ballistic impacts. This would reduce the reliance on extensive testing, which is both time-consuming and costly.

1.2 Literature Review

1.2.1 Ballistic Impact

Ballistic impact events are high velocity impacts that generally result in partial or full penetration of the target. The most extensive resources for this research area are works by Zukas et al. [1982, 1990]. Essentially texts on the subject of impact, these books emphasize the material aspects of impact phenomenology as related to the general problem area of projectile impact against target materials. The subject matter covers experimental and analytical approaches to material behavior under conditions varying from low-speed impacts to hypervelocity impacts. Numerous references for a more detailed exploration covering all aspects of ballistic impact testing are also presented. In addition to the numerous references, all of the necessary essentials to begin studying high velocity impact dynamics are provided. The fundamental principles and relevant

background information serve as the basic building blocks for the study of impact dynamics. Most of the projectiles given consideration were long rods, cylinders, and conical-shaped projectiles. These shapes are representative of bullets and military armaments, which are the most likely type of projectiles to be encountered in ballistic impact situations.

In contrast, a considerable amount of work has been completed at Wright Patterson Air Force Base for impacts with spherical projectiles. This is also generally true for impact testing conducted at the university level. The main benefit from the use of spherical projectiles is that the researcher does not have to be concerned with pitching and yawing of the projectile and, instead, can focus on more generic features such as the target response and the projectile velocity.

Czarnecki [1992] used embedded strain gages to develop a two-zone morphology model for the penetration of composite plates subjected to ballistic impact. Two quasi-isotropic laminate thicknesses (32-ply and 128-ply), configured into 8-inch x 8-inch plates were investigated. The morphology model showed the transition in damage formation by examining the reflected tensile stress wave with the compressive zone created by the projectile during shear plugging of the material. An approximate relationship between the transition depth, z, the thickness of the plate, t, the projectile speed, v_p, and the sound wave speed in the matrix material, c_L, was derived as:

$$z = \frac{2v_p t}{c_L + v_p} \tag{1.1}$$

Sun [1996] investigated scaling laws for the ballistic response with respect to impact velocity and target thickness. Experimental ballistic impact tests were

conducted on both 2024-T3 aluminum alloys (0.08-inch thickness) and graphite epoxy composite plates of varying thickness. The ballistic limits of the various composite plates were shown to increase nonlinearly with increasing thickness. By normalizing several parameters, Sun found that all of the experimental data could be represented on a single curve.

1.2.2 Impact of Curved Panels

As indicated earlier, the majority of the reported ballistic impact research has been conducted on flat plates. Over the past fifteen years, more research efforts have examined the effects of curvature on the impact response of materials but the focus has been mainly on low-velocity impact tests.

One of the earliest reported references that addressed the influence of target curvature on the impact response of composite targets is attributed to Greszczuk and Chao [1975]. In general, they found the following: (1) the area of contact was elliptically-shaped and approached a circular-shape as the radius of the cylinder was increased; (2) the area of contact decreased with decreasing cylinder radius; (3) the maximum load (resulting from the impact) decreased with decreasing cylinder radius; (4) the maximum surface pressure increased with decreasing cylinder radius; and (5) the contact duration increased with decreasing cylinder radius.

Ramkumar and Thakar [1987] compared the transient response of curved laminated composite plates to the transient response of flat composite plates.

They inferred that, as the radius of curvature decreases, curvature effects cannot be ignored.

Swanson et al. [1991] studied scaling rules between two sizes of cylinders by using airgun test data. The material used to fabricate the cylinders was IM7/55A Carbon/Epoxy (manufactured by Hercules Aerospace, Magna UT). Two sizes of cylinders, differing in linear dimensions by a factor of 3.3, were subjected to relatively low impact velocities, 11.39 m/s (37 ft/s) and 6.77 m/s (22 ft/s), by using cylindrical projectiles with various tip radii. Their results indicated that the time of the impact duration scales with the geometric scaling and that the contact force scales as the square of the geometric scale factor.

Christoforou and Swanson [1990] developed an analytical solution to model the impact loading of simply supported orthotropic cylinders. The basic inputs to the computer program were impact velocity, impactor mass, and the cylinder material and geometric parameters. Results from the simulation of 3 m/s (9.8 ft/s) impacts for various impact masses on IM7/55A carbon epoxy composite cylindrical shells with an inside diameter of 96-mm (3.8-inches) that were 419-mm (16.5 inches) in length indicated that dynamic effects were evident for small mass impacts. By comparing cylinders of various lengths, they also found that the impact dynamic response is influenced by the stiffness of the cylinder.

Lin and Lee [1990] used experimental and numerical finite element investigations to study the effect of curvature on the initiation of impact damage of composite plates and cylindrical shells. Cylindrical shell specimens with a

125-mm (4.9-inch) radius of curvature and stacking sequences of $[0_5/90_5/0_5]$* and $[90_5/0_5/90_5]$ were compared to flat plates of the same configuration. The specimens were beam-like with a 5:1 length to width ratio. A drop-weight apparatus was used for the impact testing and the impact velocities that were investigated ranged from 12 ft/s to 44 ft/s (3.7 m/s to 13.4 m/s). Impacted specimens were sectioned in order to determine the amount of damage that was generated. They concluded that the locations and areas of delamination in the flat plate were different from that of the cylindrical shell and that the cylindrical shells had more severe damage than the flat plates for the same impact velocity.

Kistler [1996] used experiments, analytical models, and finite element analyses to examine the interactions of panel geometry, boundary conditions, impactor mass, and impactor velocity during the transverse impact of composite cylindrical panels. A drop weight impact apparatus was used to impact specimens with two radii of curvature, 0.381 m (15 in) and 1.524 m (60 in), and a variety of thicknesses (8, 16, and 24 plies) from heights ranging from 60 mm to 366 mm (2.4 in to 14.4 in). The panels were fabricated into quasi-isotropic laminate configurations using AS4-3502 graphite epoxy composite material (manufactured by Hercules Inc., Magna UT). The experimental testing used a 1.13 kg (2.5 lb) mass impactor with a 12.7 mm (0.5 in) diameter hemispherical tip. Results from C-scan evaluations showed that the size of the damage zone, characterized by a maximum length, increased with increasing impact energy for these relatively low velocity impact events.

* Stacking sequence notation is discussed in detail in Chapter 2.

Palazotto, Perry, and Sandhu [1992] used a drop weight impact apparatus to investigate six symmetric stacking sequences and two panel thicknesses (12 and 24 plies) for cylindrically curved panels fabricated from AS4-3501-06 graphite epoxy composite material (manufactured by Hercules, Inc., Magna UT). The panels had surface dimensions of 8 inches x 8 inches arc length (200 mm x 200 mm) and a 12-inch (305 mm) radius of curvature. The experimental results were compared to displacement and strain results from a nonlinear finite element analysis. The impactor was dropped from heights of 1, 2, and 3.5 inches (25.4, 50.8, and 88.9 mm) for corresponding impact energies of 0.55, 1.14, and 1.89 ft-lb (0.75, 1.55, and 2.56 J), respectively. A displacement probe was utilized to identify the displacement threshold at which damage occurred in the panels. These thresholds ranged from 0.13-0.15 inches (3.3-3.81 mm) for the 12-ply specimens and from 0.07-0.10 inches (1.78-2.54 mm) for the 23-ply specimens. The non-linear finite element model, using 36-degree-of-freedom shell elements, accurately modeled both the peak displacement values and the strain in the panel at the time of damage.

A common theme amongst all of these reports (and others that were reviewed but are not specifically cited here) is the relatively low impact velocity that was investigated. No experimental reports were identified that addressed the effects of panel curvature for impact velocities capable of penetration.

1.2.3 Modeling Ballistic Impact

Zukas [1990] noted that the principal obstacle in modeling ballistic impact events is a poor knowledge of the mechanisms of failure. This lack of knowledge has necessarily resulted in simplified failure modeling. In many cases, the simple models produce results that are in substantial agreement with experimental data. The number of works that describe modeling of the ballistic impact event is voluminous and will not be described in their entirety. Some of the more relevant and recent examples will instead be discussed in some detail.

Ambur et al. [2001] used LS-DYNA (Livermore Software Technology Corporation, Livermore CA) to study the impact and penetration of thin plates by small fragment impactors. Two approaches, a tied-nodes-with-failure-option and an element-erosion-option, were utilized to simulate penetration of the target plate. In the tied-nodes-with-failure-option approach, coincident nodes are generated in selected regions and tied together using a constraint relation. The constraint is removed once the volume-weighted, effective plastic strain exceeds a specified value. In the element-erosion-option approach, elements are removed from the computation once the effective plastic strain in an element reaches a specified critical value.

A specified critical plastic strain value of 0.2 was used by Ambur et al. for simulating penetration of the aluminum target. This value corresponded to the ultimate strain at failure for the aluminum material. The impactor was modeled as a titanium fragment capable of rotation (pitch and yaw) prior to impacting the aluminum target. Friction between the titanium fragment and the aluminum

target was not considered. Numerical simulations for a range of impact velocities (220 ft/s to 1000 ft/s) and a variety of rotation values were performed. Experimental results for two cases, an impact velocity of 450 ft/s and an impact velocity of 1000 ft/s, that resulted in complete penetration of the target were compared to parametric studies of the numerical model. Results depicting the predicted target damage using the various failure options were shown but no quantitative comparison was made to experimental results.

Borvik et al. [2001] investigated the importance of the defined material model in finite element simulations of plugging failure. Only the material model was varied in the simulations and the results were compared to experimental data from the ballistic impact of 8-mm (0.3 in) thick Weldox 460 E steel plates (no manufacturer given). Eight variations of the material model were investigated with various combinations of effects including damage, temperature, strain rate, hardening, and fracture strain models. None of the coarse-mesh models were able to predict the experimentally-obtained ballistic limits to better than within 30%. Using a fine mesh, one of the material models was able to predict the ballistic limit within 2% but none of the other seven models were better than within 12% of the experimentally-obtained value.

Lee and Sun [1993] used a commercial finite element code to predict the ballistic limit of flat, AS4-3501-6 graphite epoxy composite laminates impacted by blunt-ended projectiles. Two thicknesses (16-ply and 32-ply) and three variations of a [0/90/+45/-45] stacking sequence were investigated. The panels were 100mm x 100mm (25.4 in x 25.4 in) and the projectile had a length of 24

mm (0.9 in) and a diameter of 14.5 mm (0.6 in). Thin glass plates, with conductive silver print, were used to measure the residual projectile velocity after penetration of the target. Impact velocities for the projectile ranged from 24 m/s (79 ft/s) to 91 m/s (299 ft/s). The modeling results were compared to experimental data. An analytical model, based on the conservation of energy, for predicting the ballistic limit, V_L, was given as:

$$V_L = \sqrt{V_S^2 - V_R^2} \quad \text{for } V_R > 0 \qquad (1.2)$$

where V_S is the striking velocity and V_R is the residual velocity.

In the finite element model, Lee and Sun modeled the steel projectile as non-deformable and the composite laminate was modeled as a quasi-isotropic material using an effective modulus scheme [Sun and Li]. Predicted values for the ballistic limit were within 8% of the experimental data.

1.3 Overall Technical Approach of this Research

Impact problems are extremely complex. In a general sense, there are three distinct approaches to solving impact problems. The first is an empirical approach in which experimental data is collected, correlated, and analyzed for trends. The second approach is to develop engineering models of varying complexity that approximate the impact event. And the third approach is to discretize the problem into small elements and apply the fundamental laws of physics to each element. Finite element analysis and finite difference methods are examples of the discretization method.

Each of these three approaches to the study of impact phenomena has associated advantages and disadvantages. The empirical approach is well-suited for solving a specific problem, but cannot usually be extrapolated outside of the testing parameters. Engineering models usually concentrate on one particular aspect of the problem (such as plugging, petaling, or spall) by reducing the governing equations to one- or two-dimensional algebraic or differential equations through the use of simplifying assumptions. These types of analyses usually require some additional empirical input to the model. In the case of discretization, numerical analysis has been shown to be capable of providing accurate solutions to very complex problems, but the solutions can be extremely computationally time consuming. In many cases, the best approach is a hybrid combination of all three approaches.

This combination approach has been utilized in the present study to investigate the effect of curvature on the high velocity impact response of plates. High velocity impact tests were conducted using light gas guns. These tests were used to identify the ballistic limit of the plates and to provide insight into the response of the plates across varying velocity regimes. Non-destructive and destructive post-impact analyses of the plates provided information concerning damage generation in the plates and the effects of increasing velocity and curvature. A non-linear finite element model was also used to simulate the high-velocity impact event. These results were compared to the experimental data to verify accuracy and to validate the assumptions made in the simulations.

With validity and accuracy established, the ability to conduct parametric studies was an added benefit of the finite element modeling. As expected, it was much more cost effective to simulate these parameter changes than to conduct the experimental testing of each configuration. The caveat of not extrapolating outside the range of the experimental test parameters still exists, however, and caution had to be exercised when performing simulations over parameter ranges that were broader than those validated previously. Utilizing the information gained from experimental testing and numerical analysis, an improved understanding of the effects of panel curvature during ballistic impact of both aluminum and composite panels was attained.

1.4 Content of Subsequent Chapters of this Dissertation

Chapter 2 details the experimental studies that were performed during various phases of this investigation. The experimental set-ups used and the details of the specimen fabrication are described. A brief description of ballistic limits and ballistic curves precedes presentation of the raw test data.

In Chapter 3, a numerical framework for modeling ballistic impact in both flat and curved panels is developed. The commercial finite element software used for the simulation is described along with a brief discussion of the model development process. Numerical results are presented for ballistic impact of both flat and curved aluminum panels.

Chapter 4 examines the significance of the experimental and numerical results. A chronological overview is presented that puts the research in context.

This overview is followed by a more detailed discussion and comparisons between the experimental and numerical results.

In Chapter 5, the non-destructive and destructive evaluations of the impacted panels are discussed. Results from post-impact evaluations, and documentation of observed damage are presented for both the composite and aluminum panels. Qualitative trends are identified and the results are compared to findings that have been previously reported in the literature.

Chapter 6 contains concluding remarks for this research. A summary and re-statements of some of the key findings are presented. The chapter closes with recommendations for future work that can build on the foundation established.

Chapter 2 Experimental Investigation

2.1 Overview

This chapter describes an experimental investigation of ballistic impact that was conducted on both graphite epoxy composite plates and aluminum plates with varying curvatures. The experimental tests were conducted at Wright-Patterson Air Force Base in the Gun Range "A" facility that is operated by the 46th Test Wing. The ballistic impact testing used ½-inch diameter steel spheres and a range of impact velocities that bracketed the expected ballistic limit. The ballistic limit, a term used to describe a velocity, or a range of velocities, that separates penetrating impact events from non-penetrating impact events, was established through the testing for each material and for each curvature within that particular material set. Attention was focused on this range of velocities because of the complex interactions and changes in the failure mechanisms that take place during the transition from non-penetrating impact events to penetrating impact events. A velocity measurement system and a high speed video system were used to capture both the pre- and post-impact velocities of the projectiles as well as to record the dynamic response of the plates.

2.2 Specimen Fabrication

2.2.1 Graphite Epoxy Composite Fabrication

The graphite epoxy composite specimens were fabricated from ready-to-cure sheets of unidirectional AS4/3501-6 material manufactured by Hercules Corporation of Magna, Utah. These sheets of material are manufactured such that the fibers are already incorporated into the matrix material. This process involves

the pulling of a row of uniformly spaced fibers through a resin bath containing epoxy resin dissolved in an appropriate solvent. The spacing of the fibers determines the fiber-volume content or ratio of fiber volume to total volume of the material. Heat is then applied in a controlled manner to consolidate the sheet. Release film is applied to the back of the sheet and the delivered product is a roll of material that can be cut to size and layered to create desired configurations of composite laminates.

The AS4-3501-6 lamina mechanical properties are given in Table 2.1. Initial panels, measuring 2 feet x 2 feet, were fabricated by stacking 32 plies of unidirectional material with the prescribed stacking sequence that details the fiber orientations to be described later. After stacking the unidirectional material, the panels were vacuum bagged and then placed in an autoclave for curing. The curing process involved exposing the material to elevated temperatures and pressures for a predetermined length of time. This process consolidates the individual unidirectional sheets into a solid laminate. The final thickness of the panels was 0.187 inches. Water-jets were used as the primary method of machining to fabricate 8-inch by 8-inch plates from the initial 24-inch by 24-inch panels. Tolerances for the length and width of the plates were within +/- 0.05 inches.

Table 2.1 Typical AS4-3501-6 lamina mechanical properties [Mallick,1993]

E_x = 137.9 GPa (2.0 x 10^7 psi)	E_y = 10.3 GPa (1.5 x 10^6 psi)
G_{xy} = 5.5 GPa (0.8 x 10^6 psi)	ν_{xy} = 0.3

2.2.2 Curved composite panel fabrication

Curved composite panels were fabricated in the same manner as the flat panels with the only difference being that cylindrically curved pre-forms were used for laminate lay-up and curing. The final result was composite panels with 12-inch and 4.4-inch radii of curvature. These panels were then cut into specimens with dimensions of 8-inches (linear) x 8-inches (arc). The shape of the specimens is easily visualized by taking a flat 8-inch by 8-inch plate and bending it into a cylindrical shape with the appropriate radius of curvature. Representative samples of a flat composite plate, a 12-inch radius of curvature composite plate, and a 4.4-inch radius of curvature composite plate are shown in Figure 2.1.

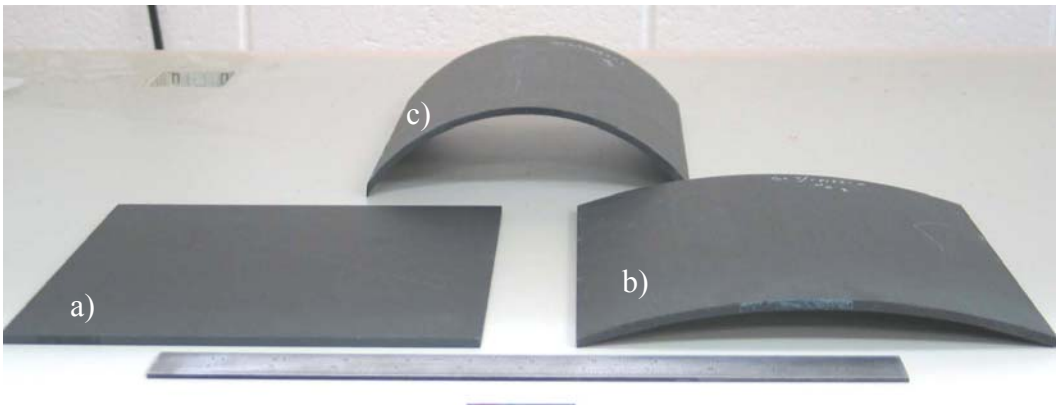

Figure 2.1 Representative samples of (a) a flat composite panel, (b) a 12-inch radius of curvature composite panel, and (c) a 4.4-inch radius of curvature composite panel. A 12-inch ruler has been included in the photograph for scaling purposes

2.2.3 Composite laminate stacking sequence

The orientation of the individual unidirectional plies that comprised the composite laminate was selected to simulate quasi-isotropic material properties and is represented in ply stacking sequence nomenclature by $[0/90/+45/-45]_{4s}$. The ply stacking sequence nomenclature defines the angle of each individual

unidirectional fiber direction with respect to a reference axis. For example, a zero-degree ply, indicated by [0], would be placed parallel to this reference axis, while a ninety-degree ply would be rotated 90° from the reference axis so that it is perpendicular to the axis. Thus, the ply stacking sequence of [0/90/+45/-45] describes four individual unidirectional plies stacked from top to bottom with the fibers oriented at the specified angle with respect to the reference axis.

A subscripted number placed behind the ply stacking sequence indicates the number of times that the stacking sequence is repeated. For example, a ply stacking sequence of $[0/90/+45/-45]_2$ is a short-hand notation for an eight ply laminate with the following order of plies from top to bottom: [0/90/+45/-45/0/90/+45/-45]. Subscripted numbers can also appear within the short-hand notation to indicate a repetition of a particular angled ply. For example, the short-hand notation $[0/90_3/0]$ refers to a five ply laminate with a zero-degree ply on top followed by three ninety-degree plies with another zero-degree ply on the bottom or [0/90/90/90/0] in expanded form.

A subscripted "s" placed behind the stacking sequence indicates that the laminate is symmetric about the mid-plane with the ply orientations repeated in reverse order. For example, $[0/60/30]_s$ is short-hand notation for a six ply laminate whose expanded form is [0/60/30/30/60/0].

The ply stacking sequence used for this research, $[0/90/+45/-45]_{4s}$, refers to a 32-ply laminate with the sequence [0/90/+45/-45] repeated four times, and then mirrored to provide symmetry about its mid-plane. The expanded form would appear as [0/90/+45/-45/0/90/+45/-45/0/90/+45/-45/0/90/+45/-45/-45/+45/90/0/-45/+45/90/0/-45/+45/90/0/-45/+45/90/0/-45/+45/90/0]. The term 'quasi-isotropic' is used to describe laminates which approximate in-plane, isotropic, elastic behavior in the xy-plane. This is generally achieved by using a mixture of ply angles (not just 0° and 90° plies) with an equal number of the various angled unidirectional plies throughout the thickness of the laminate. With this arrangement, tension tests of specimens cut at various angles should have approximately the same mechanical properties.

2.2.4 Aluminum panel fabrication

Commercially available 2024-T3 aluminum material with a thickness of 0.08 inches was purchased and fabricated into test specimens. Typical material properties for the 2024-T3 aluminum are given in Table 2.2. Flat panel specimens with dimensions of 8-inches by 8-inches were cut directly from the stock material, while the curved specimens were formed into the necessary curvatures through a rolling process and then sheared to their final dimensions. Test specimens with the following radii of curvature were formed from the stock aluminum 2024-T3 material: 12-inch, 8-inch, and 4.4-inch. Representative samples of the 2024-T3 aluminum panels are shown in Figure 2.2.

Table 2.2 Typical mechanical properties for 2024-T3 aluminum [Sun,1996]

E = 79 GPa (1.14 x 10^7 psi)	G = 30 GPa (4.3 x 10^6 psi)	ν = 0.33

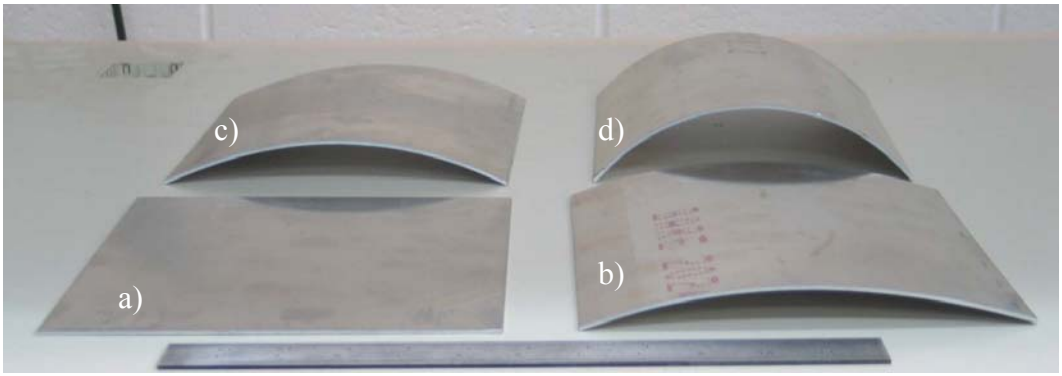

Figure 2.2 Representative samples of (a) a flat aluminum panel, (b) a 12-inch radius of curvature aluminum panel, (c) a 8-inch radius of curvature aluminum panel, and (d) a 4.4-inch radius of curvature aluminum panel. A 12-inch ruler has been included in the photograph for scaling purposes

2.3 Test Fixtures

2.3.1 Fixed-Fixed Test Fixture

Initial ballistic impact testing of the AS4/3501-6 graphite epoxy composite panels was conducted using clamped boundary conditions on all four sides of the test specimen for comparison to previous flat composite plate tests [Sun,1996]. For this purpose, two test fixtures were designed and built to accommodate the two curvatures being investigated. The test fixtures are shown in Figure 2.3 and Figure 2.4. The test fixtures were made of steel and consisted of four individual pieces that were welded together to form the base of the test fixture. A separate clamping plate was also fabricated from steel. The clamping plate secured the composite panel to the base using ¼ x 28 steel bolts spaced 2-inches center-to-

center along each edge. A small rubber insert was used around the periphery of the clamped edges to distribute the clamping pressure to the test specimen.

Figure 2.3 Test fixture for 4.4-inch radius of curvature panels. A 12-inch ruler has been included in the photograph for scaling purposes.

Figure 2.4 Test fixture for 12-inch radius of curvature panels with sample composite panel inserted. A 12-inch ruler has been included in the photograph for scaling purposes.

2.3.2 Fixed-Free Test Fixture

The biggest drawback of the fixed-fixed test fixtures, aside from cost, was that each fixture could only accommodate a single radius of curvature. To overcome this limitation, a new reconfigurable test fixture was designed and built. The new test fixture was designed to provide fixed boundary conditions along the two straight edges of the test specimen with the other two (curved) sides remaining free. Two field-goal-shaped steel frames were used to provide the straight-edge supports. The frames could be rotated so that the straight edges were properly aligned to match the various panel curvatures. The panels were held in place by clamping two ½-inch thick polycarbonate plates to the straight-edge supports. A schematic of the test fixture is shown in Figure 2.5. The steel frame supports were secured to a separate base plate (not shown in the schematic) and additional reinforcement (also not shown) was provided at the top of the straight edge to restrict movement of the fixture during the test. This test fixture setup enabled cost-efficient testing across a range of curvatures using a single, reconfigurable test fixture.

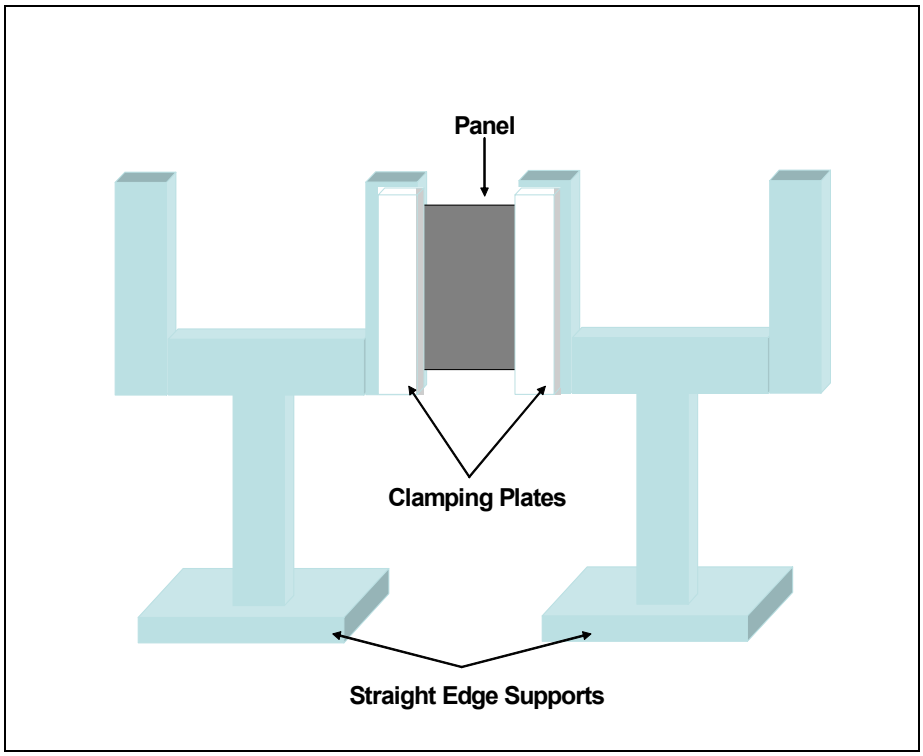

Figure 2.5 Schematic of fixed-free test fixture

2.4 Light Gas Gun

A light gas gun system is essentially a pressurized chamber, located behind the projectile, with an incorporated mechanism for opening the chamber to allow the built-up pressure to propel the projectile towards the target. The light gas gun system used for the testing is shown in Figure 2.6. This particular system consists of a gun barrel, a pressure chamber, and an electrical control valve. The inside diameter of the gun barrel is slightly larger than ½-inches. Helium gas is used as the main pressurization source and the electrical control valve allows fast-opening of the valve that seals the pressure chamber from the gun barrel. Main pressurization and triggering are activated from an isolated control room for safety purposes.

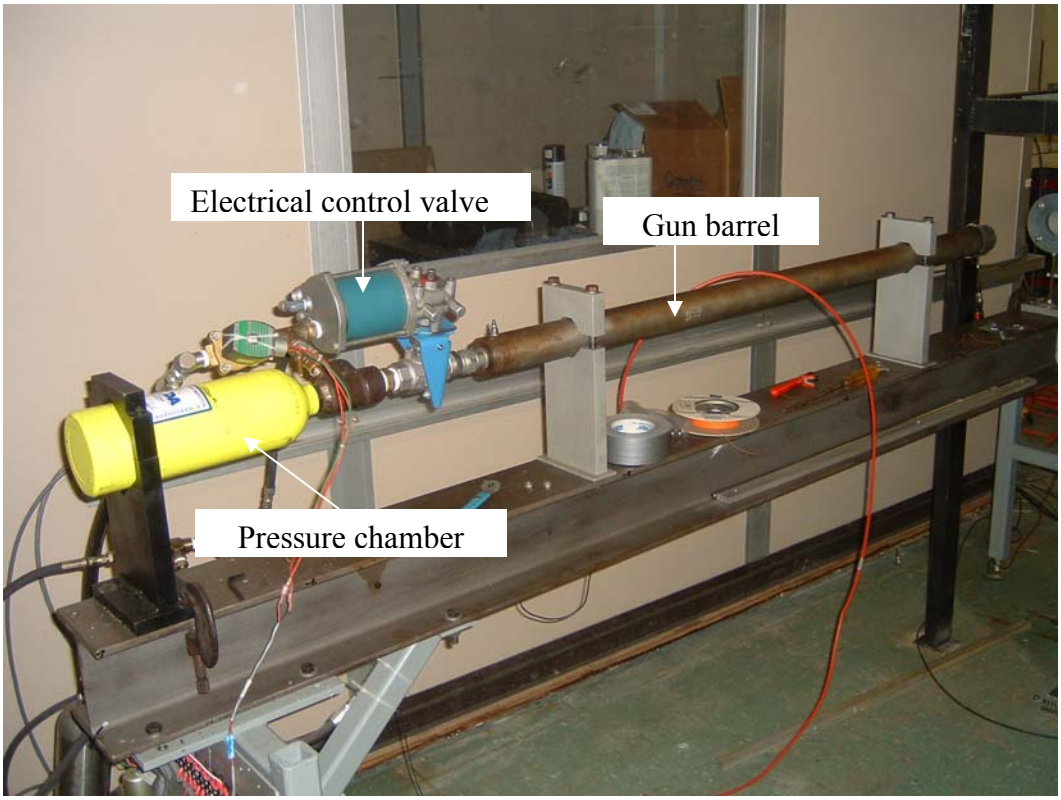

Figure 2.6 Light gas gun system

2.5 Data Acquisition

2.5.1 Velocity measurement system

A velocity measurement system, consisting of two sets of electromagnetic coils, a Nicolet System 500 digital oscilloscope (manufactured by LDS Test and Measurement LLC, Middleton, WI), and a computer, was employed to capture the pre- and post-impact velocities of the projectile.

Figures 2.7 and 2.8 show the two sets of coils used during testing. Two electromagnetic coil windings are mounted on plastic tubing at a known distance apart. The induction of each coil winding changes when a conductive object passes through it and a voltage change is registered on the Nicolet System each time this occurs. The voltage records from each pair of coil windings provide a

measure of the times, Δt_1 and Δt_2, that the projectile takes to traverse the distance between each pair of coil windings, Δx_1 and Δx_2, respectively. Figure 2.9 shows representative traces of the voltage output recorded on the Nicolet during a test.

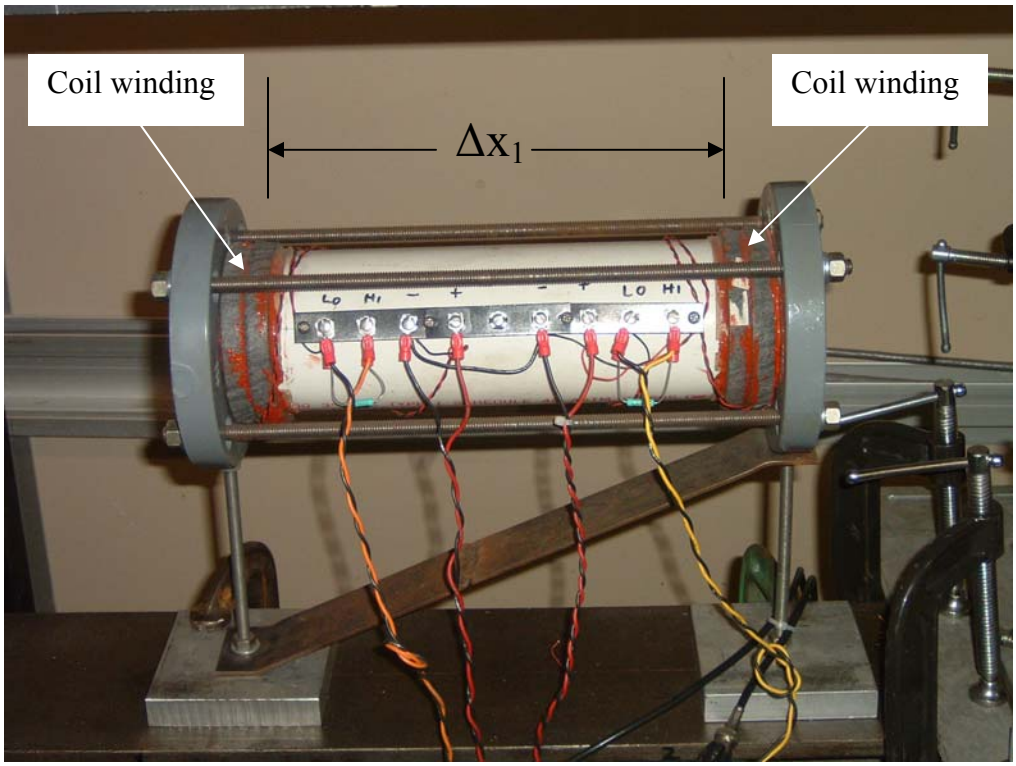

Figure 2.7 Front electromagnetic coils

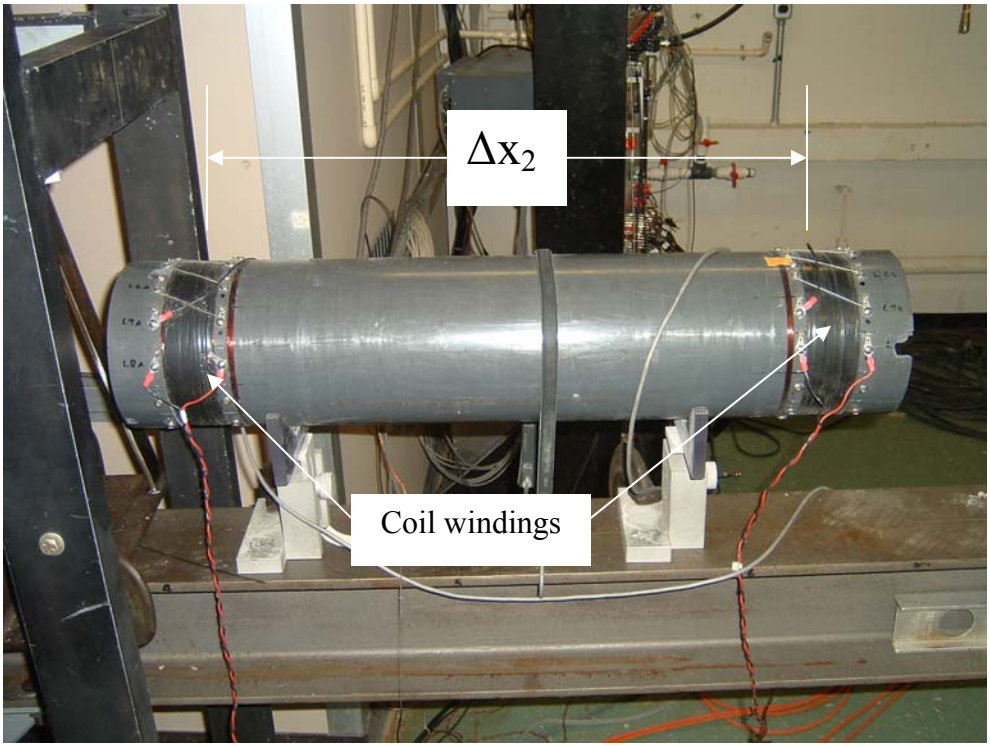

Figure 2.8 Rear electromagnetic coils

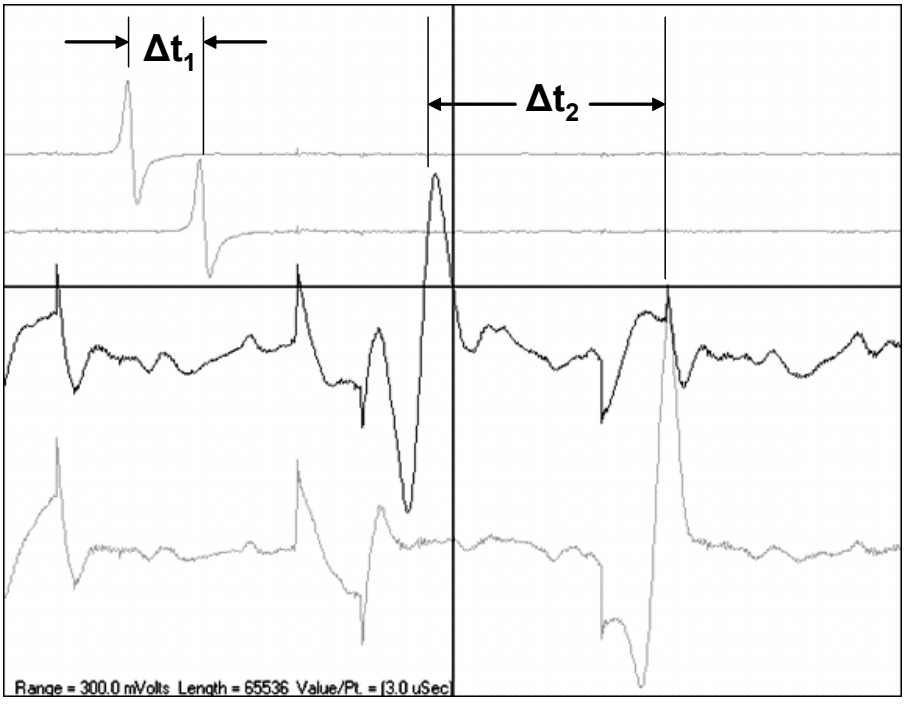

Figure 2.9 Sample data acquired from the electromagnetic coil system

The top two traces show the voltage change registered from the two coil windings in front of the target. The bottom two traces show the voltage change registered from the two coil windings located behind the target. These bottom traces also show the presence of electromagnetic noise in the system but the information of interest can still be readily extracted. The velocity of the projectile is determined by dividing the effective separation distance of each pair of coils by the measured time differences, Δt_1 and Δt_2, in the signals. The time difference is measured at the peaks of the two signals as depicted in Figure 2.9.

For both the front and rear coils, the effective separation distance of the windings was calibrated using a variety of other velocity measurement systems, most notably break paper and light screens. In this process, a series of tests were conducted where projectiles were fired from the gas gun system at various pressures. The break paper or light screens were positioned at the front and rear of one of the electromagnetic coils and the projectile velocities were calculated by dividing the measured separation distance of the break papers or light screens by the elapsed time as determined by a digital counter that captured the triggering of the break paper or light screens. These calculated velocities were used in conjunction with the time difference, Δt, measured from the coil signals to back-calculate an effective coil separation distance. This process was then repeated for the other set of coils. Once calibrated, the effective separation distance was considered a fixed value for the fixture and was used in future experiments without further calibration.

There are several distinct advantages to using the electromagnetic coil system over other velocity measurement techniques. First, the coil system is reusable. The coils that were used in these experiments have been in service for approximately ten years. Secondly, the electromagnetic coil system has the ability to capture the rebound velocities of the projectile for non-penetrating impact events. Lastly, the system is able to more accurately measure the post-penetration velocities of the projectile. Break paper systems require replacement after each test and are incapable of measuring the rebound velocity. Additionally, rear-mounted light screens and break paper systems are most often triggered by ejected material from the rear of the impacted specimen resulting in erroneous measurements of the post-penetration projectile velocity.

2.5.2 High speed video system

A high speed video system, with framing rates up to 60,000 frames per second, was employed to capture qualitative and quantitative information about the plate response to ballistic impact. The high speed video system consists of two Phantom™ high speed video cameras (Phantom™ V7 and Phantom™ V5 manufactured by Vision Research, Inc., Wayne, NJ), high intensity lighting, a laptop computer for control and data acquisition, and image analysis software for quantifying the response of the plate. The high speed video system is triggered when the projectile breaks a thin wire that is secured across the gun muzzle as shown in Figure 2.10. The breaking of the wire disrupts the 5V DC potential that was being carried and the cameras are programmed to trigger when they register this falling signal.

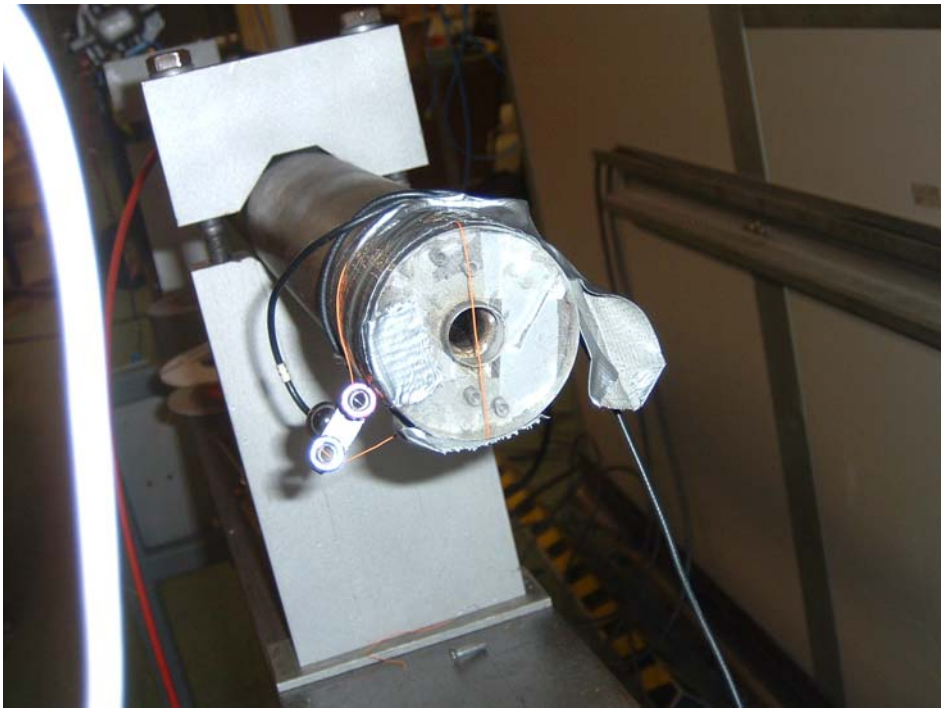

Figure 2.10 Muzzle-wire trigger for camera system

The two-camera system provides the ability to capture three-dimensional data through digital image correlation and photogrammetry [Mikhail,2001]. Figure 2.11 shows the relative positioning of the two cameras in the experimental set-up. Spatial calibration of the cameras is accomplished in the software by establishing known reference points on a fixed target that can be seen by both cameras. The x, y, and z coordinates of these points are used to back-calculate the camera locations based on the camera focal lengths. After calibrating the positions of the cameras, reference points or gratings are physically marked on the target at points of interest and image analysis software is used to track the dynamic response for each of these reference points.

Images from a representative recording of a ballistic impact are shown in Figure 2.12. This particular recording shows a 12-inch radius of curvature

aluminum panel being penetrated by a ½-inch diameter steel sphere with an initial velocity of 617 ft/sec. The high-speed video was recorded at 15,000 frames per second. Sample video files depicting impacts on both aluminum and composite panels are included in Appendix A.

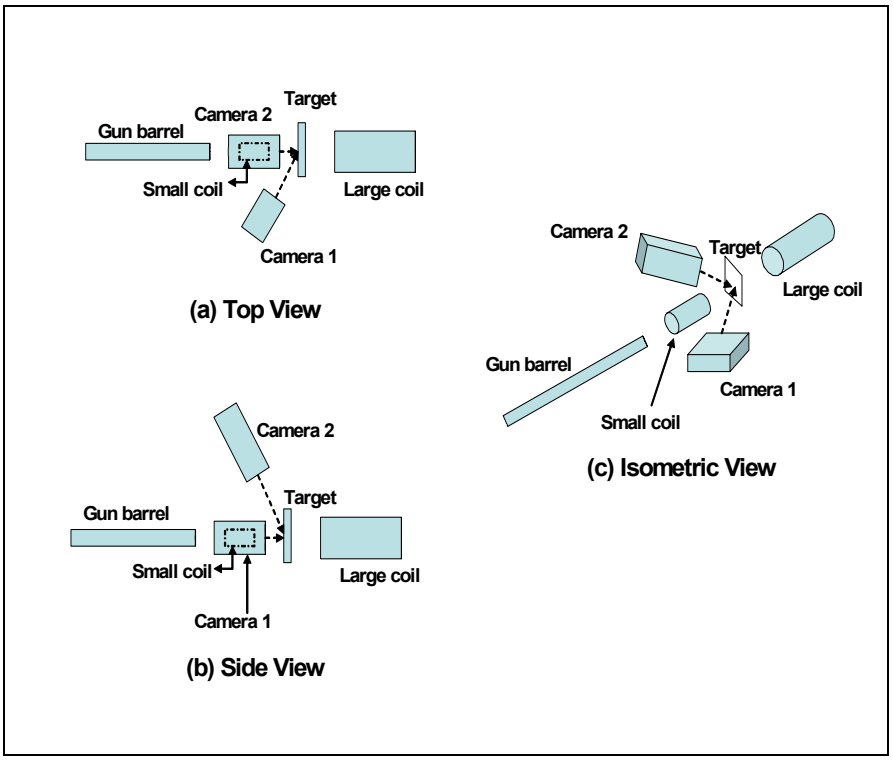

Figure 2.11 Various views of camera set-up: (a) top view, (b) side view, and (c) isometric view

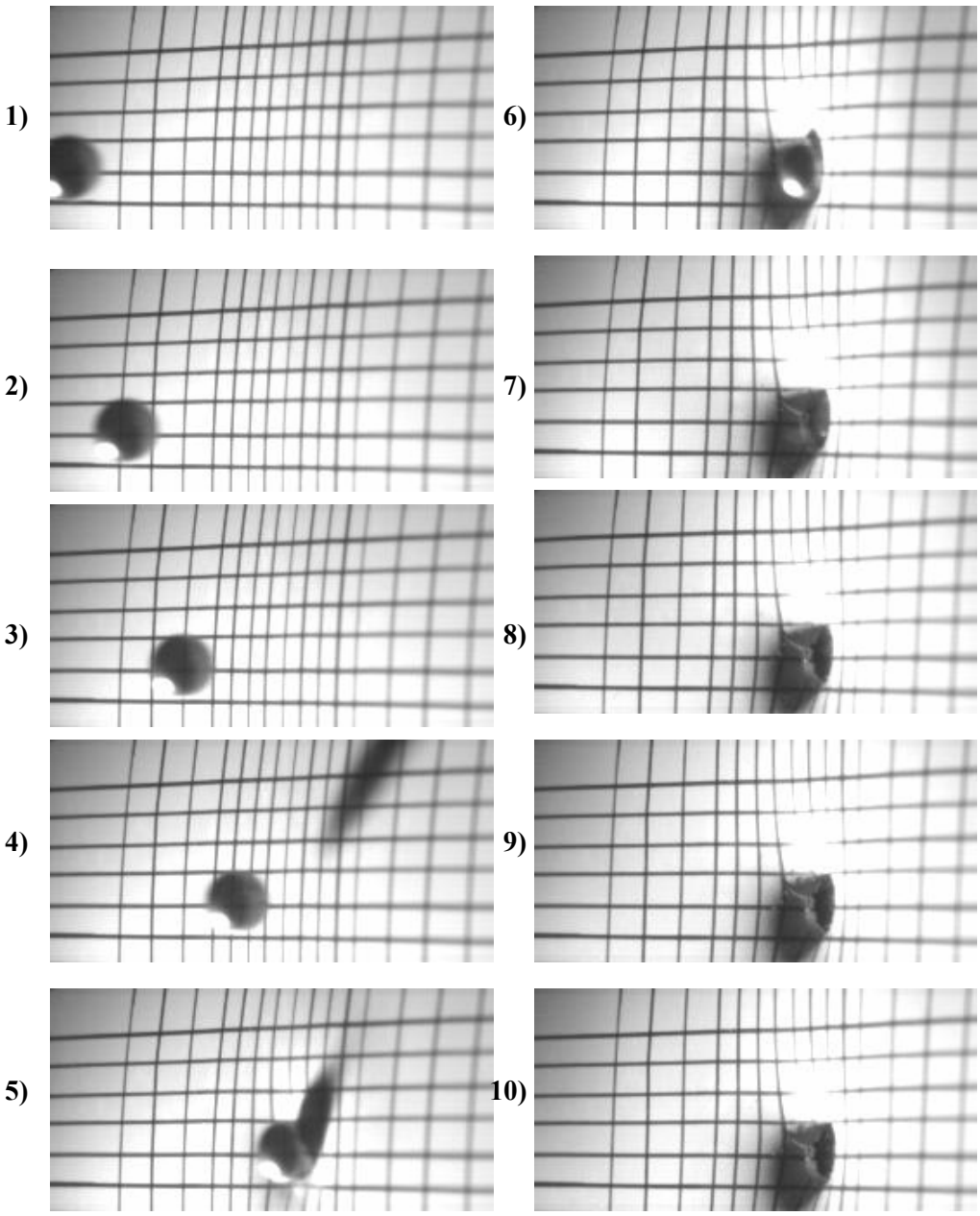

Figure 2.12 Images showing projectile penetration during a 617 ft/sec impact on a 12-inch radius of curvature aluminum panel with an ink-drawn reference grating. The video was recorded at 15,000 frames/sec

2.6 Test Procedure

The following standard test procedure was a range safety requirement at the Gun Range "A" facility that is operated by the 46th Test Wing at Wright Patterson Air Force Base, OH and was followed for all of the ballistic impact testing:

1. Configure/Set up test fixture
2. Turn on helium pressure in trailer
3. Turn on power to electromagnetic coils and data acquisition system
4. If necessary, set up high speed video
5. Close trigger ball valve
6. Insert projectile into gun barrel
7. If necessary, set up gun barrel wire trigger
8. Set regulator on nitrogen bottle to approximately 110 psi
9. If necessary, turn on lights for high speed video
10. Close and lock all test area doors
11. Charge helium bottle to desired test pressure
12. Turn weapon key lock to "weapon ready"
13. Press "system ready" button
14. Arm data acquisition system
15. Press "test" button
16. Press "arm" button
17. Activate siren
18. After 5 second audible count down, press "fire" button
19. Press "end test" button
20. Turn weapon key lock to safe position and remove
21. If necessary, turn off lights for high speed video
22. If necessary, save high speed video recordings
23. Record projectile velocities from data acquisition
24. Close valves on nitrogen cylinder and helium trailer
25. Remove specimen from test fixture

2.7 Description of Ballistic Curves and Ballistic Limit

To ensure that the terminology being used is unambiguously understood, a brief discussion on the construction of ballistic curves follows. A ballistic curve is a graphical representation of the results from several individual ballistic tests with the residual projectile velocity plotted versus the initial impact velocity of the projectile. In general, the impact event results in either penetration of the

target or non-penetration of the target. The latter is hereafter referred to as a rebound event.

The initial direction of travel of the impacting projectile is taken to be the positive direction. Penetration events are then associated with positive residual projectile velocity (travel continues in the same direction) and rebound events are associated with negative residual projectile velocity. On rare occasions, the projectile embeds itself into the target. This event corresponds to a zero residual projectile velocity. A hypothetical ballistic curve is shown in Figure 2.13.

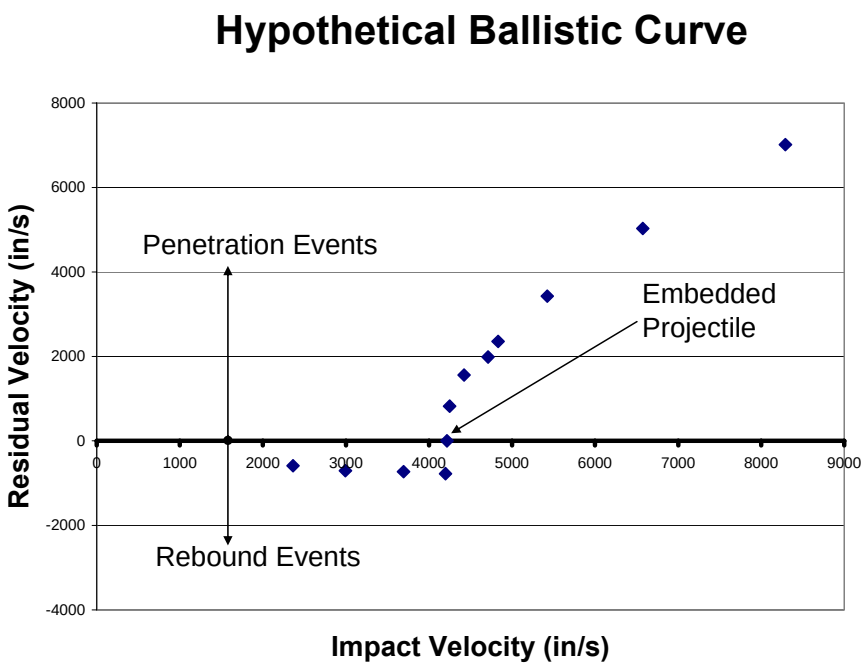

Figure 2.13 Hypothetical ballistic curve

For the purposes of this research, the ballistic limit is defined as the value that results from averaging the highest impact velocity that results in a rebound with the lowest impact velocity that results in penetration. Similarly, the ballistic limit region is defined as the range of impact velocities that encompass the

transition from rebound to penetration events. The procedures followed for the calculation of the ballistic limit in the present research will be presented in Chapter 4.

2.8 Test data

For each test performed as part of this study, the time histories of the signals generated by the electromagnetic coils were recorded by the data acquisition system. These signals were then used to calculate the initial impact velocities and residual impact velocities of the projectiles. Tables 2.3-2.8 list the pre-impact and post-impact velocity measurements for each ballistic test. Tables 2.3 and 2.4 pertain to composite panels of 4.4-inch and 12-inch radius of curvature, respectively. Tables 2.5-2.8 pertain to ballistic impact testing of the aluminum panels of 4.4-inch, 8-inch, 12-inch, and infinite radius of curvature, respectively. The same information is shown in ballistic curve format in Figures 2.14-2.19. The average projectile mass was 8.57 grams (0.0189 lbm) with a standard deviation of +/- 0.05 grams. Additionally, the weight of the ejected plug has been recorded for the aluminum panel test results for those cases where the plug could be recovered.

Table 2.3 Experimental results for composite, 4.4-inch radius of curvature

Impact Velocity (ft/sec)	Residual Velocity (ft/sec)
301	-114
350	-111
367	-103
370	0
372	0
373	-86.6
376	0
377	-75.6
377	-85.7
379	81.6
379	70.4
385	91.6
421	200
520	380
550	422

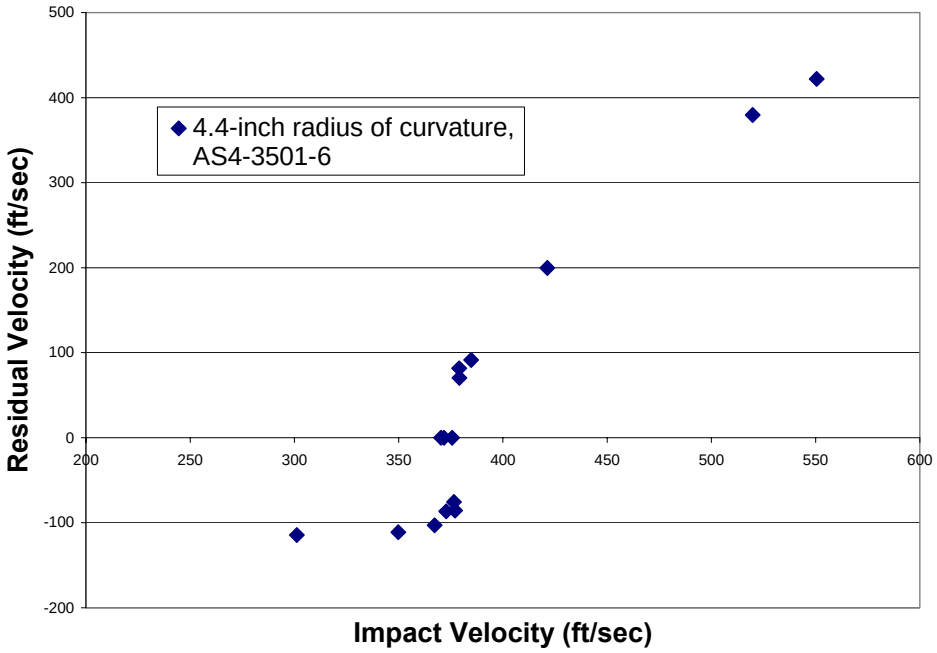

Figure 2.14 Experimental results for composite, 4.4-inch radius of curvature

Table 2.4 Experimental results for composite, 12-inch radius of curvature

Impact Velocity (ft/sec)	Residual Velocity (ft/sec)
303	-55.3
336	-60.7
346	-75.0
348	-80.3
350	-76.1
352	-68.4
358	-71.7
358	47.7
358	91.2
359	-75.5
363	71.7
364	-83.2
366	-79.0
368	116
368	89.1
370	74.3
371	111
416	216
519	380

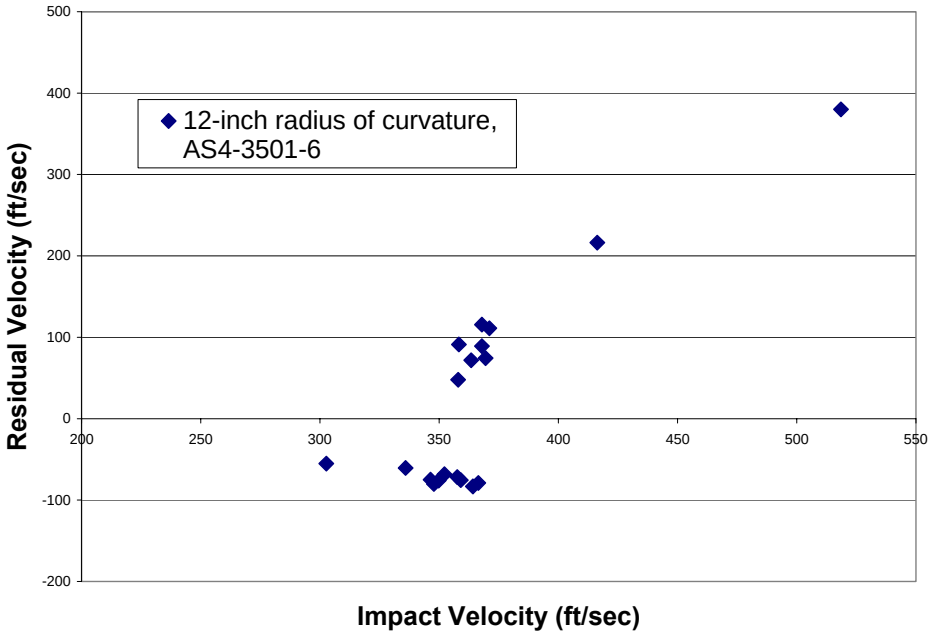

Figure 2.15 Experimental results for composite, 12-inch radius of curvature

Table 2.5 Experimental results for aluminum, 4.4-inch radius of curvature

Impact Velocity (ft/sec)	Residual Velocity (ft/sec)
402	-61.9
430	-67.9
482	-85.7
490	73.9
515	187
525	186
590	344
619	382
890	732

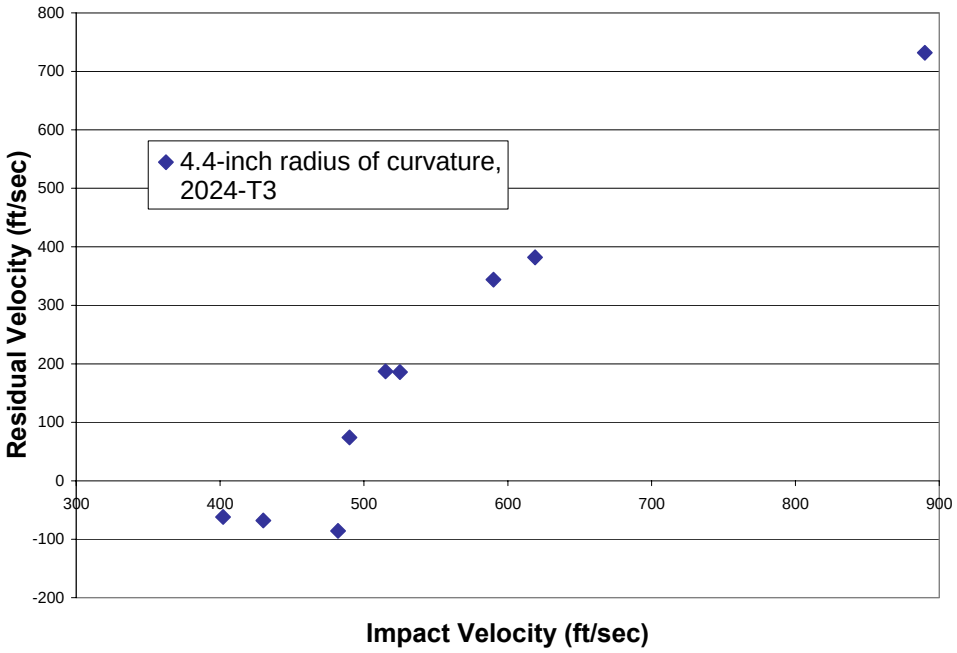

Figure 2.16 Experimental results for aluminum, 4.4-inch radius of curvature

Table 2.6 Experimental results for aluminum, 8-inch radius of curvature

Impact Velocity (ft/sec)	Residual Velocity (ft/sec)	Plug wt (grams)
393	-66	
459	-47.9	0.2059
490	-77.5	0.2233
502	-75	0.2293
512	133	0.2322
522	185	0.2386
542	243	0.2426
844	675	0.3614
900	749	0.376

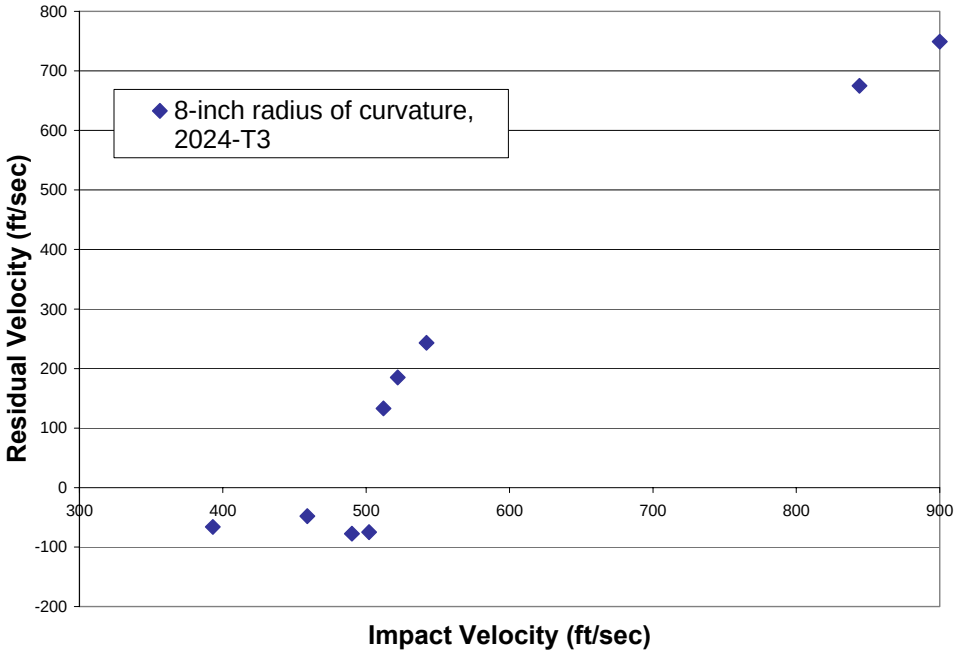

Figure 2.17 Experimental results for aluminum, 8-inch radius of curvature

Table 2.7 Experimental results for aluminum, 12-inch radius of curvature

Impact Velocity (ft/sec)	Residual Velocity (ft/sec)	Plug Wt (grams)
341	-170	
397	-48.3	
442	-49.6	
477	-49.2	0.2168
480	-50.5	
486	-51.2	0.2152
494	-50.9	0.2225
498	171	
504	146	
506	100	0.2276
517	157	0.2295
617	403	
684	494	
723	540	
874	638	

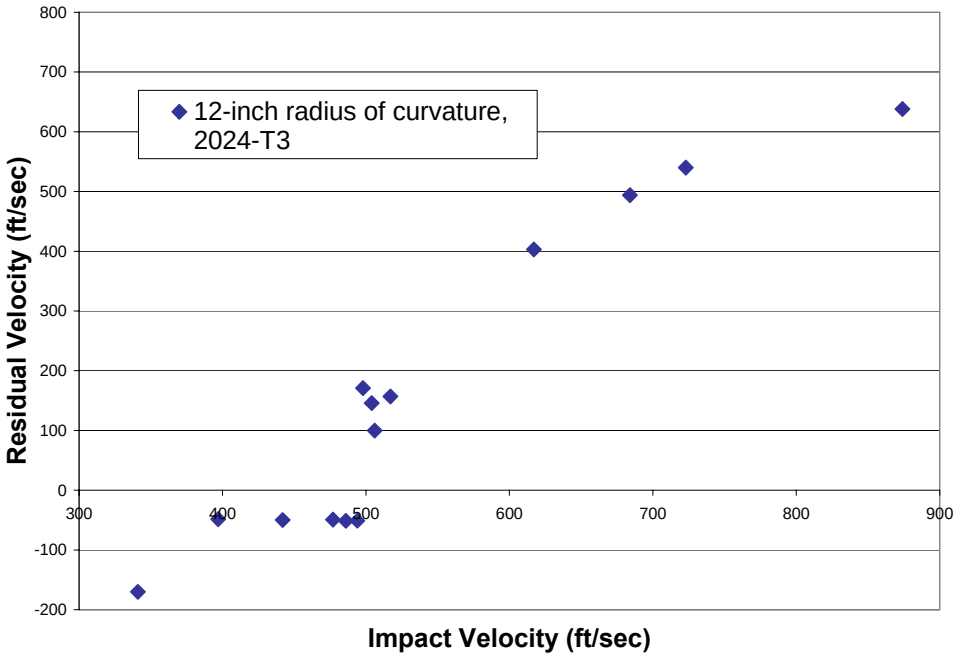

Figure 2.18 Experimental results for aluminum, 12-inch radius of curvature

Table 2.8 Experimental results for aluminum, flat (infinite radius of curvature)

Impact Velocity (ft/sec)	Residual Velocity (ft/sec)	Plug wt (grams)
419	-25.1	0.2154
456	-42.4	0.1986
461	-44.8	0.2719
474	-35.5	0.2053
482	90	0.2118
482	101	0.2093
505	207	0.2181
794	631	0.3304

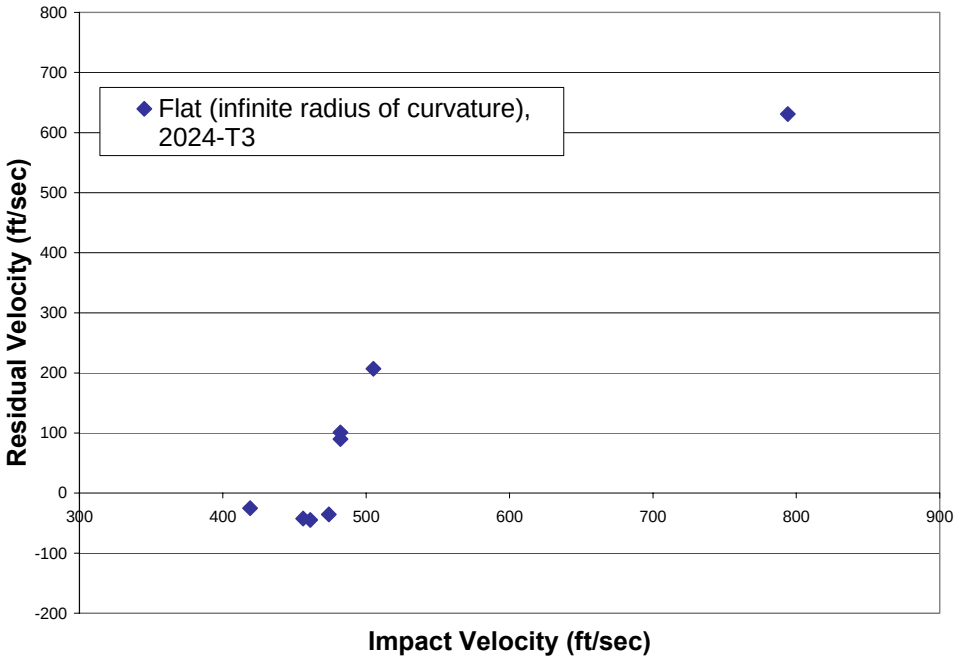

Figure 2.19 Experimental results for aluminum, flat (infinite radius of curvature)

2.9 Chapter Summary

Results of an experimental investigation into the effects of panel curvature on the ballistic impact response have been presented in this chapter. Two materials, AS4-3501-6 graphite epoxy composite and 2024-T3 aluminum, were selected for examination. The experimental set-up and specimen fabrication have been discussed in detail. Two panel curvatures, a 4.4-inch radius of curvature and a 12-inch radius of curvature, were tested for the graphite epoxy composite material. Four panel curvatures, a 4.4-inch radius of curvature, an 8-inch radius of curvature, a 12-inch radius of curvature, and an infinite radius of curvature (flat plate), were tested for the aluminum material. In total, seventy-six experimental ballistic tests were conducted. Table 2.9 shows an overall summary of the experimental testing. A more in-depth discussion regarding the significance of the experimental results will be presented in Chapter 4. The next chapter describes computational simulation studies of the ballistic impact event.

Table 2.9 Experimental ballistic testing summary

Material	AS4-3501-6		Aluminum 2024-T3			
Radius of curvature (inches)	4.4	12	4.4	8	12	infinite
Number of tests	15	19	9	9	16	8
Lowest velocity tested (ft/sec)	301	303	402	393	341	419
Highest velocity tested (ft/sec)	550	519	890	903	1637	794

Chapter 3 Numerical Analysis

3.1 Overview

An important objective for the research effort described in this dissertation was the desire to rapidly and reliably simulate and predict the ballistic impact event using a commercially-available finite element code. This would allow parametric studies on the effect of curvature to be completed in an economical fashion. An iterative process was established whereby ballistic impact experiments were initially used to validate and refine preliminary numerical models. Exercising the numerical model then provided guidance for additional experimental work.

LS-DYNA^{TM}, a commercial finite element code developed by Livermore Software Technology Corporation, Livermore CA, was used as the primary numerical solution tool. This code was specifically developed for simulations of dynamic events and has been used in this study to simulate the ballistic impact event for both flat and curved plates.

3.2 Introduction to LS-DYNA

LS-DYNA is a general purpose, multi-physics, simulation software package and is not limited to any particular type of simulation. Finite element codes use either an explicit or implicit time integration solver. LS-DYNA's ability to model non-linear dynamic events accurately and inexpensively is made possible through the use of an explicit analysis solver. In an explicit analysis, the internal and external forces are summed at each nodal point, and a nodal acceleration is computed by dividing the nodal force by the nodal mass. The

solution is then advanced by integrating the acceleration twice with respect to time [LSTC, 2003]. In contrast, an implicit analysis solver, which is generally more suited for static applications, computes a global stiffness matrix, inverts it, and applies it to the nodal, out-of balance force to obtain a displacement increment.

LS-DYNA has evolved continuously since its inception as DYNA3D in 1976, and in its present form, has numerous capabilities in terms of element selection, material modeling, and contact interfaces. Table 3.1 lists some samples of the software capabilities. The LS-DYNA software is primarily limited by the storage capacity of the computer on which it is being run.

Table 3.1 Sample LS-DYNA software capabilities

Analysis capabilities:	**Element library:**
• Nonlinear dynamics • Rigid body dynamics • Quasi-static simulations • Linear statics • Thermal analysis • Fluid analysis • Underwater shock • Failure analysis • Crack propagation • Multi-physics coupling	• Solids • 8-node thick shells • 4-node shells • Beams • Welds • Discrete zero length beams • Trusses and cables • Nodal masses • Lumped inertias
Material models:	**Contact algorithms:**
• Metals • Plastics • Glass • Foams • Fabrics • Honeycombs • Composites • Concrete & soils • High explosives • User-defined materials	• Flexible body contact • Flexible body to rigid body contact • Rigid body to rigid body contact • Edge-to-edge contact • Eroding contact • Tied surfaces • Rigid walls • Draw beads

Input of model data is achieved through the use of an independent preprocessor. In this case, the preprocessor utilized was Finite Element Model Builder ^{TM} (FEMB), developed by Engineering Technology Associates located in Troy, MI. Table 3.1 lists the current FEMB database specifications/limitations.

Table 3.2 FEMB database specifications/limitations

Points	200,000
Lines	100,000
Surfaces	2,500
Edge Points	100,000
Control Points	150,000
Grids	100,000
Elements	225,000
Properties	1,000
Nodes	225,000

3.3 Model Development

This section details the necessary steps to develop the finite element model for use in LS-DYNA. The following topics are discussed: building the part geometry, meshing the geometry, assigning element types, assigning material models, defining the contact algorithm, setting up boundary conditions, and setting up initial conditions.

3.3.1 Part Geometry

For the simulation of ballistic impact, we are concerned with two unique parts: the projectile (a ½ inch diameter steel sphere) and a target (a flat or curved plate). After creating unique part identifiers in FEMB, we can begin to define the geometry of each part. The steel sphere is created from a ½ inch diameter circle. This circle is transformed into a surface of revolution by rotating it about an axis that passes through its center. The plate geometry is created by connecting line segments of the proper length and orientation to model the boundary of the plate. This is trivial for the flat plates (four eight-inch line segments in the same plane)

and only slightly more involved for the curved plates. Instead of straight line segments on all four sides, the curved plates use two straight line segments and two arc segments to represent the desired curvature of the plate. A single arc segment is first created and then the second arc segment can be properly located by copying the first arc segment and translating its position. The two line segments are then created by connecting the ends of the two arc segments.

3.3.2 Finite Element Meshing

With the model geometry specification completed, the next step is to provide a finite element mesh for each part. Advances in pre-processor capabilities have greatly increased the ease of creating finite element meshes. For a plate geometry consisting of four individual line segments, the mesh is automatically generated by using the four-line plate meshing option in FEMB. The only other information required is the desired number of elements along each line segment and a visual verification that the automatic mesh is acceptable.

For the initial testing, the mesh size was selected as 40 elements along each side (40x40) for a total of 1600 elements in the plane of the 8-inch x 8-inch plate. Mesh size selection is dependent on the time response of events in the analysis. Simulations involving high gradients of strain require finer meshes in order to accurately model those gradients. The required mesh size is determined after the entire model is complete by analyzing successively finer mesh sizes until the analysis results converge. A convergence study was conducted and the results will be presented in a later section. The final mesh size selected was 150 elements along each side (150x150) for a total of 22500 elements. Symmetry

conditions could have been utilized to reduce the model size, and the associated computational time, but were not implemented.

Recall that the projectile geometry was generated as a surface of revolution. This surface was utilized to create a mesh consisting of 384 solid elements to represent the ½-inch diameter sphere. With the finite element meshes of the plate and the impacting sphere generated, the next steps were to assign element properties and material properties to each part.

3.3.3 Element Formulation

The flat and curved plates were modeled using Belytschko-Tsay (BT) shell elements [Belytschko,1981]. The LS-DYNA Theory Manual [LSTC, 1998] indicates that the BT shell element is usually the shell element formulation of choice. Its computational efficiency is derived from a combined co-rotational and velocity-strain formulation. The co-rotational coordinate system is an embedded element coordinate system that deforms with the element and is defined in terms of the nodal coordinates of the four corner nodes of the element.

For the velocity-strain displacement relations, the displacement of any point in the shell is described by a nodal translation and a nodal rotation. The velocity of any point in the shell, v, is given by

$$v = v^m - z \cdot e_3 \times \Theta \qquad \textbf{(3.1)}$$

where v^m is the velocity of the mid-surface, z is the distance along the thickness direction of the shell, e_3 is the unit vector normal to the main diagonal of the element, Θ is the angular velocity vector, and x represents a vector cross product. The co-rotational components of the velocity strain, d_{ij}, are given by

$$d_{ij} = \frac{1}{2}\left(\frac{\partial v_i}{\partial x_j} + \frac{\partial v_j}{\partial x_i}\right) \quad \textbf{(3.2)}$$

Substitution of Equation 3.1 into Equation 3.2 yields the velocity-strain relations, which are approximated at a finite number of sample points within the shell. Details concerning the solid elements that are used to model the spherical projectile are neglected since the projectile is modeled as a rigid body.

3.3.4 Material Models

Assignment of material properties is accomplished via selection of an appropriate material model. LS-DYNA has approximately 100 material models available for use in its database and the ability to create user-defined material models is also provided. As previously mentioned, the spherical projectile was modeled as a rigid (non-deforming) body. The flat and curved plates were modeled using an elasto-plastic material (Mat_Piecewise_Linear_Plasticity) in which an arbitrary stress versus strain curve, and arbitrary strain rate dependency, can be defined [LSTC, 2003].

A failure criterion based on plastic strain was also included. This failure criterion allows elements to be deleted from the model when a specified plastic strain is reached in the element. This facilitates modeling perforation of the target material during studies of ballistic impact.

3.3.5 Contact-Impact Algorithm

An important consideration in the treatment of impact problems is the interaction between the two entities when they come into contact. In LS-DYNA, the contact-impact algorithm defines the treatment of sliding and contact along interfaces. Interfaces are defined as either master or slave interfaces and the

respective nodes of each interface are defined as master nodes and slave nodes. During contact, slave nodes are required to slide on the master surface until a tensile force develops between the slave nodes and the master surface.

Consider the time-dependent motion of the projectile and the panel. In their undeformed configuration at time zero, the projectile and the panel occupy regions B^1 and B^2, respectively. Initially the intersection, $\cap$, of the two regions satisfies:

$$B^1 \cap B^2 = 0 \qquad \textbf{(3.3)}$$

After the analysis is started, the projectile and panel occupy regions b^1 and b^2 and are bounded by surfaces δb^1 and δb^2. The deformed configurations are not allowed to penetrate and must satisfy:

$$\left(b^1 - \partial b^1\right) \cap b^2 = 0 \qquad \textbf{(3.4)}$$

As long as $\left(\partial b^1 \cap \partial b^2\right) = 0$, the equations of motion remain uncoupled. When $\partial b^1 \cap \partial b^2 \neq 0$, an interface force is applied between the slave node of the panel and the contact point of the projectile. The magnitude of the applied interface force is proportional to the amount of penetration and may be thought of as placing normal interface springs between all penetrating nodes and the contact surface. To avoid affecting the computed time step, the interface stiffness is set to be approximately the same order of magnitude as the stiffness of the interface element normal to the interface. Static and dynamic coefficients of friction between the surfaces are also defined within the contact-impact algorithm.

3.3.6 Boundary and Initial Conditions

Boundary conditions in LS-DYNA were utilized to simulate the holding of the plate by the test fixture during testing. The test fixture constraints were idealized as being 'fixed' in LS-DYNA. Thus, nodes identified as belonging within the test fixture were fixed in all six degrees of freedom and no motion was allowed. In actuality, the test fixture constraints are not truly fixed but fall somewhere between being fixed and simply supported.

The firing of the projectile from the gas gun was simulated in LS-DYNA by assigning an initial velocity to the nodes that make up the finite element model of the sphere. Modeling the range of impacts that comprise the ballistic impact testing was achieved by modifying the initial velocity of the projectile in this manner for each desired impact velocity.

3.4 Numerical Modeling Results

Section 3.3 detailed the required steps to construct the finite element model for modeling the ballistic impact response of flat or curved plates. At this point, the focus shifted to exercising the model to produce results that could be compared to the experimental data presented previously. A building block approach was employed to progress from the simplest case of flat, isotropic, homogeneous, metallic plates to the more complex curved, isotropic, homogeneous, metallic plates, and finally to flat and curved, quasi-isotropic, composite plates. Parametric studies were conducted at various stages to provide a better understanding of the effects of particular parameters on the modeled ballistic

impact response. In all cases, initial impact velocities were selected based on the initial impact velocities measured during the experimental testing.

3.4.1 Modeling the Ballistic Impact Response of Flat and Curved Aluminum Plates

In the spirit of the building block approach, the first model employed consisted of a relatively coarse finite element grid, with 40 elements per side, for a total of 1600 elements. The element size is directly related to the time step of the analysis (the minimum time step used in the explicit analysis is determined by dividing the length of the element by the wave speed of the material), and, as such, variations in the results could be expected for various element sizes.

A convergence study was therefore conducted to determine the appropriate element size for use in the models. An initial value for the failure strain was arbitrarily selected ($\varepsilon_f = 0.1$) and kept constant for the duration of the convergence study. Figure 3.1 shows the predicted ballistic impact response for four different mesh densities. Convergence of the results can be better illustrated by examining the relative change in the predicted ballistic limit as the mesh density is increased. The relative change in predicted ballistic limit from one mesh to another, e.g., 40x40 compared to 80x80, is expressed as a percentage difference.

These results are shown in Table 3.3 as the mesh size was changed from 40x40 to 80x80, 80x80 to 150x150, and 150x150 to 200x200. These results show that the percent difference in the predicted ballistic limit decreased as the finite element mesh density was increased. Further increases in mesh density should result in correspondingly smaller variations in the predicted response but the

associated computation time will continue to increase. The 150x150 finite element mesh was chosen as a suitable compromise between increased numerical accuracy and computational efficiency and was employed for all subsequent modeling efforts.

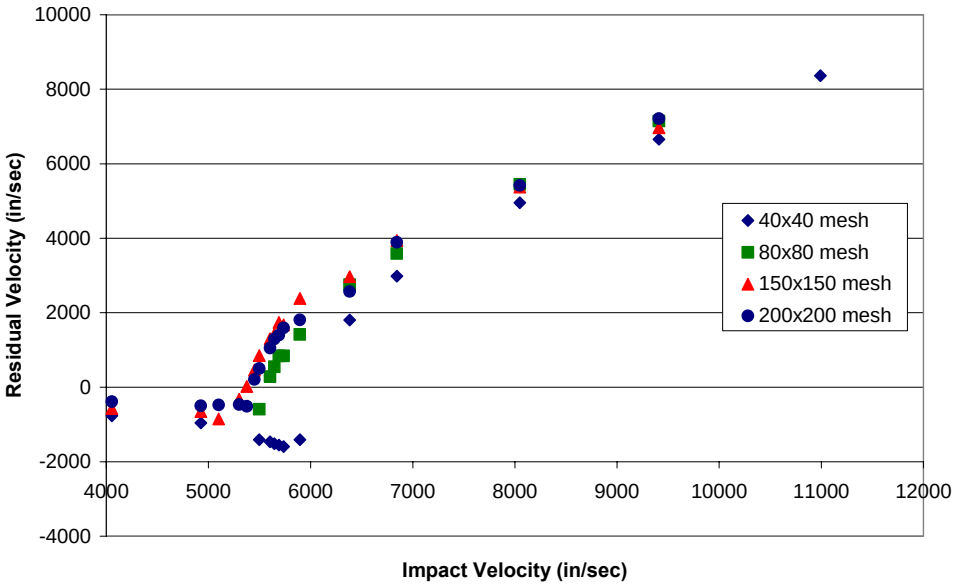

Figure 3.1 Finite Element Mesh Convergence Study

Table 3.3 Convergence of numerical results as mesh size was changed

Change in mesh size	% difference in predicted ballistic limit
40x40 to 80x80	9.6%
80x80 to 150x150	3.8%
150x150 to 200x200	1.4%

As shown in the convergence study, the final modeling results can be highly dependent on user-specified input parameters. A sensitivity study was conducted to ascertain the relative impact of parameter variations on the modeled ballistic impact response. Parameters that were of most interest included the elastic modulus, the coefficient of friction, and the plastic failure strain. The

modeled ballistic impact response was found to be most sensitive to variations in the specified value for the plastic failure strain and, for this reason, the plastic failure strain was selected as the fitting parameter for the modeling effort. All of the other input parameters were considered constant material properties (after initial selection) and were not used to provide a better fit of the numerical model to the experimental data.

With the convergence and sensitivity studies completed, the next step was to fit the flat aluminum panel modeling results to the experimental data and then to model the curved aluminum panels. The failure strain value used in the aluminum panel modeling was established by running the numerical model for the flat aluminum panel with various values for the failure strain and comparing the numerical results to experimental ballistic impact results in the literature [Sun 1996]. As shown in Figure 3.2, the value that provided the best fit to the experimental data was $\varepsilon_f = 0.055$. This value was then kept constant for the numerical modeling of all remaining aluminum panel configurations.

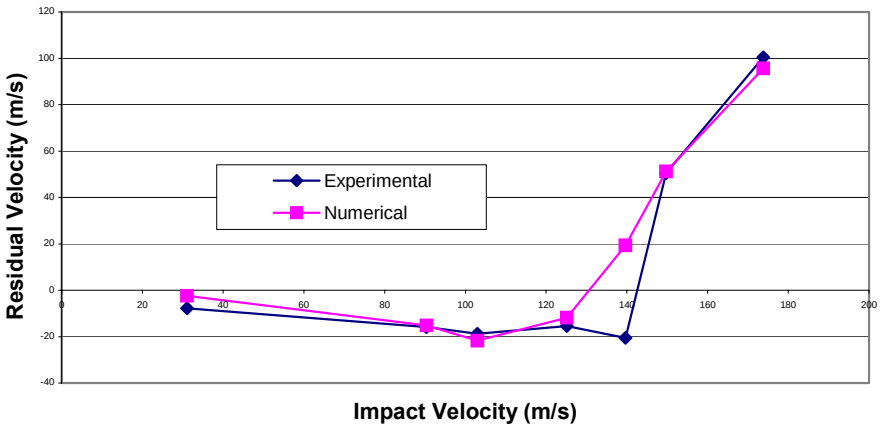

Figure 3.2 Comparison of numerical results, with a failure strain value of 0.055, to existing experimental data

The following radii of curvature were modeled: infinite (flat), 25-inch, 12-inch, 8-inch, 6-inch, and 4.4-inch. The numerical results for each configuration are presented in tabular form in Tables 3.4-3.9. The results from all of the configurations are shown together graphically in Figure 3.3. From a numerical standpoint, the results are consistent within the framework that has been defined. More detailed discussion of the numerical results and comparisons to experimental data will be addressed in the next chapter.

Table 3.4 Numerical results for ballistic impact of flat aluminum panels

Impact Velocity (in/sec)	Residual Velocity (in/sec)
5646	-1514
5690	-1552
5735	-1594
5896	-1407
5905	-1735
5925	-503
5950	-616
6000	1230
6100	857
6200	1238
6300	1636
6383	1807
6844	2981
8048	4951
9410	6659

Table 3.5 Numerical results for ballistic impact of 25-inch radius of curvature aluminum panels

Impact Velocity (in/sec)	Residual Velocity (in/sec)
5646	-1857
5690	-1787
5735	-1804
5896	-1804
5905	-1889
5925	-1808
5950	-1795
6000	-1803
6100	-1572
6200	971
6300	718
6383	1424
6844	2755
8048	4834
9410	6549

Table 3.6 Numerical results for ballistic impact of 12-inch radius of curvature aluminum panels

Impact Velocity (in/sec)	Residual Velocity (in/sec)
5646	-2515
5690	-2478
5735	-2439
5896	-2198
5905	-2159
5925	-2189
5950	-2122
6000	-2119
6100	-2111
6200	509
6300	281
6383	970
6844	2551
8048	4750
9410	6495

Table 3.7 Numerical results for ballistic impact of 8-inch radius of curvature aluminum panels

Impact Velocity (in/sec)	Residual Velocity (in/sec)
6100	-2437
6200	-2317
6300	-2351
6383	-1285
6400	-203
6500	286
6600	1165
6700	1676
6800	1996
6844	2209
8048	4569
9410	6312

Table 3.8 Numerical results for ballistic impact of 6-inch radius of curvature aluminum panels

Impact Velocity (in/sec)	Residual Velocity (in/sec)
6100	-2184
6200	-2168
6300	-921
6383	182
6844	2284
8048	4552
9410	6303

Table 3.9 Numerical results for ballistic impact of 4.4-inch radius of curvature aluminum panels

Impact Velocity (in/sec)	Residual Velocity (in/sec)
5646	-2095
5690	-2187
5735	-1922
5896	-1819
5905	-489
5925	374
5950	405
6000	315
6100	392
6200	955
6300	1511
6383	1786
6844	2833
8048	4817
9410	6481

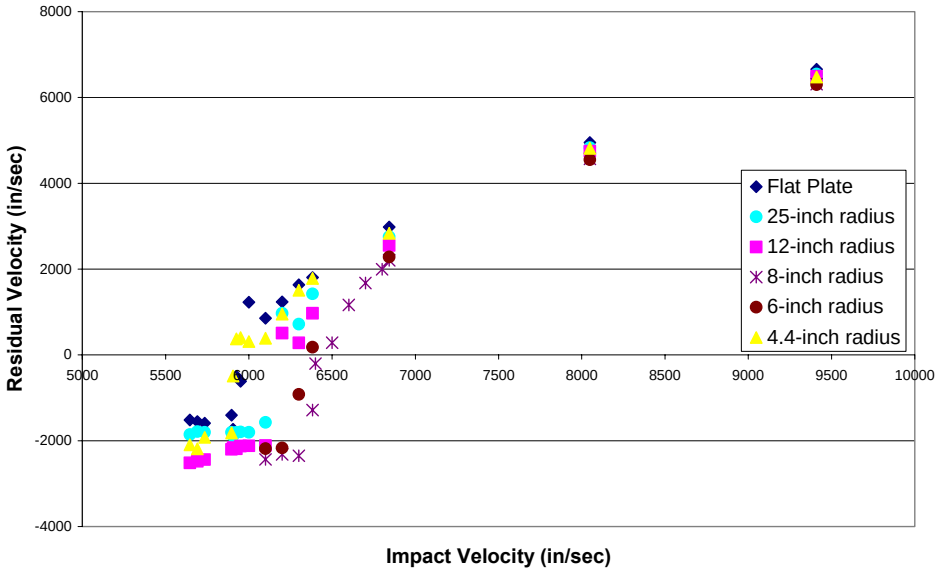

Figure 3.3 Modeled Ballistic Impact Response for Aluminum Plates with Different Radii of Curvature

3.4.2 Effect of Residual Stress on the Modeled Ballistic Impact Response

During the numerical analysis of the curved aluminum panels, one item of concern was whether or not the residual stress induced in the plates by the fabrication process had an effect on the impact response. It is known [Dieter,1986] that the rolling process used to form the curved panels results in residual stresses in the post-formed plate, but it was not known if these residual stresses were significant enough that they had to be taken into account during the modeling.

A numerical study was therefore performed to estimate the effect of residual stress on the ballistic response of the plates.

The maximum value which a residual stress can reach is the yield stress of the material. For an approximation, a residual stress equal to one-half of the yield stress was introduced into the material before impact. A linear distribution was used through the thickness with compression on the impact face and tension on

the rear face of the plate. It should be noted that the distribution of residual stress used in the simulation is not entirely representative of the residual stress distribution that would actually be present in the rolled plate. The residual stress system in a body must be in static equilibrium. Therefore, the total force acting on any plane through the body and the total moment of the forces acting on any plane must be zero. In this instance, the residual stress state imposed on the numerical model is not in static equilibrium. A more representative distribution would have been self-equilibrating, both through the thickness, and in the planes of the upper and lower surfaces. Note that the specified compressive residual stress on the impact surface is of greater magnitude, and is distributed over a larger area, than would normally be expected in practice. Despite not being mathematically correct, the prescribed residual stress distribution was deemed sufficient to estimate whether or not the presence of residual stresses would be a factor in the predicted ballistic response.

The results of the analysis are shown in Figure 3.4. Over the range of velocities of interest, the basic impact response trends remained the same. For velocities that resulted in predicted non-penetration of the plate, the residual stress does not appear to have any significant effect on the residual velocity of the projectile. In the ballistic limit region, for plates with the superimposed residual stress, the predicted residual velocity of the projectile is slightly below that predicted for plates with no residual stress. One possible explanation for this difference is that the material model simulates penetration by deleting elements after they have reached a threshold value of plastic strain. Therefore, for the same

projectile impact velocity, the effective plastic strain in the elements with the superimposed residual stress will differ from the elements that have no residual stress applied. The resulting change in the ballistic limit was an increase of less than three percent and it was concluded that the residual stresses due to rolling of the curved aluminum plates would not play a significant role in the predicted ballistic impact response.

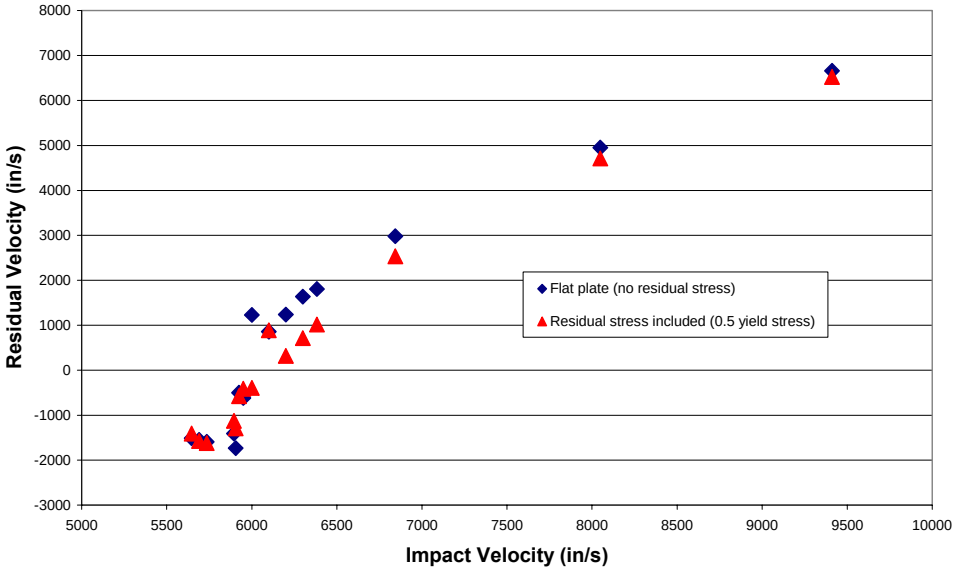

Figure 3.4 Effect of Residual Stress on Modeled Ballistic Impact Response of Aluminum Panels

3.4.3 Modeling the Ballistic Impact Response of Flat and Curved Composite Panels

One of the greatest benefits of composite material is the ability to tailor the material properties by varying how the composite laminate is layered. This through-thickness variation plays an important part in the overall performance and response of a component to external loads and can sometimes be of great importance in the numerical modeling of the response of a composite material. In this case, however, it seemed computationally inefficient to model the detailed

through-thickness properties of the laminate since micro-mechanical information, such as the stress distribution on a ply-by-ply basis, would not be compared to the experimental data. The use of an effective modulus to model the in-plane properties of the composite material was further justified by the fact that the composite laminate lay-up used for this research was specifically designed to provide quasi-isotropic material properties.

With these modeling simplifications adopted, an effective modulus for the composite laminate was initially derived using the rule of mixtures [Mallick,1993], whereby the material properties associated with the fiber material and matrix material are apportioned according to their respective volume fraction. The material properties and volume fractions for the graphite fibers and the matrix material are shown in Table 3.10. The effective modulus was then calculated from

$$E_{eff} = E_F * V_F + E_M * V_M \quad \textbf{(3.5)}$$

where E_F is the elastic modulus of the fiber material

E_M is the elastic modulus of the matrix material

V_F is the volume fraction of the fiber material

V_M is the volume fraction of the matrix material

Table 3.10 Material properties and volume fractions for graphite fiber and matrix material used to calculate the effective elastic modulus

E_F (psi)	V_F	E_M (psi)	V_M	E_{eff} (psi)
30×10^6	0.6	0.5×10^6	0.4	18.2×10^6

Similar to the aluminum panel modeling, a specified plastic failure strain value was used to facilitate the perforation process in the model. Again, the value used in the model, $\varepsilon_f = 0.066$, was determined by fitting the numerical modeling results for the flat composite panel to existing experimental data [Sun, 1996]. This value was then kept constant for the remaining composite panel configurations.

This initial effort at modeling the in-plane properties led to some significant differences between the model predictions and experiments. It was therefore necessary to perform additional experimental testing in order to resolve these modeling inconsistencies. Consequently, no results from the preliminary simulations of ballistic impact for the composite panels are presented in this chapter. A thorough discussion of the developments and results from iterative experimental testing and numerical modeling for the composite panels will instead be presented in its entirety in Chapter 4.

3.5 Chapter Summary

In this chapter, the numerical framework for simulating the ballistic impact of ½-inch diameter steel projectiles on flat and curved panels has been discussed. The finite element software and the process of developing the finite element model were described. Some of the more important topics, such as element size selection and the contact algorithm, were discussed in greater detail. Numerical results for the ballistic impact of aluminum panels were presented for six different panel curvatures. Numerical results for the ballistic impact of

composite panels were not presented due to issues associated with the modeling of the composite panels and the need to conduct additional experimental testing. These results will, instead, be presented in Chapter 4, in conjunction with a discussion of the experimental results.

Chapter 4 Discussion

4.1 Overview

In the previous chapters, the emphasis has been on reporting how the experimental and computational investigations were conducted and presenting the results that were obtained. Little or no attention was given to interpretation, discussion, and comparison of the results. In this chapter, the emphasis shifts to addressing the significance of the results and their implications for the objectives of this research.

A chronological overview is presented first that puts this research in context. This is followed by a more detailed discussion and a comparison of the experimental and numerical results. The overall objectives remain: (a) understanding the effects of panel curvature on the ballistic response of both aluminum and composite panels; and (b) establishing a framework for efficient, economical, and reliable simulations of ballistic impact events of this kind.

4.2 Chronological Development of the Research

Due to the high costs associated with experimental ballistic testing, the evolutionary development of the research presented here is similar to the approaches previously advocated by Zukas [1990] and Recht [1990]. Zukas noted that, "…the judicious combination of carefully controlled experiments, analytical models, and numerical simulations can lead to improvements in our understanding of impact physics and the development of improved models of material behavior at high strain rates." Recht adds that, "…a rewarding

evolutionary approach to developing models of the penetration processes is to iterate experiment and analysis."

Following in these footsteps, the research reported in this dissertation began with a desire to better understand the effects of curvature on the ballistic response of composite panels. As described previously in Chapter 2, these panels were fabricated from unidirectional composite sheets that were layered to yield quasi-isotropic material properties for the resulting 32-ply laminate. Experimental ballistic testing was conducted on curved composite panels of two different radii of curvature to identify the ballistic limits for each configuration and to obtain data regarding the residual projectile velocity for impact velocities that spanned a range from well below the ballistic limit to well above it. Similar information from ballistic impact studies of flat panels of the same laminate configuration had previously been conducted by Sun [1996].

The results showed that the ballistic limit increased as the curvature of the panel was increased. However, because the initial experimental investigation involved only two curvature configurations, the data was insufficient to support a hypothesis as to the type of relationship, in particular one that would hold for other curvatures as well. The high costs of experimental ballistic testing and material fabrication made it impractical to conduct an extensive series of tests on additional curvatures to further explore the relationship between panel curvature and the ballistic limit. Validated numerical modeling was therefore pursued as a cost-effective approach to satisfy the dual need for additional data and development of an improved understanding.

A building block approach, in which additional complexity was incorporated as simpler tasks were mastered, was followed for the numerical modeling effort. First, a series of analyses were performed, using LS-DYNA, that modeled the ballistic impact of 0.08 inch thick, flat panels with isotropic and homogeneous material properties representative of aluminum 2024-T3. Predicted residual projectile velocities were compared to experimental data previously reported by Sun [1996] with good results. The objective of this first effort was to demonstrate the viability of using commercial software, in this case LS-DYNA, to model the ballistic impact response.

The next step was to model the impact response of curved aluminum plates. Five panel curvatures were modeled, with two of the curvatures (a 12-inch radius of curvature and a 4.4-inch radius of curvature) matching the curvatures used in the earlier experimental testing on composite panels. The other curvatures were selected to provide intermediate information covering the progression from a flat (infinite radius of curvature) panel to a highly curved (4.4-inch radius of curvature) panel.

Preliminary results from the numerical modeling appeared reasonable but could not be verified due to the absence, in the literature, of existing ballistic impact data for curved aluminum panels. Two key insights emerged from the preliminary numerical modeling: 1) The relationship between panel curvature and ballistic limit was found to be parabolic rather than monotonic in nature; and 2) this parabolic nature suggested the existence of an optimal panel curvature for maximizing the ballistic limit. The need to validate the numerical modeling, and

to further explore these two insights, led to a decision to undertake experimental ballistic testing of curved aluminum panels.

Flat aluminum (2024-T3) panels and panels with three sets of curvatures were fabricated for testing. Two of the curvatures, a 12-inch radius of curvature and a 4.4-inch radius of curvature, matched the previously tested composite panels. The third curvature, an 8-inch radius of curvature, was chosen based on the predictions from the numerical analysis, which indicated an optimal radius of curvature of approximately 8 inches for maximizing the ballistic limit.

The data collected during the earlier experimental testing of the composite panels provided only the impact and residual velocities of the projectile. In an effort to also quantify the dynamic response of the panel, high-speed video was incorporated into the experimental setup. Digital image correlation software was then used to obtain dynamic displacement information at various points on the surface of the impacted panel. These measurements were used to further validate the numerical modeling of the impact response by comparing the predicted panel response to the observed experimental data at these specific locations. When the aluminum panel testing was completed, repeat tests of several flat and curved composite panels were conducted to obtain dynamic material response data utilizing the high-speed video analysis system. This data provided additional comparisons between the observed composite panel response and the results from numerical predictions.

Good agreement was obtained between the experimental results and the numerical predictions for both flat and curved aluminum panels. The focus of the

investigation then shifted towards the more complex task of modeling the ballistic impact of flat and curved panels fabricated from composite laminates. Because of the quasi-isotropic nature of the composite panels, it seemed reasonable to model the composite laminate material properties using the rule of mixtures [Mallick,1993]. In this approach, the material properties associated with the fiber material and matrix material are apportioned according to their respective volume fraction to obtain effective material properties. The initial results using this approach showed poor agreement in both the displacement magnitude and response time between the experimental data and the numerical predictions. This, in turn, generated questions regarding the validity of the assumed composite material properties and the impact of these assumed values on the results obtained from the numerical model.

To resolve these questions, ballistic impact tests were conducted on strain-gage-instrumented composite panels to determine the wave propagation characteristics of the laminates and, hence, to infer the effective material properties. These experiments showed that the initial approach for modeling the composite material properties using the rule of mixtures (and the associated wave speed that was calculated from these properties) was not appropriate for this application. The effective modulus derived from the wave speed measurements was significantly lower than the effective modulus calculated using the rule of mixtures. The resulting "flexural-wave-based effective elastic modulus" that was inferred from the experimental data was therefore adopted for the numerical modeling and the analyses were repeated. This change resulted in good

agreement between the experimental results and the numerical analyses. With this issue satisfactorily laid to rest, attention turned to the failure analysis of both the composite and aluminum panels.

This chronological overview was provided to place the complete research path in perspective for the reader. The sections that follow will revisit some of the areas above in more depth and the significant results will be presented and discussed.

4.3 Effect of Panel Curvature on the Ballistic Impact Response

4.3.1 Introduction

At its inception, the objective of this research was to explore and identify the effects of panel curvature on the ballistic impact response of composite laminates. Material specifications, test set-up, test procedures, and the results have been previously reported in Chapter 2. This section provides a more in-depth discussion of the results obtained and summarizes the key findings.

4.3.2 Ballistic Impact Response of Composite Panels with Different Radii of Curvature

The individual ballistic curves that were constructed from the experimental testing of the 12-inch radius of curvature and 4.4-inch radius of curvature composite laminates were shown in Chapter 2. Experimental ballistic impact results for flat (infinite radius of curvature) composites laminates were previously reported by Sun [1996] and are included here for comparison purposes. Ballistic curves consolidating these experimental results are shown in Figure 4.1.

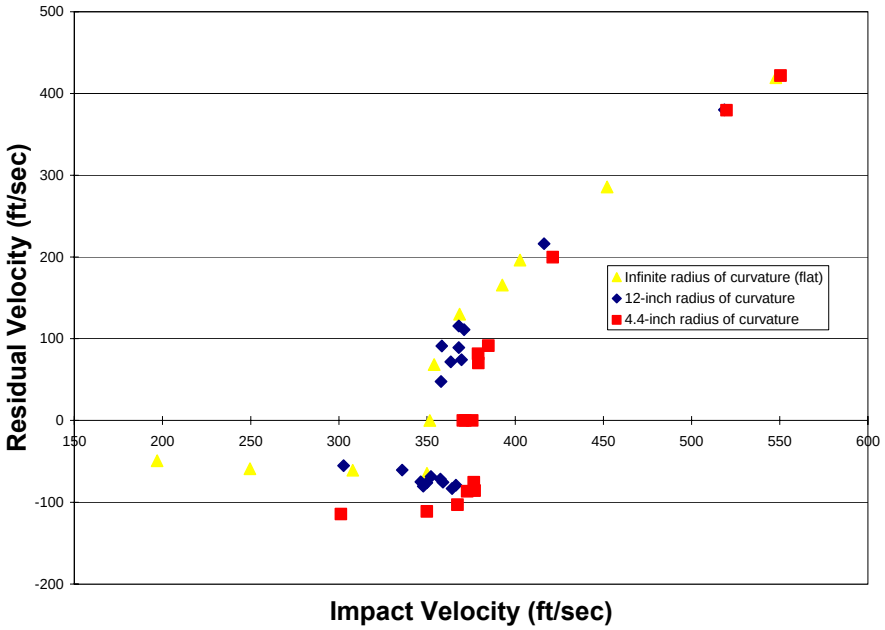

Figure 4.1 Ballistic curves of composite panels with three different radii of curvature

The consolidation of all the experimental data into a single graph facilitates a visual comparison of the ballistic impact response for the three different configurations. The most noteworthy effect of curvature is the increase in the ballistic limit as the radius of curvature of the panel is decreased.

Figure 4.2 shows an enlarged view of the data from the transition region of the ballistic curves shown in Figure 4.1. The points used in defining the ballistic limit for each configuration are highlighted. It should be noted that due to experimental scatter and the prescribed definition of the ballistic limit, an overlap in the transition from rebound to penetration events, as shown for the 12-inch radius of curvature configuration in Figure 4.2, can result in the ballistic limit being calculated using an impact velocity from a rebound event that is greater

than the lowest impact velocity that results in penetration of the target. Also note that there are three points for the 4.4-inch radius of curvature configuration, and one point for the infinite radius of curvature configuration, that lie on the x-axis. These points, representing zero residual velocity for the projectile, correspond to tests in which the projectile became embedded in the panel. By virtue of the definition, these points are not used in the calculation of the ballistic limit.

Figure 4.3 shows the experimentally determined ballistic limit for each configuration (a space is shown for an 8-inch radius of curvature configuration for future comparison purposes) and the increase in the ballistic limit with a decrease in the radius of curvature is clear.

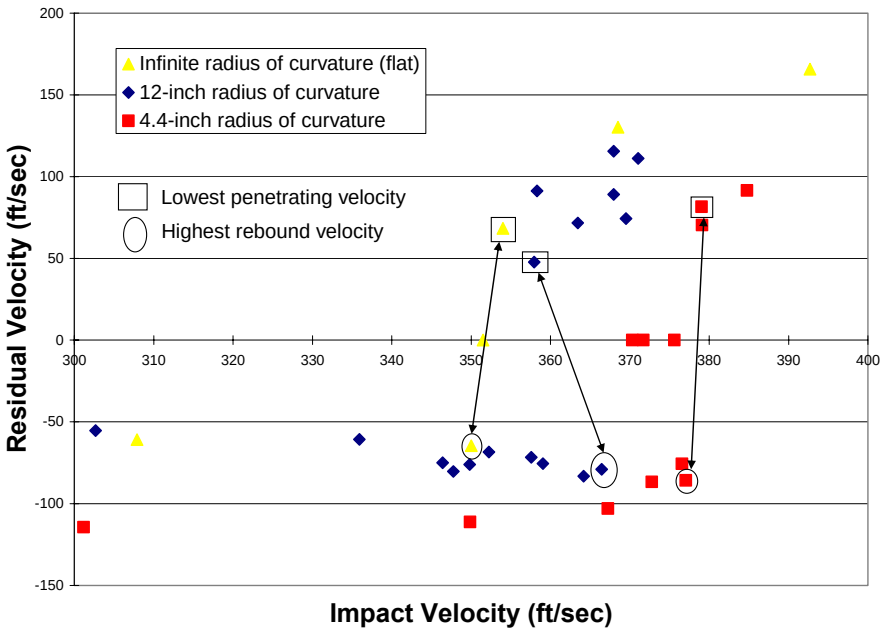

Figure 4.2 Enlarged view of the ballistic limit region for the data shown in Figure 4.1. The data used to calculate the ballistic limit are highlighted.

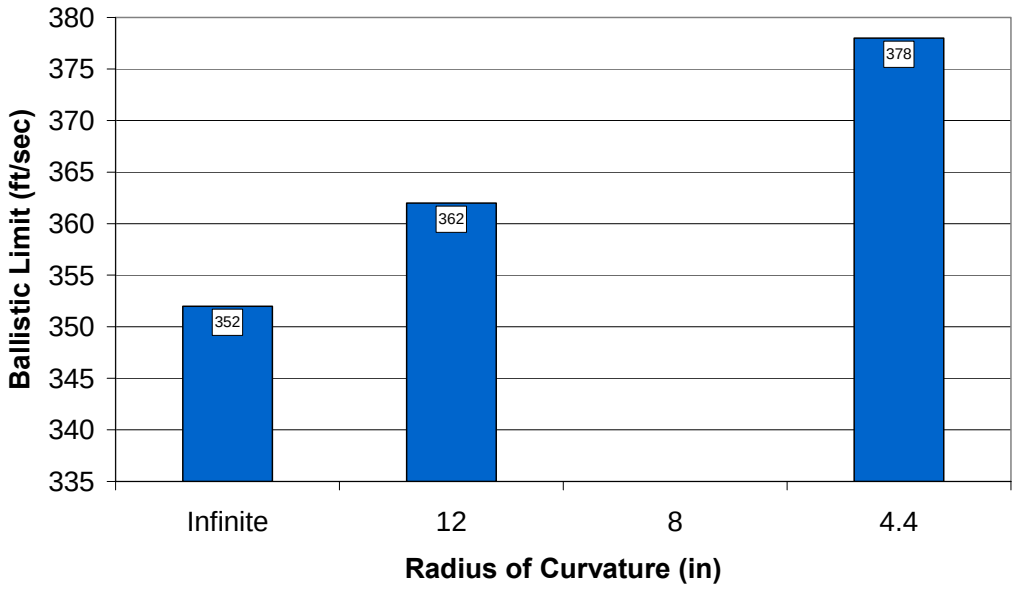

Figure 4.3 Measured ballistic limit for composite panels

While the experimental data for the composite panels could be interpreted as showing that the ballistic limit increases monotonically with decreasing radius of curvature, this cannot be conclusively stated due to the limited number of curvatures tested. Ideally, testing of additional curvatures would provide additional insights and more thoroughly explore the relationship between panel curvature and the ballistic limit. However, as discussed previously, the high costs associated with extensive experimental ballistic testing made this approach impractical and numerical modeling of the ballistic impact event was therefore pursued as a cost-effective approach to gaining additional insight into the effects of panel curvature. This was done first for curved aluminum panels and then for composite laminates.

4.3.3 Numerical Modeling of the Ballistic Impact Response of Curved Aluminum Panels

Models were created that were representative of five panel curvatures ranging from slightly-curved to highly-curved. The specific radii of curvature modeled were a 25-inch radius of curvature, a 12-inch radius of curvature, an 8-inch radius of curvature, a 6-inch radius of curvature, and a 4.4-inch radius of curvature. Two of these radii of curvature (R=12 inches and R=4.4 inches) were selected to match the curvatures of the composite panels that had already been tested experimentally. Figure 4.4 provides a visual comparison of the five panel curvatures.

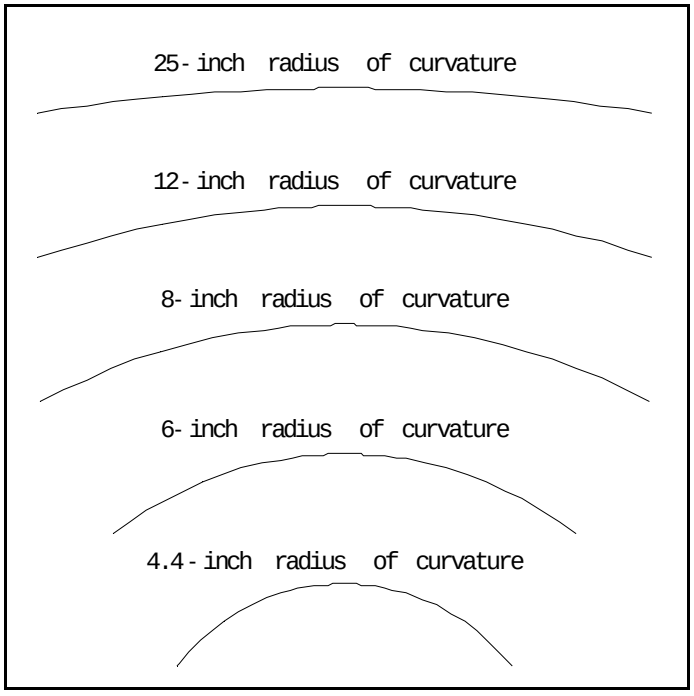

Figure 4.4 Comparison of the five aluminum panel curvatures modeled numerically

Ballistic curves for each curvature were generated by repeating the finite element analyses with different specified impact velocities spanning the range of interest. The resulting ballistic curves are shown in Figure 4.5. The ballistic limit for each radius of curvature was calculated and the results are shown in Figure 4.6.

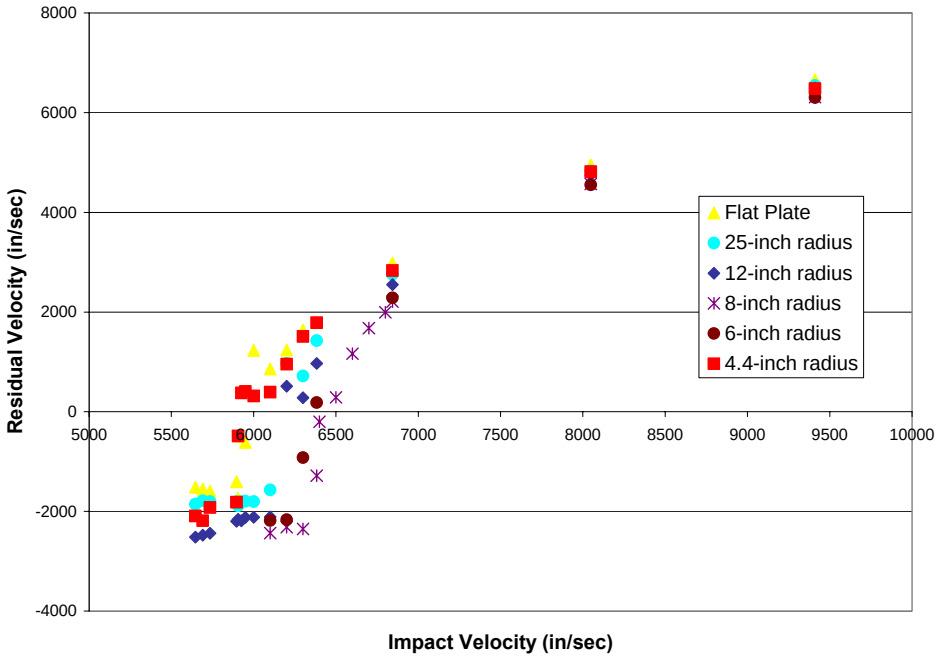

Figure 4.5 Numerically determined ballistic curves for aluminum panels with varying radii of curvature

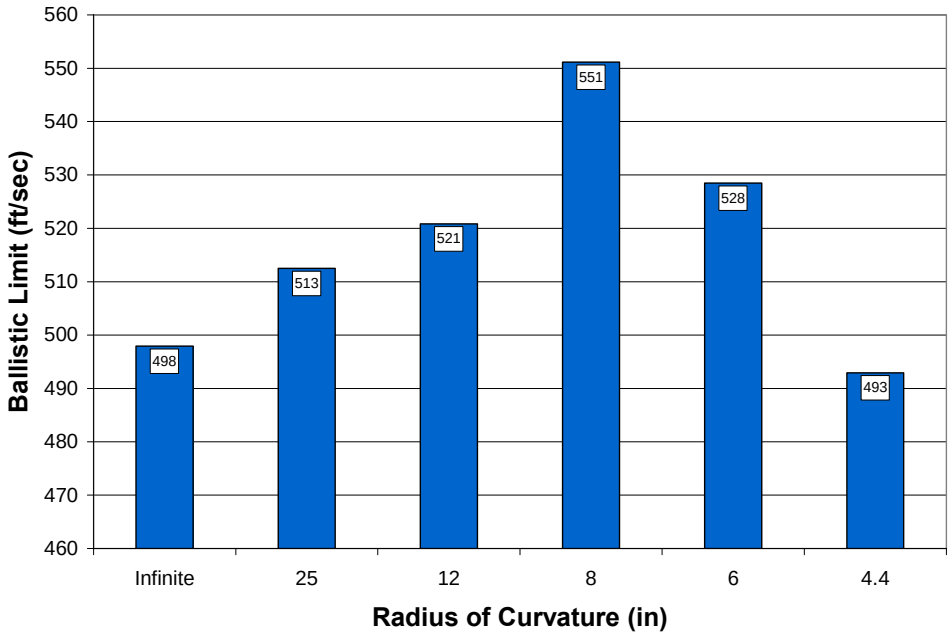

Figure 4.6 Numerically determined ballistic limits for aluminum panels with varying radii of curvature

These numerical results indicate that the relationship between panel curvature and the ballistic limit is not monotonic, as previously suggested by the experimental results from the composite panels, but is actually parabolic in nature. The parabolic nature of this relationship further suggests that there is an optimal value for panel curvature that results in a maximum ballistic limit. The numerical and experimental results, however, involve two rather different sets of material (aluminum vs. composite) and, as such, it would be premature to state that the identified ballistic limit-curvature relationship is solely a manifestation of geometry, and therefore valid regardless of material. Continuing with the iterative approach advocated earlier, experimental ballistic testing of curved aluminum panels was conducted to validate the numerical modeling results.

4.3.4 Experimental Investigation of the Ballistic Impact Response of Curved Aluminum Panels

Details describing the experimental test set-up, test specimen fabrication, and experimental test procedure were previously discussed in Chapter 2. The individual ballistic curves that were constructed from the experimental testing of the flat (infinite radius of curvature), 12-inch radius of curvature, 8-inch radius of curvature, and 4.4-inch radius of curvature were also shown in Chapter 2. Ballistic curves containing the experimental results from all four of the different aluminum panels tested are shown in Figure 4.7.

Again, the consolidation of all the experimental data into a single graph facilitates a visual comparison of the ballistic impact response for the four different configurations. The calculated ballistic limits for the aluminum panels are shown in Figure 4.8. The experimental results also show that the ballistic limit increases as the radius of curvature is decreased from infinity to 8 inches. Further decrease of the radius of curvature to 4.4 inches resulted in a lower ballistic limit. These results agree qualitatively with the results from the numerical analysis and provide experimental validation supporting the existence of an optimal radius of curvature for maximizing the ballistic limit.

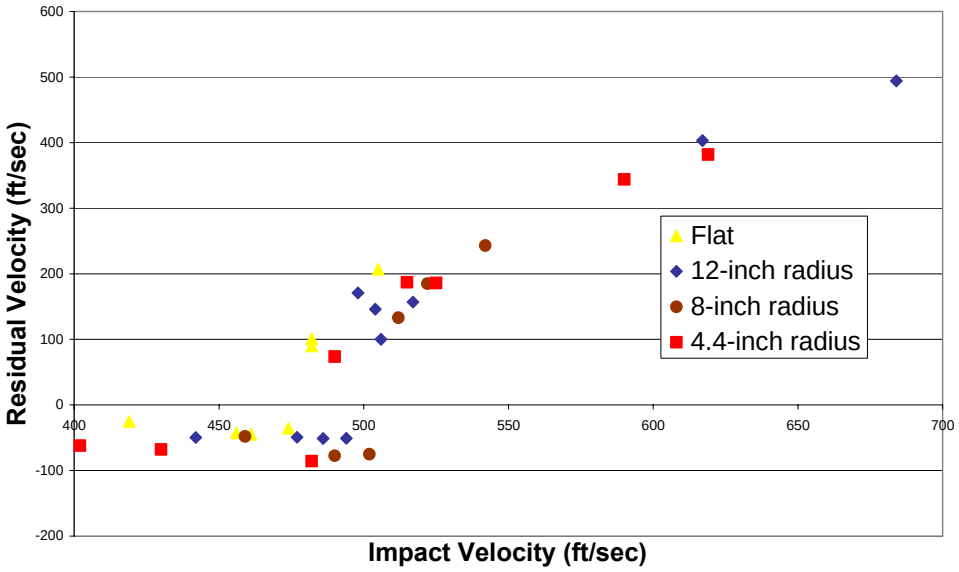

Figure 4.7 Experimentally-determined ballistic curves for aluminum panels with four different radii of curvature

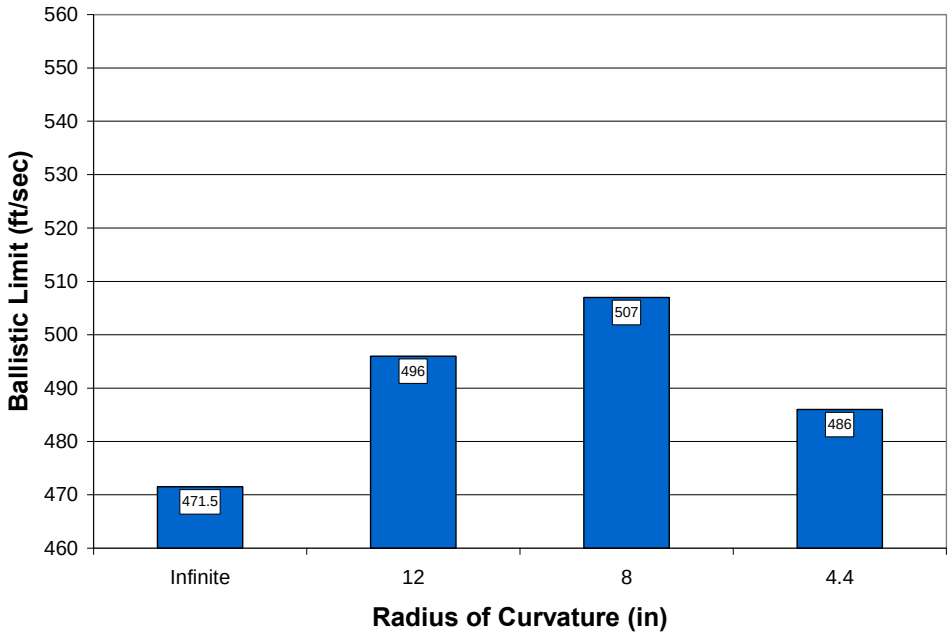

Figure 4.8 Experimentally-determined ballistic limits for aluminum panels with four different radii of curvature

4.3.5 Comparison of Predicted Ballistic Response with Experimental Results

Numerical modeling of the ballistic impact response of curved aluminum plates was presented in Section 4.3.3. These results are revisited here in conjunction with the experimental data of Section 4.3.4 in order to show the agreement between the two. It should be noted that numerical modeling offers many variables that can be varied in order to achieve better agreement with experimental results. In this effort, representative material properties for aluminum 2024-T3 were utilized in the modeling and the only variable allowed to vary for the purpose of model fitting was the threshold value for the failure criterion. Once a suitable value was obtained, this parameter was kept constant for each configuration. This was viewed as a valuable measure of how well the software modeled the actual impact event. Good agreement was found for all of the curvatures. Figures 4.9, 4.10, 4.11, and 4.12 show comparisons of the numerical and experiment results for the ballistic response for the flat (infinite radius of curvature), 12-inch radius of curvature, 8-inch radius of curvature, and 4.4-inch radius of curvature aluminum panels, respectively.

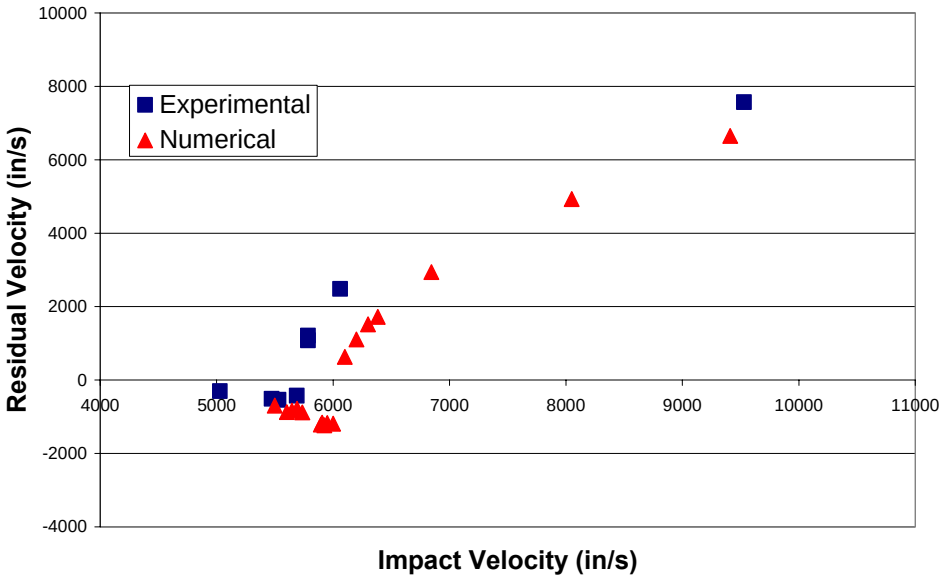

Figure 4.9 Comparison of experimental and numerical ballistic response for flat aluminum panels

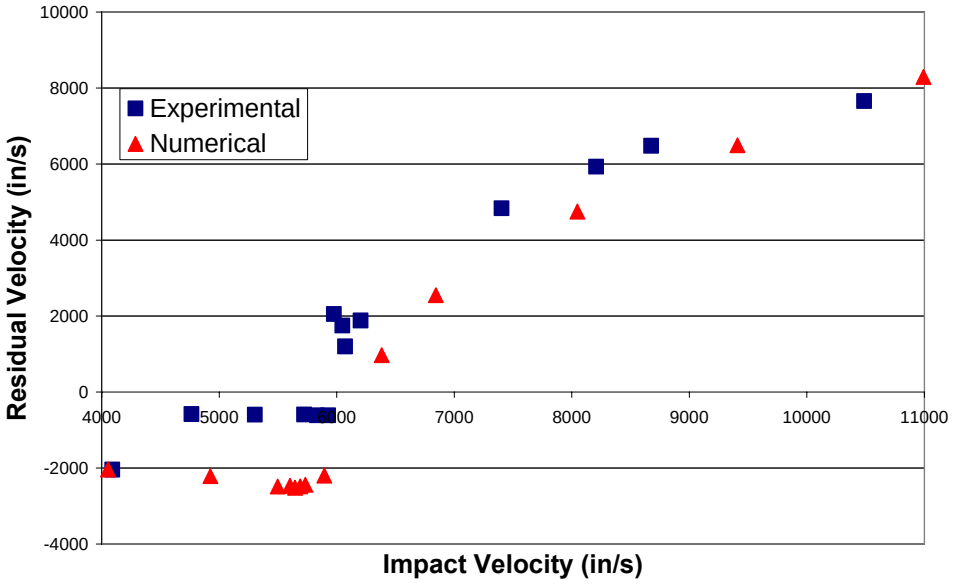

Figure 4.10 Comparison of experimental and numerical ballistic response for 12-inch radius of curvature aluminum panels

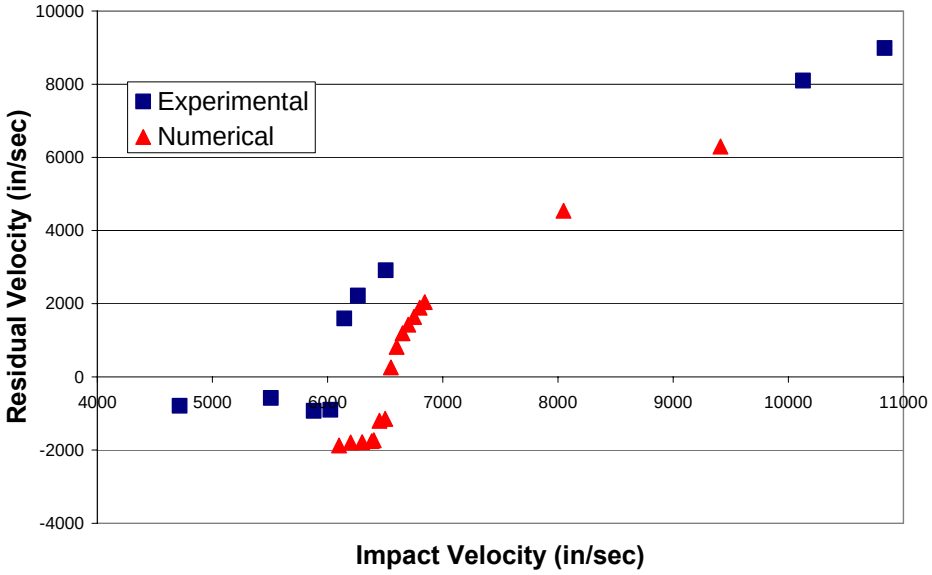

Figure 4.11 Comparison of experimental and numerical ballistic response for 8-inch radius of curvature aluminum panels

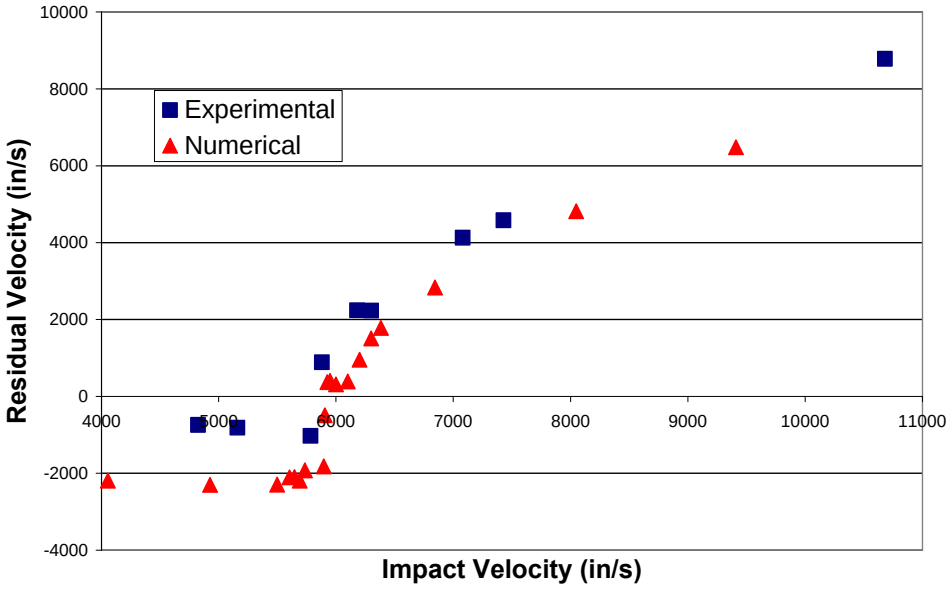

Figure 4.12 Comparison of experimental and numerical ballistic response for 4.4-inch radius of curvature aluminum panels

4.3.6 Further Validation of the Numerical Modeling of Ballistic Impact of Aluminum Panels

The experimental ballistic response data used to validate the numerical modeling effort consisted solely of information related to the initial and residual velocity of the projectile. Given the objective of extending the numerical modeling approach to model the composite panels, the accurate representation of the panel response to ballistic impact was a primary concern. High-speed video and digital image correlation analysis of the video-graphic records was therefore incorporated into the experimental procedure to provide dynamic displacement measurements at various points on the impacted panels. These measurements were used to further validate the numerical modeling by comparing the predicted panel response to the observed experimental data at specific locations. The high-speed video system utilized to capture this information was described in Chapter 2. A representative case is presented here for discussion.

4.3.7 Dynamic Deformation Measurement of Aluminum Panel Response to Ballistic Impact

The dynamic deformation of a 12-inch radius of curvature aluminum panel resulting from an impact by a 1/2-inch diameter steel sphere with an initial velocity of 397 ft/sec is presented. A dot-grid system was placed on the panel prior to impact to provide reference points for tracking in the digital imaging software. Two high-speed Phantom™ cameras were used to digitally capture the impact event. Prior to capturing the impact event, the relative locations of the cameras were determined by photographing a calibration specimen (the

calibration specimen contains reference markers at known locations and is used in the digital imaging software to calibrate each of the high-speed cameras).

After calibration was complete, the cameras were used to capture the impact event. The image sequences from the impact event were loaded into the digital image software package and viewed simultaneously. At each time step, the reference tracking points from the dot-grid system on the panel were identified for each camera view. By combining the calibrated camera information with the identified reference tracking points, the digital imaging software was able to calculate the three-dimensional coordinate data for each of the reference tracking points. This step was repeated for each additional time step and resulted in a time-history progression of the coordinate data for each of the reference tracking points.

This information was then recast as dynamic displacement data by subtracting the pre-impact event coordinates of each reference point. Dynamic displacement data was recorded for six reference tracking points. A limited viewing area and the obstruction of points by the traveling projectile restricted the number of reference tracking points available for the entire duration of the impact event. The relative locations of the tracked points with respect to the impact location are shown in Figure 4.13. The out-of-plane dynamic displacement data for the six points are shown in Figure 4.14.

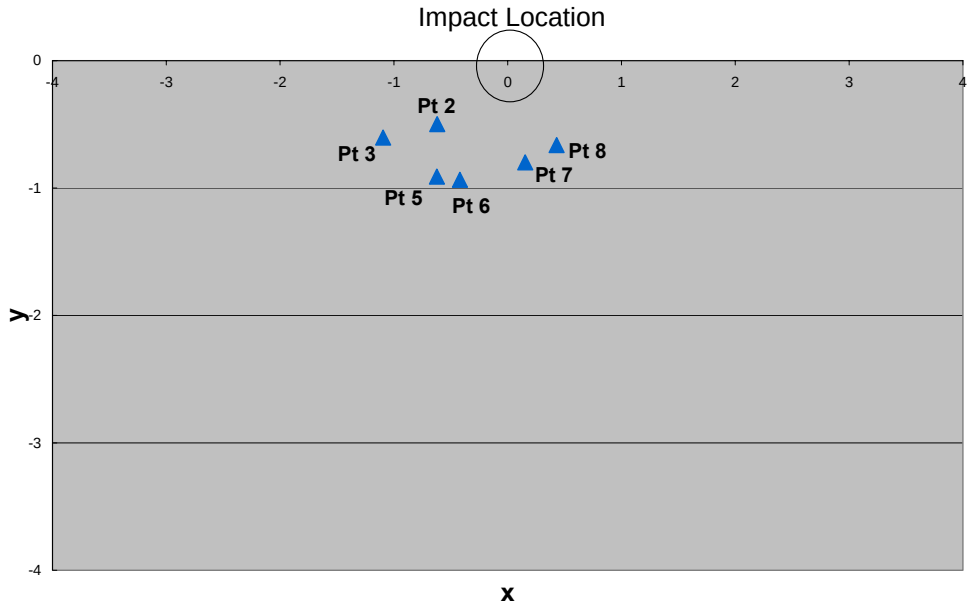

Figure 4.13 Locations of tracked points for 397 ft/sec projectile impact on a 12-inch radius of curvature aluminum panel (only the bottom half of the panel is shown)

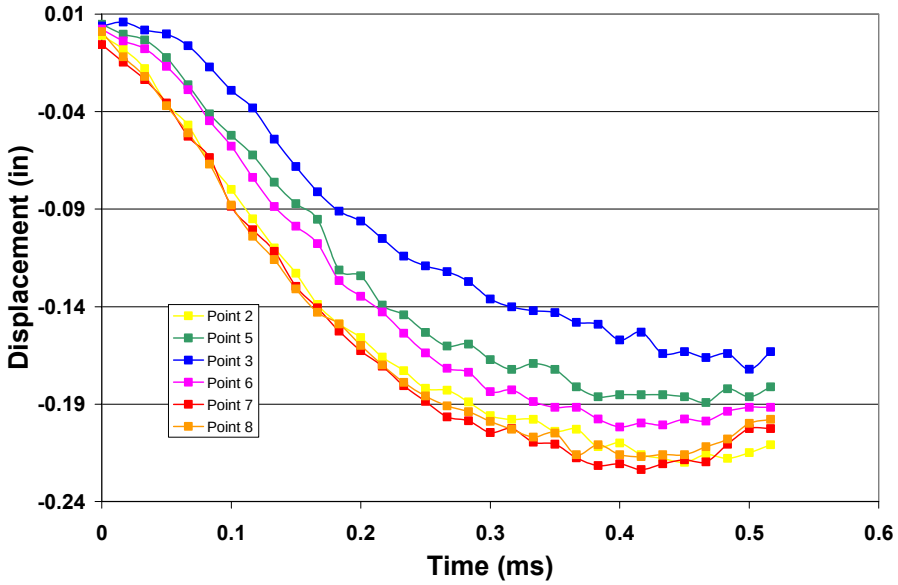

Figure 4.14 Experimental out-of-plane dynamic displacement data for selected points on a 12-inch radius of curvature aluminum panel impacted by a ½-inch diameter steel sphere at 397 ft/sec

4.3.8 Comparison of Predicted Aluminum Panel Response with Experimental Dynamic Displacement Data

The initial coordinates of the six tracked points were determined from the image analysis software prior to the impact event. This coordinate data was used to identify the element in the numerical model that would best match the experimental tracking locations. The out-of-plane nodal displacement data was extracted for each of the four nodes of the element that contained the tracked point. The results were then averaged to provide data for comparison to the experimental measurements. No changes were made to the variables of the numerical model.

The predicted panel response is shown in Figure 4.15. The calculated results from the image analysis software (previously shown in Figure 4.14) are presented again in Figure 4.16 for easier comparison. The predicted panel response agrees well with the image-analysis-calculated panel response in terms of magnitude and time-sequencing of the displacement data. The maximum out-of-plane displacements for each tracked point are shown in Table 4.1, and the results for five of the six points are within ten percent of the values calculated from the video-graphic images. The results for four of the six tracked points are within five percent of their predicted values indicating that the numerical model is accurately capturing the dynamic response of the aluminum panels to ballistic impact.

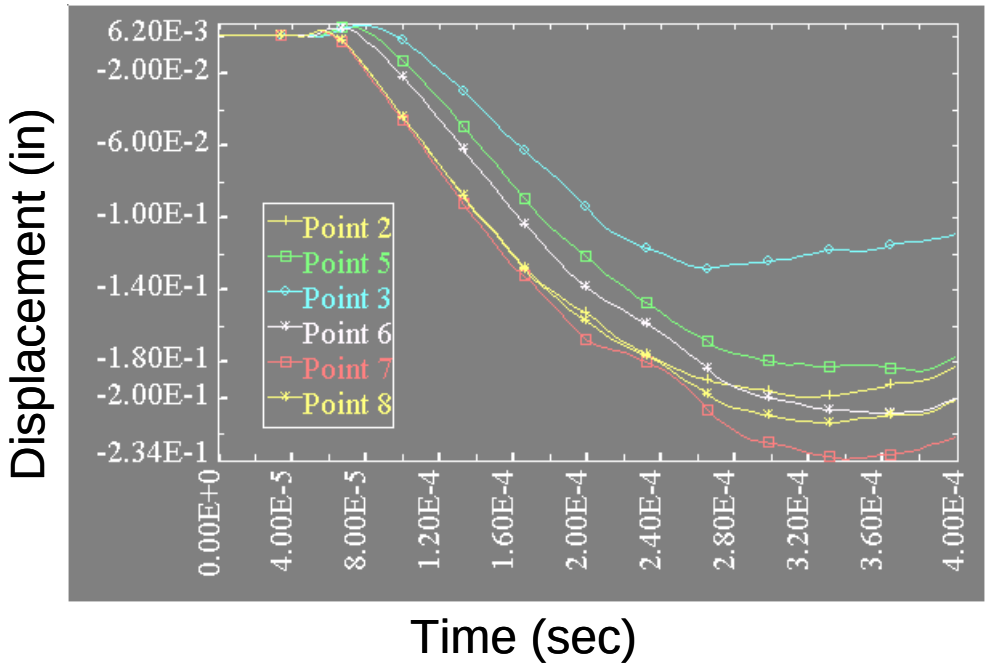

Figure 4.15 Predicted out-of-plane displacements for selected points on a 12-inch radius of curvature aluminum panel impacted by a ½-inch diameter steel sphere at 397 ft/sec

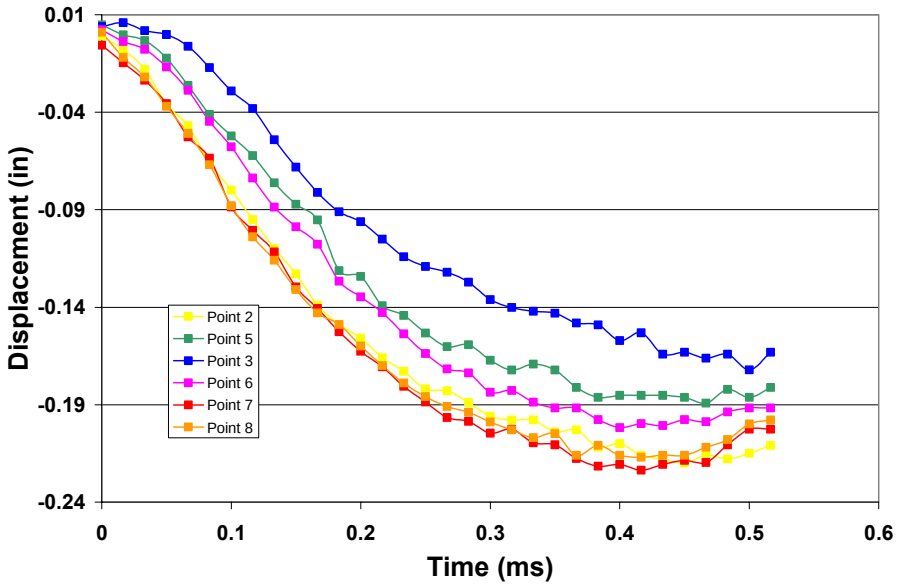

Figure 4.16 Experimental out-of-plane displacement data for selected points on a 12-inch radius of curvature aluminum panel impacted by a ½-inch diameter steel sphere at 397 ft/sec

Table 4.1 Maximum out-of-plane displacement values at tracked locations for numerical predictions and experimental observations of ballistic impact on an aluminum panel

POINT #	LS-DYNA max displacement (in)	Experimental max displacement (in)	Percent difference
2	-0.200	-0.220	9.5%
3	-0.129	-0.172	29%
5	-0.186	-0.189	1.6%
6	-0.209	-0.202	3.4%
7	-0.234	-0.224	4.4%
8	-0.215	-0.216	0.5%

4.3.9 Summary of the Effect of Panel Curvature on the Ballistic Impact Response

In this section, the relationship between panel curvature and ballistic limit has been examined. Initial experimental data from ballistic impacts on composite panels verified the existence of a curvature effect, but the number of curvatures examined was insufficient to fully quantify the relationship. Additional experimental and numerical studies of ballistic impact on curved aluminum panels were conducted to further explore the relationship between panel curvature and the ballistic limit. These results showed that the relationship between panel curvature and the ballistic limit was parabolic in nature, suggesting that there exists an optimal panel curvature with respect to maximizing the ballistic limit of the panel. The numerical modeling utilized a single parameter, the plastic failure criterion, for model fitting. Once this was established from preliminary analyses on a given material, it was left unchanged for all subsequent analyses. The

detailed results agreed well with the experiments. Additional validation of the numerical model was accomplished by comparing the predicted response of the panel with experimentally-determined dynamic displacement measurements at selected locations during ballistic impact events.

In the next section, developments associated with the more complex task of modeling the ballistic impact of composite panels are addressed.

4.4 Development of a Flexural-Wave-Based Effective Elastic Modulus Concept for the Modeling of the Ballistic Impact of Curved Composite Panels

4.4.1 Introduction

It was pointed out previously (in Chapter 3) that there were uncertainties associated with the appropriateness of a "rule-of-mixtures" formulation for defining the effective material properties needed to model the ballistic impact event in composite laminate panels. There were also concerns about the through-thickness (shell element) modeling simplification that had been used. A logical next step was to first validate the predicted panel response from the numerical modeling against experimental data. The high-speed video system and the digital image analysis software were therefore used to make dynamic displacement measurements on a flat composite panel impacted by a ½-inch diameter steel sphere traveling with an initial velocity of 322 ft/sec.

The experimentally-derived out-of-plane displacements for several selected points on the surface of the flat composite panel are shown in Figure 4.17. The initial comparison to the predicted panel response from the numerical

analysis was not favorable. The predictions of both the magnitudes of the displacements and the time-sequencing of when the maximum displacements occurred were significantly different from the observed experimental values. The magnitudes of the predicted maximum displacements were approximately half of the experimental values and the maximum displacements were achieved at significantly earlier times than seen experimentally.

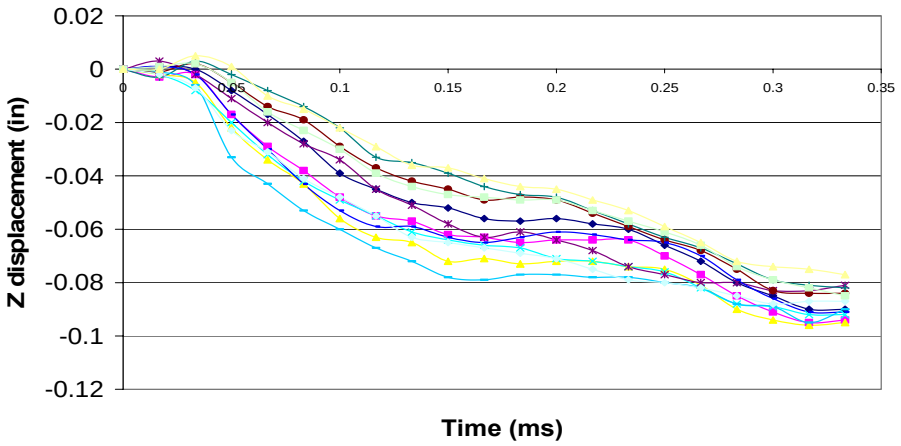

Figure 4.17 Experimentally-derived out-of-plane displacements for selected points on the surface of a flat composite panel undergoing ballistic impact at 322 ft/sec

4.4.2 A Flexural-Wave-Based Effective Elastic Modulus Approach

It was hypothesized that both of these differences between computational predictions and experimental observations were related to the effective modulus value used in the numerical modeling. Reducing the value of the effective elastic modulus in the model was therefore explored as a way to bring the predicted numerical displacements into better agreement with the experimental data.

There were two underlying reasons supporting this line of thought. First, the elastic modulus is directly proportional to the flexural rigidity of the material.

A reduction in this parameter would reduce the stiffness of the panel and increase the predicted magnitude of the out-of-plane displacements resulting from a transverse impact. Second, the stress wave velocity is also directly proportional to the elastic modulus of the material. In the numerical model, the prescribed stress wave velocity determines the speed at which a disturbance is propagated from one node to the next. Reducing the elastic modulus would therefore result in a slower stress wave velocity, which would in turn, also slow down the response of the panel to the external disturbance.

A reduced value for the elastic modulus (0.8×10^6 psi instead of 18.2×10^6 psi) was input into the numerical model and the analysis was performed again (all other impact parameters remained unchanged). The numerical results obtained using this reduced effective elastic modulus and the original effective elastic modulus are compared in Figure 4.18. These results support the earlier hypothesis that use of a reduced elastic modulus in the numerical model would both increase the magnitude of the calculated out-of-plane displacements and slow down the panel response.

If the objective were to simply obtain better fitting data, one could continue arbitrarily adjusting the value used for the elastic modulus in the numerical modeling. A more sound approach is to experimentally explore the question of what is the most appropriate value of the elastic modulus to specify in numerical modeling efforts of this kind. This would provide a technical justification for specifying a particular value of the elastic modulus for use in the numerical model. More importantly, guidance would be available for future

investigators on how best to achieve the goal of reliable and accurate predictions of ballistic impact events involving composite structures. The path followed and the results obtained are described in the following section.

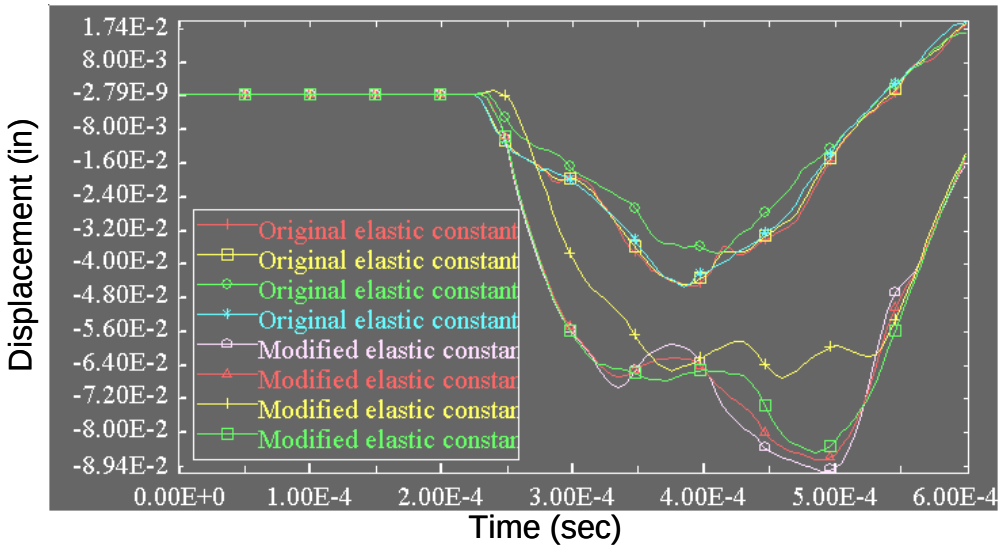

Figure 4.18 Comparison of numerically-predicted out-of-plane displacements for a model using an effective elastic modulus and a model using a reduced effective elastic modulus

4.4.3 Further Investigation and Validation of a Flexural-Wave-Based Effective Elastic Modulus Approach

While the results discussed above suggested that a reduced effective modulus should be used, there was no readily-available physical justification for its use. A series of strain-gage instrumented composite panels were therefore subjected to ballistic impact in an effort to measure the flexural wave speed in the composite material. The purpose of these tests was to obtain an estimate for the effective elastic modulus from the measured flexural wave speed for comparison against the values that had been used in the numerical modeling.

Six strain gages, three on the front face and three on the rear, were mounted on a flat composite panel that was subsequently subjected to a ballistic

impact. The strain gages were CEA-13-062UW-350 manufactured by Micro-Measurements Division, Raleigh, NC. The locations of the three gages on the front face are shown in Figure 4.19. The gages on the front face were given the designations SG1, SG2, and SG3. The gages on the rear face were placed directly opposite the three gages on the front face and were given the designations SG4, SG5, and SG6.

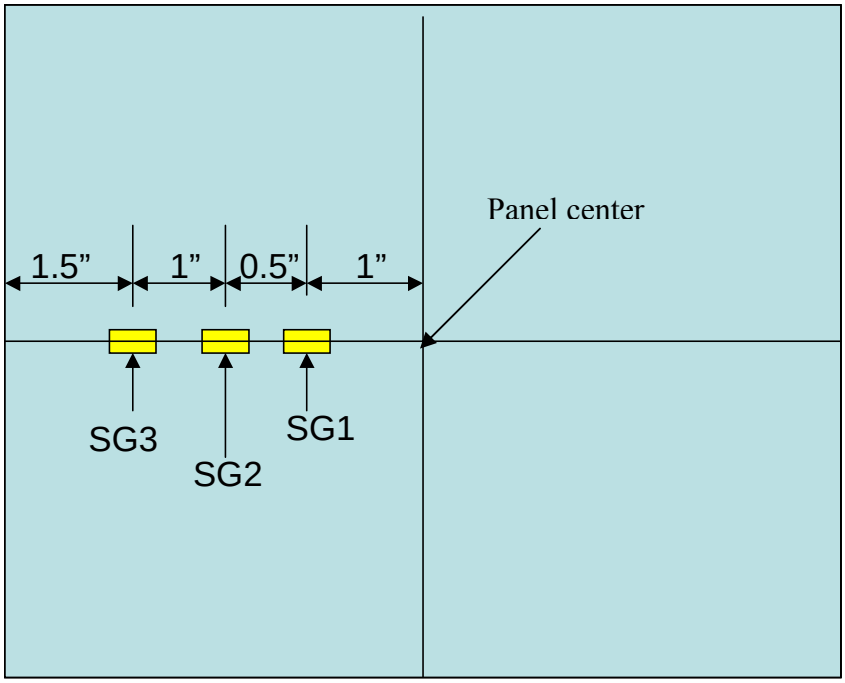

Figure 4.19 Front-view of strain gage locations on a flat composite panel.

With this notation, the pairing of front and rear gages was as follows: SG1-SG4, SG2-SG5, and SG3-SG6. The placement of gages on the front and rear surface was designed to isolate the response associated with panel bending. This was accomplished by subtracting the response of the front surface gage from the response of the counterpart gage located directly opposite and on the rear surface. Contributions of in-plane effects to the strain gage response would be of the same sign on both the front and rear surfaces and would therefore be canceled out when

the signals from the pairs of front and rear face gages were subtracted from one another. However, strain contributions due to bending would be of opposite sign and would remain after the subtraction operation.

The strain gage located closest to the impact location, SG1, failed at the onset of the impact event and no results were obtained for the first strain gage pair, SG1-SG4. The responses from the remaining strain gage pairs are shown in Figures 4.20 and 4.21. Figure 4.20 shows the individual strain gage response from SG2 and the gage located directly on the opposite side, SG5. Figure 4.21 shows the same type of information for SG3 and SG6. The strain gages were not individually calibrated and, as a result, the amplitudes of the voltage responses may vary.

Recall that the gages are located directly opposite one another on the front and rear faces of the plate. Similar signals (with a corresponding sign difference) would therefore be expected, as seen in Figure 4.21 for the strain gage responses from SG3 and SG6. However, this is not the case for SG5 in Figure 4.20. This suggests that SG5 failed shortly after the impact event. This failure does not affect the leading edge of the signal but it does cause distortions in the rest of the curve. The subtraction operation was performed for each strain gage pairing and the resultant paired responses, SG2-SG5 (2^{nd} set) and SG3-SG6 (3^{rd} set), are shown in Figure 4.22. Ideally, the amplitudes of the two curves should be similar. The lower amplitude at the beginning of the SG2-SG5 resultant curve is attributed to the failed strain gage (SG5).

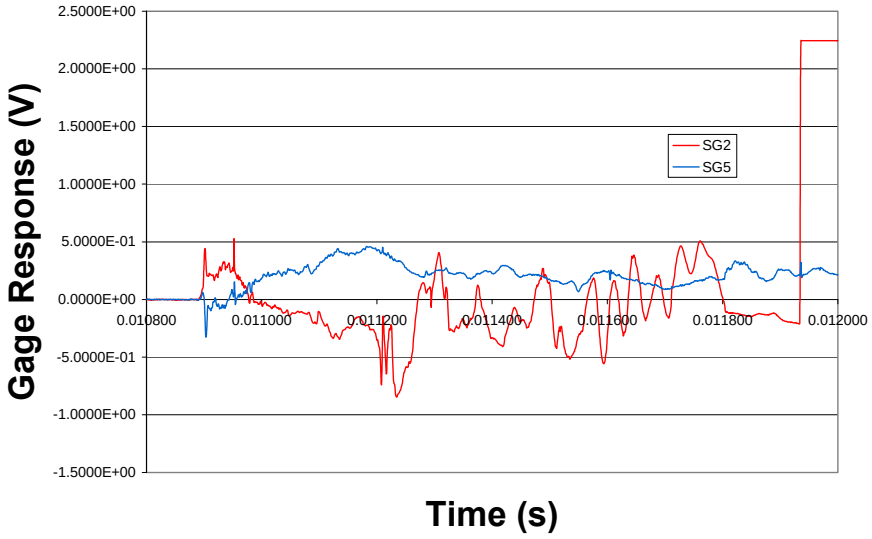

Figure 4.20 Strain gage responses for strain gage pairs SG2 and SG5

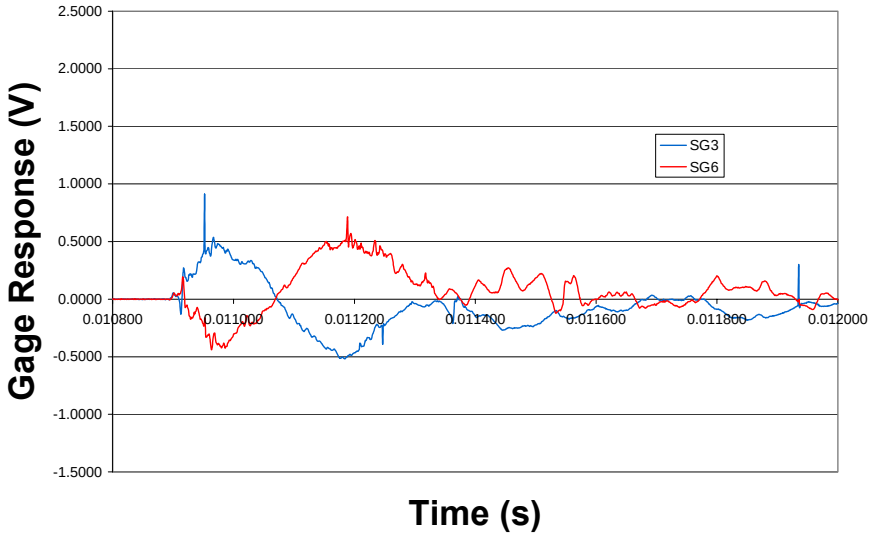

Figure 4.21 Strain gage responses for strain gage pairs SG3 and SG6

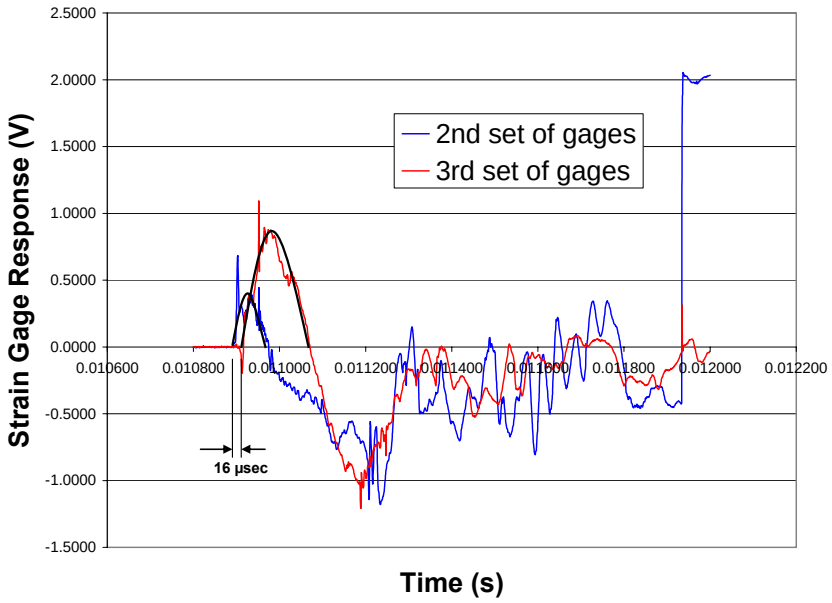

Figure 4.22 Paired strain gage responses resulting from the subtraction of responses from pairs of front and rear face strain gages. Leading edges are highlighted and the time delay between the two sets of gages is shown.

These paired responses show the measured strain in the panel resulting from bending due to the transverse impact. More importantly, the leading edge of each response represents the arrival of the bending wave at the strain gage location. By knowing the separation distance between the two paired strain gages, and the arrival time of the bending wave at each pair, the bending wave speed in the composite material can be calculated. The separation distance between SG2-SG5 and SG3-SG6 was one inch. From the paired responses shown previously in Figure 4.22, the difference in arrival times from the two responses was found to be 16 µsec. This results in a calculated bending wave speed of 62,500 in/sec.

Assuming that this is the appropriate wave speed that should be implemented in the numerical model, a value for the effective elastic modulus that

corresponds to this wave speed can be estimated. In the numerical model, the wave speed is calculated as

$$c = \sqrt{\frac{E}{\rho(1-\upsilon^2)}} \qquad \textbf{(4.1)}$$

The original values used in the numerical model for the density and Poisson's Ratio are assumed to be correct. Using these values and the experimentally-obtained bending wave speed, the corresponding elastic modulus is found to be 0.51 x10^6 psi. This is the value for the effective elastic modulus that must be specified in the set of material parameters input to the numerical model in order to simulate the experimentally-observed bending wave speed. In contrast, the effective elastic modulus that was originally calculated using the rule of mixtures was 18.2 x 10^6 psi, more than thirty times greater than the experimentally-derived value. These results, in conjunction with the previous poor numerical correlation to experimental data, indicate that the use of an effective elastic modulus derived using the rule of mixtures is not appropriate for modeling these kinds of dynamic events. Typical values reported in the literature [Mallick,1993] for the tensile modulus of epoxy matrix material range from 0.4-0.6 x 10^6 psi. It would therefore appear that a flexural-wave-based effective elastic modulus value, which in this particular case was on the same order as the tensile modulus of the matrix material, would be more appropriate for this particular modeling effort.

4.4.4 Comparison of Results for Composite Panels from Flexural-Wave-Based Effective Elastic Modulus Numerical Modeling and Experiments

With the experimental justification for its use satisfactorily demonstrated, a flexural-wave-based effective elastic modulus of 0.51×10^6 psi was implemented in the numerical model and the predictions for the ballistic impact response of the composite panels were repeated. As expected, the predicted dynamic displacement measurements from the modified analysis showed much better agreement with the experimental results.

With confidence established in the modeling of the composite panel response, the numerical models were then used to generate ballistic curves for the flat (infinite radius of curvature), 12-inch radius of curvature, and 4.4-inch radius of curvature composite panels for comparison to the experimental ballistic curves. These results are shown in Figures 4.23, 4.24, and 4.25.

The calculated values for both the experimentally-determined and numerically-determined ballistic limits for the composite panels are given in Table 4.2 and shown graphically in Figure 4.26. Also given in Table 4.2, and shown in Figure 4.26, is the numerically-derived ballistic limit for a composite panel with an 8-inch radius of curvature, a configuration that was not tested experimentally for the composite material. The experimental and numerical results match remarkably well over the entire range of impact velocities and the numerically calculated ballistic limit values are within 2% of the experimental values. As seen in Figure 4.26, the numerical model predicts that an optimal radius of curvature, as observed previously for the aluminum panels, also exists for the composite panels.

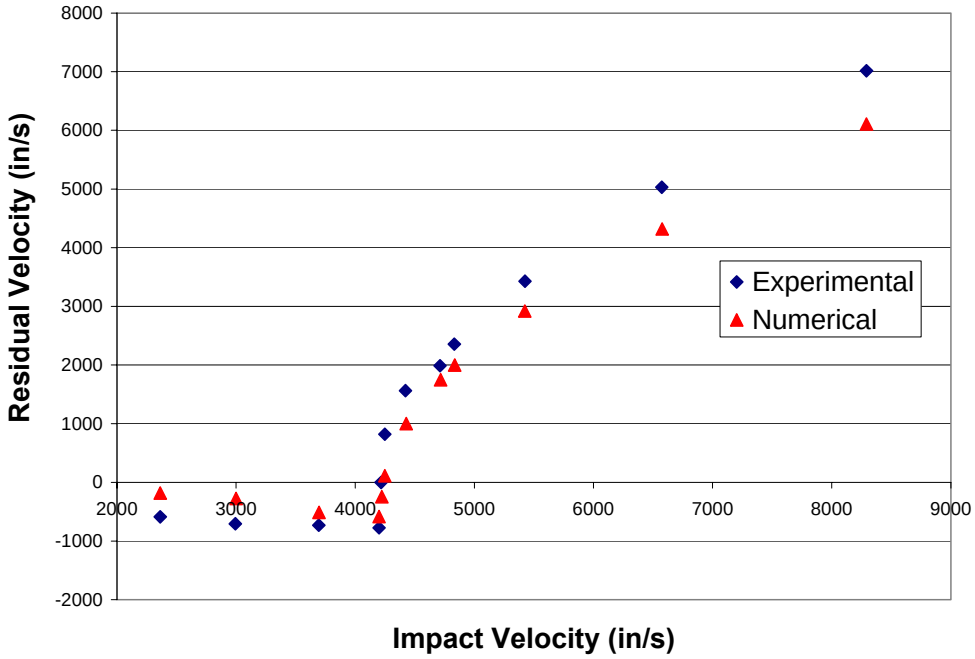

Figure 4.23 Comparison of numerical and experimental ballistic curves for an infinite radius of curvature composite panel

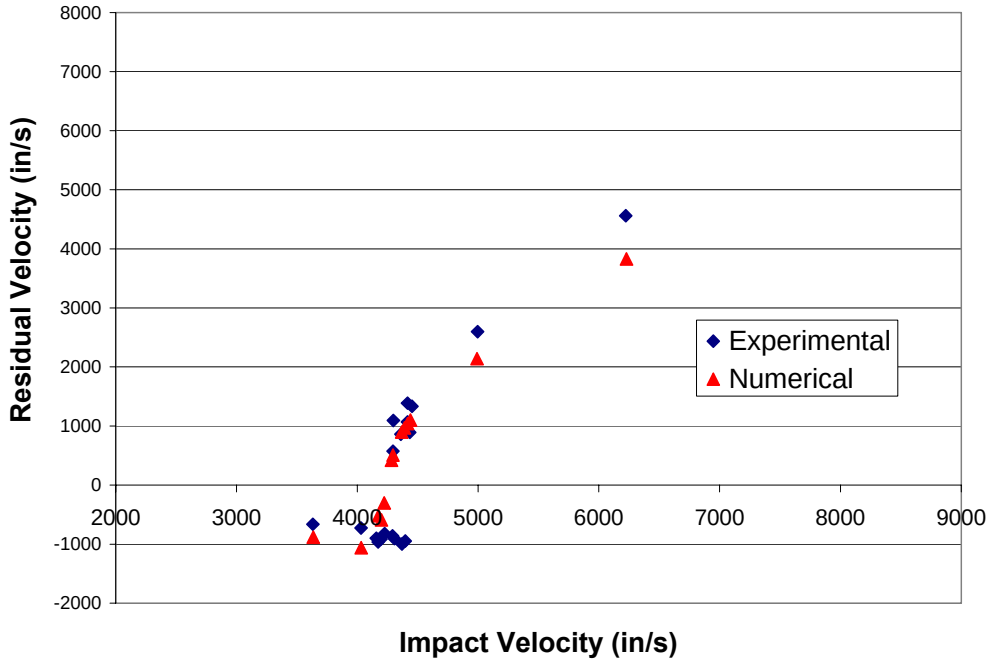

Figure 4.24 Comparison of numerical and experimental ballistic curves for a 12-inch radius of curvature composite panel

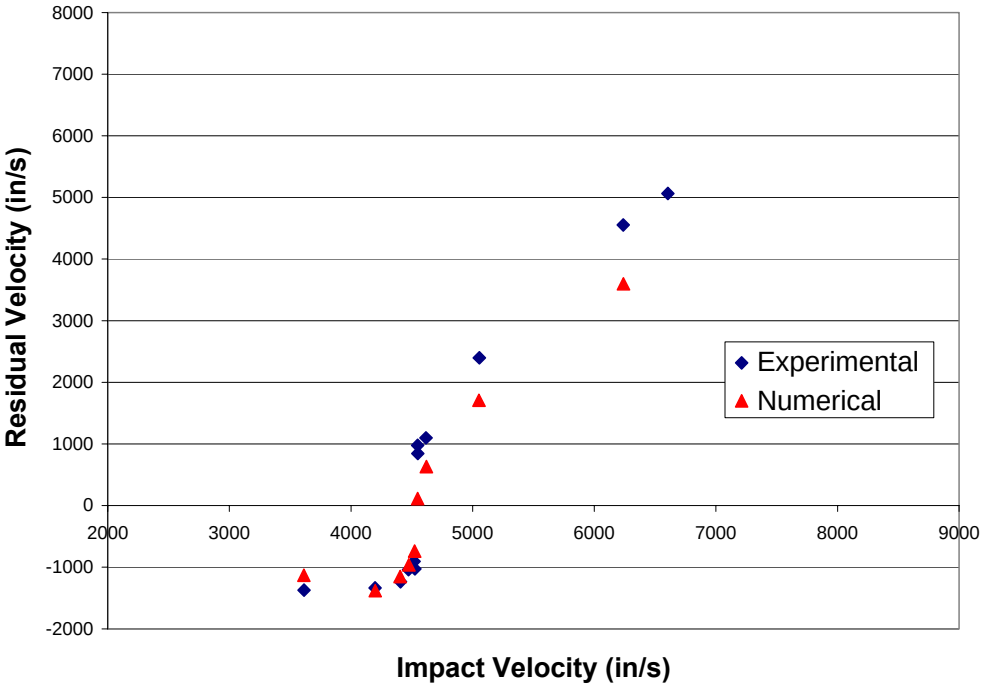

Figure 4.25 Comparison of numerical and experimental ballistic curves for a 4.4-inch radius of curvature composite panel

Table 4.2 Comparison of experimentally-obtained and numerically-derived ballistic limits for AS4-3501-6 graphite epoxy composite panels

Radius of Curvature	Experimental Ballistic Limit	Numerical Ballistic Limit	Percent difference
Infinite	352 ft/sec	353 ft/sec	0.28 %
12 inches	362 ft/sec	355 ft/sec	1.95 %
8 inches	N/A	389 ft/sec	N/A
4.4 inches	378 ft/sec	378 ft/sec	0 %

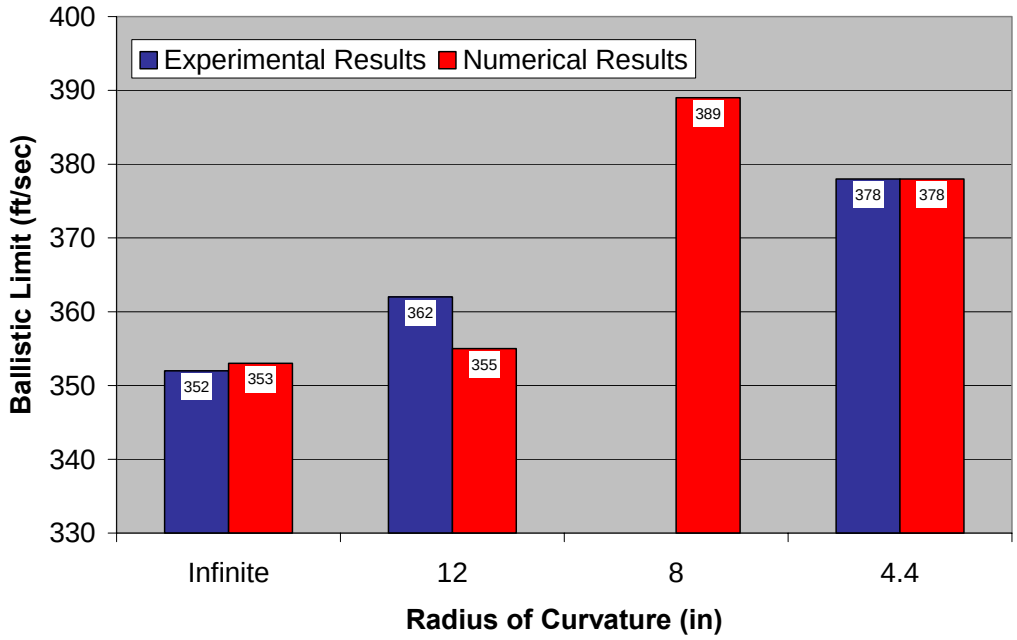

Figure 4.26 Experimental and numerical ballistic limits showing a numerically predicted optimal curvature for the composite panels

4.4.5 Summary of Results for Composite Panels

Two modeling simplifications were initially implemented to reduce the complexities associated with the modeling of the composite material properties. First, the lay-up of the composite material was selected to yield quasi-isotropic material properties and, for this reason, a shell-element formulation was employed that modeled the composite material as a single layer through the thickness. Secondly, the orthotropic in-plane properties of the composite material were modeled as isotropic using an effective elastic modulus that combined the fiber and matrix material properties into a single value based on the rule of mixtures.

The predicted panel response using these modeling simplifications did not agree well with experimental results. Strain-gage-instrumented ballistic testing

showed that a more appropriate value for an effective modulus was on the order of the tensile modulus of the matrix material. The use of this flexural-wave-based effective elastic modulus in the numerical modeling resulted in excellent agreement with the available experimental data. Further numerical modeling suggested the existence of an optimal radius of curvature with respect to maximization of the ballistic limit for curved composite panels; an observation similar to that made previously for the curved aluminum panels. The next section discusses this optimal radius of curvature phenomenon further.

4.5 Energy-based Mechanistic Justification for the Observed Effect of Curvature on the Ballistic Limit

4.5.1 Introduction

An important finding resulting from the experimental and numerical investigation into the effects of panel curvature on the ballistic impact response was the existence of an optimal curvature for maximizing the ballistic limit. This phenomenon was clearly seen in both the experimental and numerical studies of aluminum. In the composite panels, this phenomenon was not observable directly during the experimental phase but was clearly seen in the numerical studies that were performed. Given the excellent correlation between the experimental observations and the numerical predictions for radii of curvature values of infinity, 12-inches, and 4.4-inches, there is no reason to believe that the predicted results for an 8-inch radius of curvature for the composite panels are in any way anomalous or simply an artifact of the numerical modeling.

An energy-based mechanistic explanation for this particular effect of panel curvature is presented in this section. The approach taken in developing this explanation follows Langhaar [1962]. With respect to solving elasticity problems using energy methods, Langhaar states that, "…certain features of the solution of the problem may be clarified without a complete knowledge of the solution." As such, energy based methods are utilized here to develop a mechanistic argument for the existence of an optimal curvature without necessarily developing a complete knowledge of the effects of curvature.

4.5.2 Ballistic Impact Energy Balance

The kinetic energy balance as a result of a ballistic impact can be written as:

$$\tfrac{1}{2}mV_i^2 = \tfrac{1}{2}mV_r^2 + E \qquad \textbf{(4.2)}$$

where E is the deformation (strain) energy absorbed by the panel. This deformation energy includes both the plastic and elastic strain energy. The difference between the initial and residual kinetic energies of a projectile after a ballistic impact describes the amount of energy absorbed by or imparted to the target. The energy absorbed by the target can be of two forms: elastic or inelastic. Elastic energy response is related to elastic deformation and vibration of the panel. Inelastic energy response is related to plastic (non-recoverable) deformation and fracture energy. The elastic and inelastic responses of a target are competing mechanisms for dissipation of the energy imparted to the target. As the amount of energy imparted to a target increases, the target will continue to

deform elastically, and eventually plastically, so long as the work required to deform the material is less than the amount of work required to create new surfaces and hence initiate fractures.

4.5.3 Strain Energy of Deformed Shells

The discussion is first restricted to impacts that do not involve the creation of new surfaces. In this case, the only response of the target is through deformation processes. Inasmuch as a curved panel can be viewed as a portion of a shell, the general equations for thin shells are applicable to curved panels. The components of strain energy of a deformed shell are the bending-strain energy U_b and the membrane-strain energy U_m. The membrane-strain energy is associated with mid-surface stretching. It is assumed that the shell resists the transverse loading mainly through bending action and that the membrane-strain energy can be neglected. The bending-strain energy, U_b, is found to be [Ugural,1981]

$$U_b = \tfrac{1}{2} D \iint_A [(\chi_x + \chi_y)^2 - 2(1-\upsilon)(\chi_x \chi_y - \chi_{xy}^2)]dxdy \qquad \textbf{(4.3)}$$

where A represents the surface area of the shell and χ_x, χ_y, and χ_{xy} represent changes in curvature.

The bending-strain energy equation provides the first subtle insight into the manifestation of curvature effects. Because the bending-strain energy of a deformed shell is a function of changes in curvature, and not just the initial curvature, there is a potential for the existence of non-monotonic relationships with respect to curvature.

As an example, consider the elastic impact process of a projectile impacting a fixed plate. During impact, the projectile and the plate are subjected to equal and opposite forces and impulses through a mutually shared contact interface. Waves propagate through both structures transforming stress and strain states and inducing changes in motion. Before the elastic strain energy relaxes, the projectile and some disturbed area of the plate attain equal velocities. After the elastic strain energy relaxes, a relative velocity develops between the projectile and the plate, and the two separate.

Because the bending-strain energy is a function of changes of curvature, there exists the potential for an ideal configuration state (i.e., initial radius of curvature) which minimizes the energy required to satisfy the attainment of equal velocities for the projectile and the unknown disturbed area of the plate. While no proof has been provided to support the ideal configuration state hypothesis, the point of the exercise was to demonstrate that the effects of curvature are represented in the governing equations of motion and that the amount of storable energy in a deforming plate is affected by both the initial curvature and, more importantly, the change in curvature of the panel.

In the following section, the absorbed deformation energies resulting from experimental ballistic impact events are examined in an effort to establish a relationship between panel curvature, deformation energy, and the ballistic limit of the panel.

4.5.4 Effect of Curvature and Deformation Energy

The experimental results plotted in Figure 4.27 show that the absorbed deformation energy for impacted aluminum panels continues to increase linearly as the initial velocity (and initial kinetic energy) of the projectile approaches the ballistic limit of the panel. In addition, the slope of the linear increase is nearly the same for all panel curvatures as shown in Figure 4.28, which is a collection of the data shown in Figure 4.27.

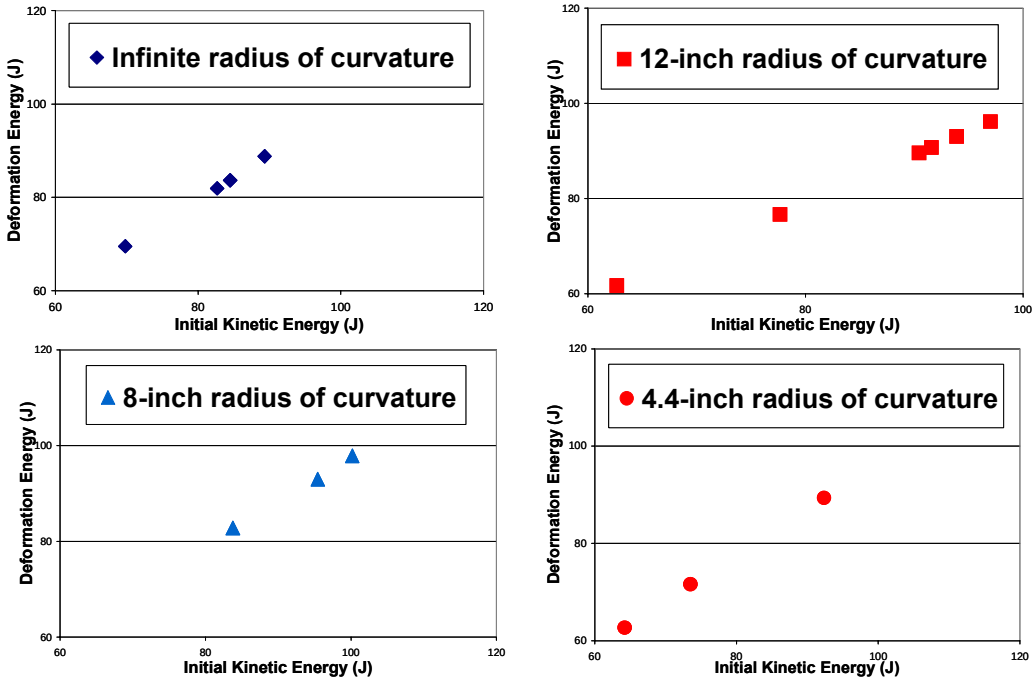

Figure 4.27 Experimental results showing the increase in deformation energy as the initial kinetic energy is increased for aluminum panels with different radii of curvature

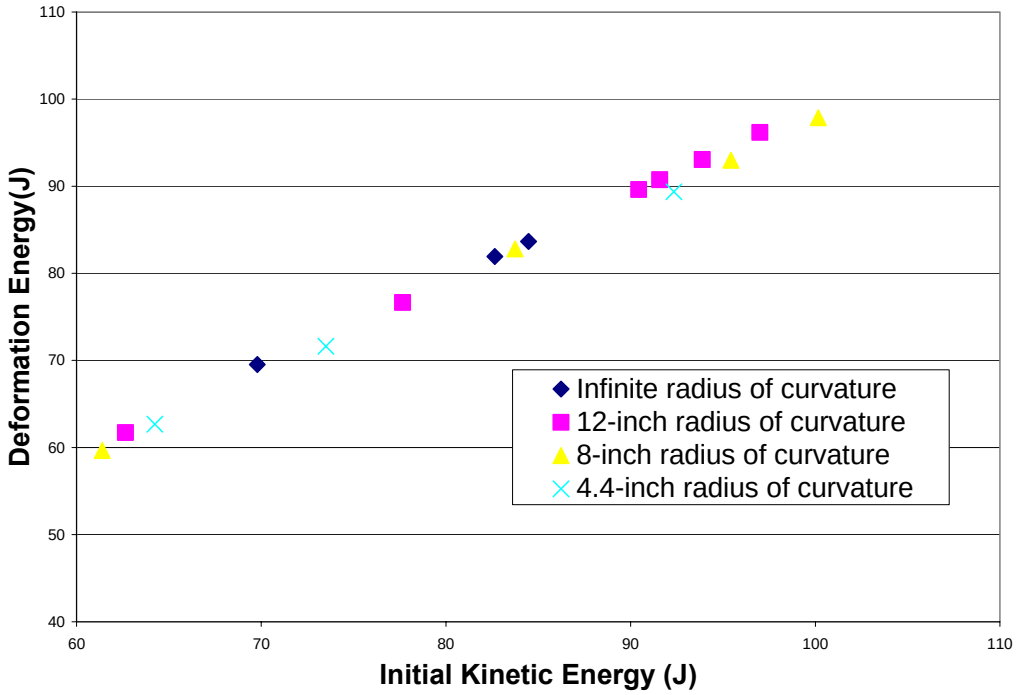

Figure 4.28 Experimental results for four aluminum panel curvatures showing the similarity in the rate of (linear) increase in deformation energy

The ballistic limit defines the transition from rebound events (mostly elastic processes) to penetration events (inelastic processes) and is assumed to occur at a constant threshold value of deformation energy that is material dependent. This material dependency assumption is supported by the good correlation of numerical results to experimental results in the present study, where the numerical analysis were carried out using a constant threshold value for failure based on a plastic failure strain criterion. Based on this information, it is hypothesized that, by comparing the assumed, material-dependent, threshold value of deformation energy to the absorbed deformation energy of the panel, an indication of how close a particular impact velocity is to the ballistic limit of the material can be obtained.

Figure 4.29 shows the absorbed deformation energy amounts, calculated from the numerical analysis results, for aluminum panels with six different radii of curvature, that were impacted using identical initial projectile velocities (identical initial kinetic energy). Superimposed on the figure is a hypothetical threshold value of deformation energy that represents the amount of deformation energy needed to reach the ballistic limit of the material.

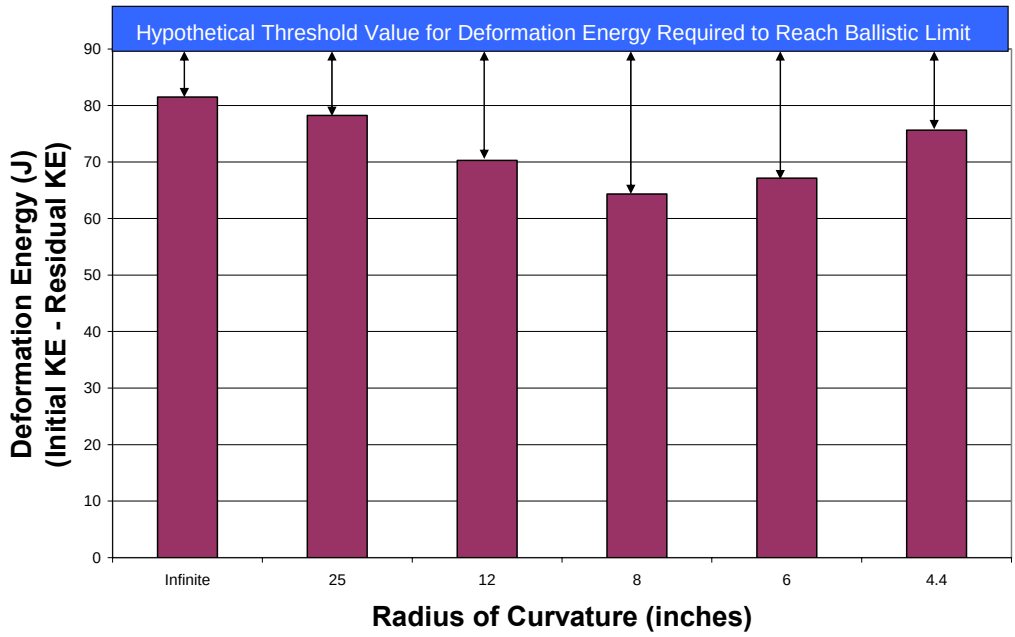

Figure 4.29 Absorbed deformation energy and hypothetical threshold value for aluminum panels with different radii of curvature resulting from 5640 in/sec impact

As seen in the figure, the 8-inch radius of curvature panel has the smallest amount of absorbed deformation energy of all the panel configurations for identical impact energies. The experimental results showed that the deformation energy increases linearly with increases in projectile velocity (or initial kinetic energy) until the ballistic limit is reached. The 8-inch radius of curvature panel

should therefore have the highest ballistic limit for the configurations shown, based on the assumed existence of a material-dependent deformation energy threshold. The non-monotonic relationship between panel curvature and ballistic limit is similarly evident from the differential between absorbed deformation energy and the assumed threshold level across the various panel curvatures.

4.6 Chapter Summary

In this chapter, the experimental and numerical results reported previously for ballistic impact of both aluminum and composite panels were revisited for discussion and comparison. The numerical models were shown to be capable of consistently and reliably modeling the post-impact residual velocity of the projectile, the threshold (ballistic limit) separating penetrating and non-penetrating impact events, and the panel response (out-of-plane deformation) to the impact event, provided that the appropriate (flexural-wave-based) effective elastic modulus was used in the simulation of ballistic impact events for composite panels.

The existence of an optimal curvature for maximizing the ballistic limit was shown experimentally for the aluminum panels and numerically for both the aluminum and composite panels. A simple energy-based mechanistic justification for the existence of an optimal curvature was also discussed.

In the next chapter of this dissertation, the focus shifts from experimental and numerical ballistic impact testing to the examination of post-impact damage in both the composite and aluminum panels.

Chapter 5 Non-Destructive and Destructive Evaluation of Impacted Panels

5.1 Overview

In the previous chapters, consistent and reliable numerical modeling of the ballistic impact response of curved and flat panels for both aluminum and a graphite-epoxy composite laminate was demonstrated. A fitting parameter, the failure strain had to be specified in the model, in addition to the usual material properties. One area of interest that the numerical modeling did not specifically address was the quantitative estimation of ballistic impact damage. In its present form, the numerical model simulates perforation of the impacted panel by deleting elements when the element strain exceeds a specified value. One fairly superficial technique for comparing numerical simulations and experiments would be to compare the area of the deleted elements with the exit-hole size in the impacted panels. However, while this might be a valid comparison for aluminum panels, this would not sufficiently address the various damage mechanisms, such as delamination and matrix cracking, which are known to occur in impacted composite panels.

Post-impact evaluations, and documentation of observed damage, were carried out and the results are presented in this chapter for both the composite and the aluminum panels. Non-destructive, ultrasonic, C-scans were completed for the impacted composite panels. A destructive, de-ply technique was also employed in selected cases to examine the ply-by-ply damage that occurred through the thickness of the composite panels. Results from the destructive evaluation were compared to the non-destructive C-scan results and good

correlation between the two was observed. For the impacted aluminum panels, exit-hole sizes were documented and some changes in the failure mechanisms were observed over the range of impact velocities that were studied.

While an in-depth study of the damage in impacted panels has not been performed as part of this research effort, those results that were obtained are being included and discussed. The objective is threefold. Firstly, there is the desire to look for qualitative trends in the damage induced by ballistic impact over a range of impact velocities. Secondly, there is a desire to compare the results from this study with some findings that have been reported in the literature, wherein for example, the maximum damage in a laminated composite panel has been seen to occur at neither the front nor the rear surface of the panel, but rather in the interior plies. Thirdly, the information documented in this chapter could prove useful to future investigators who wish to explore issues like micro-mechanical damage modeling, or the modeling of through-thickness damage development, in ballistic impacted curved composite laminates.

5.2 Non-destructive Evaluation of Composite Panels

Briefly stated, the C-scan technique [Doherty,1993] identifies damage regions in the specimen by measuring changes in the attenuation of an ultrasonic wave as the wave passes from intact areas to damage zones within the plate. This method can identify only the projected extent of internal damage and is thus limited in its ability to identify damage on a ply-by-ply basis. Despite this limitation, the technique is useful in showing the changes in failure patterns for increasing impact energies. All of the non-destructive C-scans were completed at

the Non-Destructive Evaluation Branch of the Materials and Manufacturing Directorate of the Air Force Research Laboratory at Wright-Patterson Air Force Base in Dayton, OH.

Representative C-scan results from 12-inch radius of curvature and 4.4-inch radius of curvature panels impacted at varying impact velocities are shown in Figures 5.1 and 5.2, respectively. These figures reveal a trend that is commonly seen in ballistic impact studies on composite panels, namely that the damage area decreases with increasing impact velocity. This decrease in damage area is associated with a change in the failure mechanism as the impact velocity is increased. In the velocity regime that does not result in penetration of the target, inter-ply delaminations, or separations between adjacent plies, are the primary damage mode. As the impact velocity increases, the failure mechanism shifts to perforation of the material and the delamination zones do not extend as far. These results confirm what many other researchers have previously recognized; lower velocity impact events result in larger damage areas than correspondingly higher impact velocities.

Measurements of the size of the damage zone were made on the C-scan images recorded for each of the composite panels. The results for the 12-inch radius of curvature and the 4.4-inch radius of curvature composite panels are shown in Figures 5.3 and 5.4, respectively. The ballistic limit and a ballistic limit region, defined as ±15 ft/sec from the ballistic limit, are also shown in the figures. For clarity, the measured damage zone sizes for the data points located within the defined ballistic limit region are averaged together and the results for the 12-inch

radius of curvature panels and the 4.4-inch radius of curvature panels are shown together in Figure 5.5. This figure better illustrates the decrease in the size of the damage zone as the impact velocity is increased. In addition, these results show that the 4.4-inch radius of curvature panels generally suffered a larger damage area than the 12-inch radius of curvature panels for comparable impact velocities. All of the C-scans are included for reference in Appendix B.

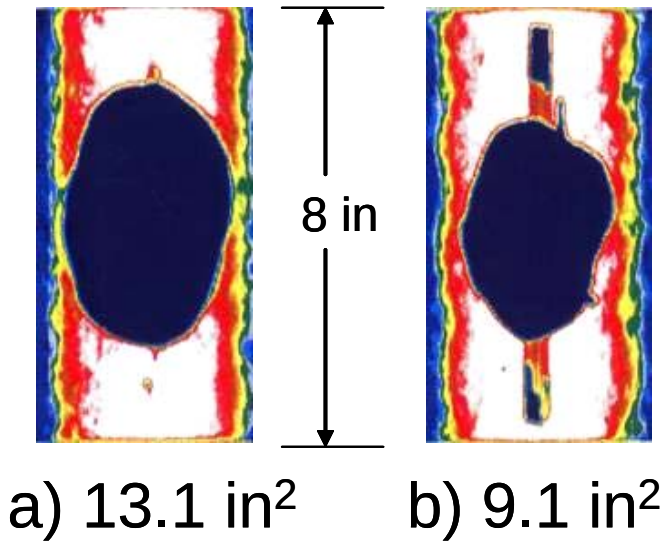

Figure 5.1 C-Scan damage and measured damage area for 12-inch radius of curvature composite panels showing a decrease in damage area with increasing impact velocity: a) 303 ft/sec b) 346 ft/sec c) 358 ft/sec d) 519 ft/sec

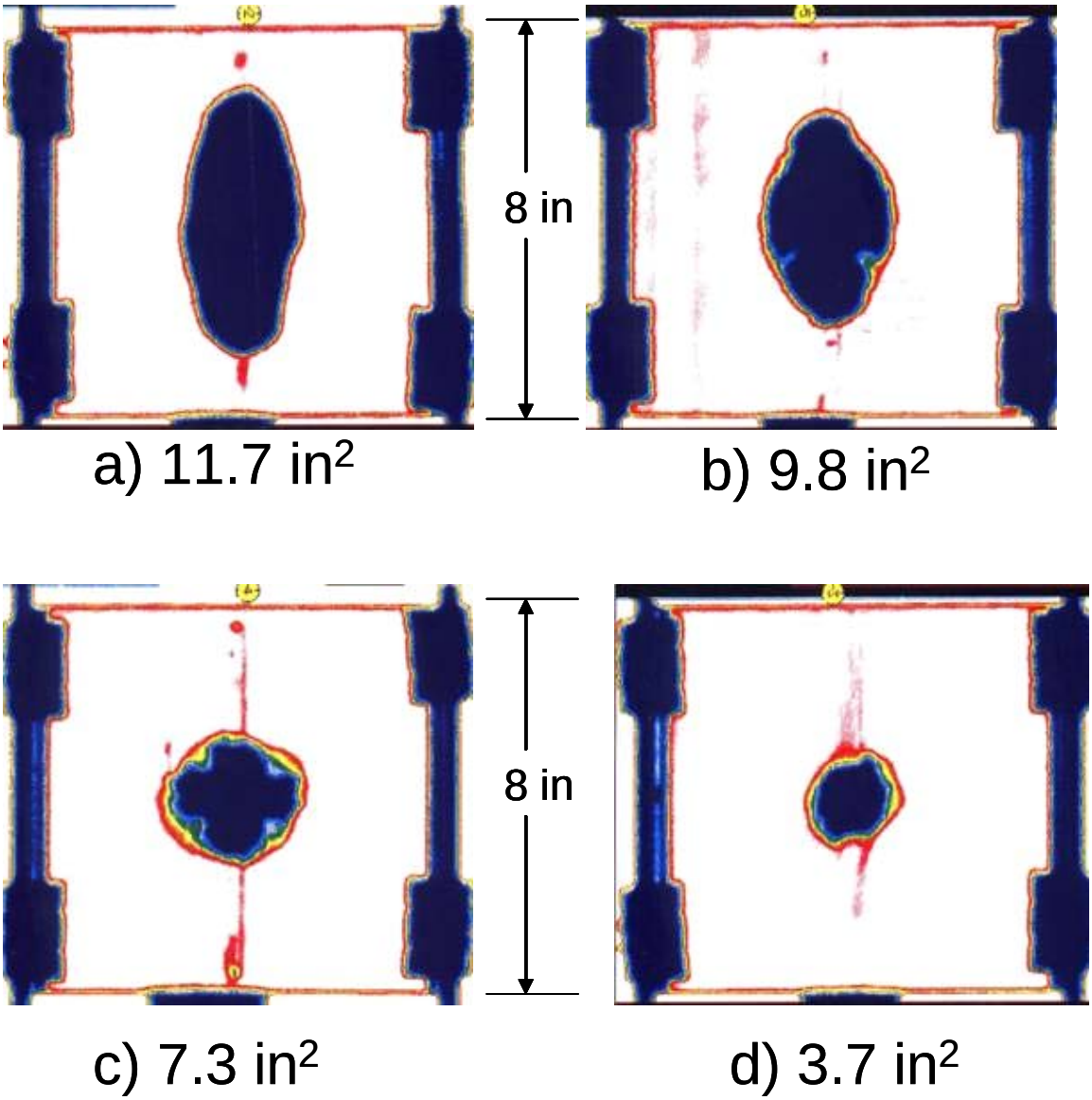

Figure 5.2 C-Scan damage and measured damage area for 4.4-inch radius of curvature composite panels showing a decrease in damage area with increasing impact velocity: a) 301 ft/sec b) 350 ft/sec c) 379 ft/sec d) 550 ft/sec

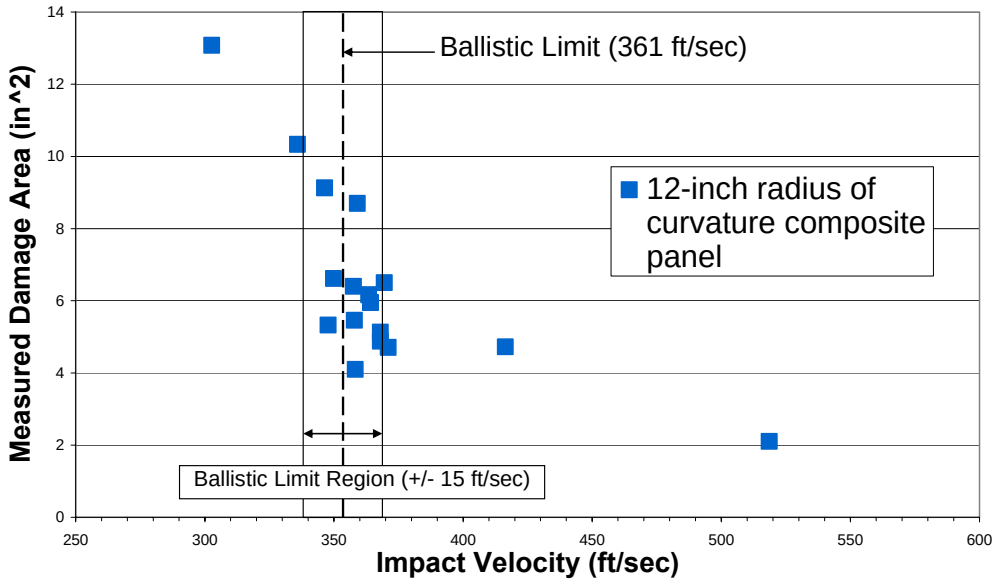

Figure 5.3 Damage area (measured from C-Scan) as a function of impact velocity for 12-inch radius of curvature composite panels, showing a decrease in the size of the damage zone with increase in impact velocity.

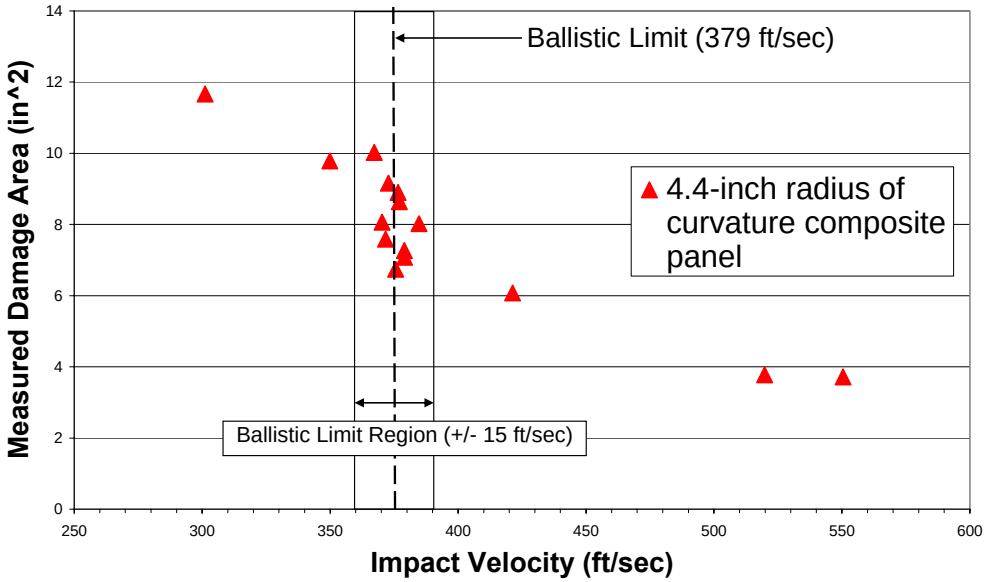

Figure 5.4 Damage area (measured from C-Scan) as a function of impact velocity for 4.4-inch radius of curvature composite panels, showing a decrease in the size of the damage zone with increase in impact velocity

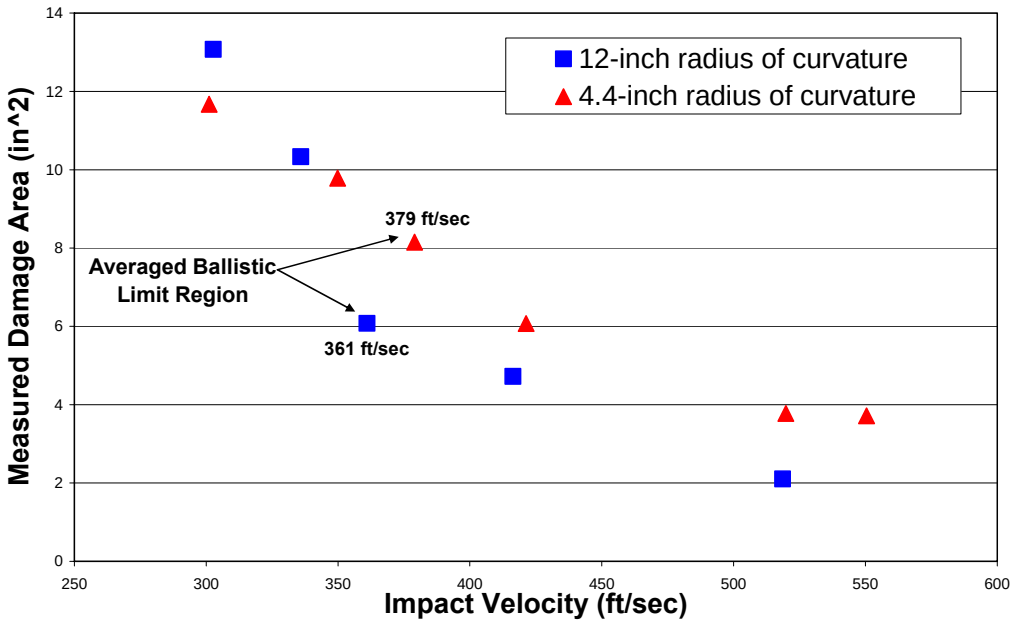

Figure 5.5 Damage area measured from C-scans for 12-inch and 4.4-inch radius of curvature composite panels. Measurements within ±15 ft/sec of the ballistic limit have been averaged and plotted at the ballistic limit to clarify the figure.

5.3 Destructive Evaluation of Composite Panels

While the non-destructive, C-scan evaluations were helpful in identifying the extent of internal damage, no information was available on the distribution of the damage through the thickness of each panel. A destructive de-ply technique was therefore employed to gain insights into the ply-by-ply distribution of damage and to determine if there was an effect of panel curvature on the distribution of damage in impacted composite panels.

The destructive de-ply technique involves injecting a colored, penetrating agent into the damaged area of the composite, heating the composite specimen so that the resin is burned off, and removing the individual plies one-by-one for

inspection. The penetrant used for this research was a 2% solution of gold-chloride in a carrier of isopropyl alcohol, which results in a yellow tinting of the surfaces that are wetted.

To facilitate injection into the damaged area, the composite panels were first sectioned in half, through the impact location, with a diamond-bladed saw. One of the sections was injected with the dye penetrant and the remaining half of the sectioned panel was preserved for future studies. After injection of the penetrant, the sectioned composite panels were heated in an oven at 600°F for approximately 2 hours. This elevated temperature caused the resin of the composite material to pyrolyze and, after cooling, the individual plies could be lifted off one-by-one using a sharp knife. The de-plied surface was then inspected under a microscope or photographed for later examination of damaged areas.

The results from a representative de-plied specimen are shown in Figures 5.6-5.15. Only the last ten interfaces of the 12-inch radius of curvature composite panel are shown. The impact velocity was 348 ft/sec and the projectile did not penetrate the panel. Each figure shows the delaminated area for the interface identified by the arrow marked on the panel ply stacking sequence.

[0/90/+45/-45/0/90/+45/-45 … -45/+45/90/0/-45/+45/90/0/-45/+45/90/0/-45/+45/90/0]

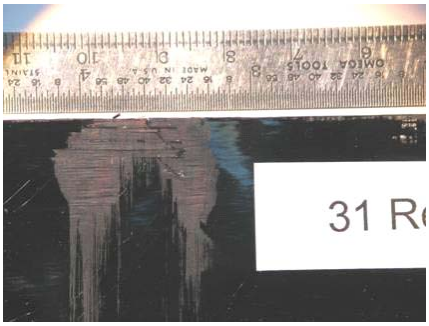

Figure 5.6 De-plied 12-inch radius of curvature specimen with interface location shown

[0/90/+45/-45/0/90/+45/-45 … -45/+45/90/0/-45/+45/90/0/-45/+45/90/0/-45/+45/90/0]

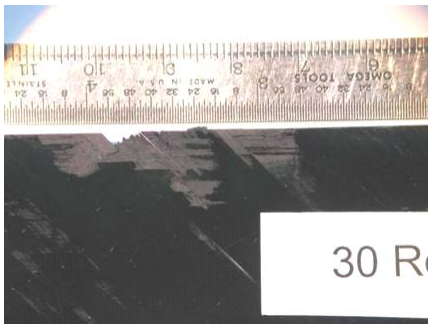

Figure 5.7 De-plied 12-inch radius of curvature specimen with interface location shown

[0/90/+45/-45/0/90/+45/-45 … -45/+45/90/0/-45/+45/90/0/-45/+45/90/0/-45/+45/90/0]

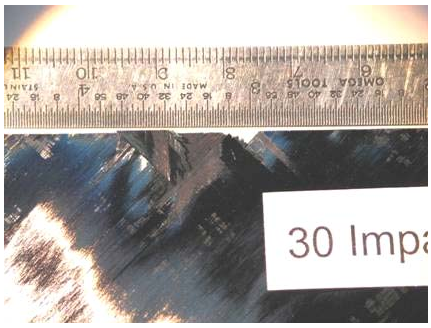

Figure 5.8 De-plied 12-inch radius of curvature specimen with interface location shown

[0/90/+45/-45/0/90/+45/-45 … -45/+45/90/0/-45/+45/90/0/-45/+45/90/0/-45/+45/90/0]

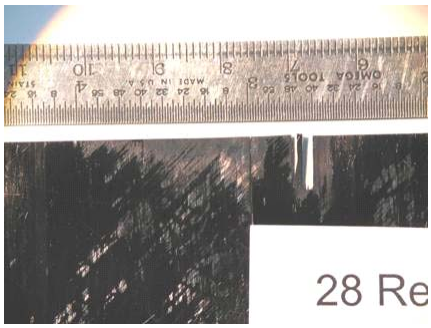

Figure 5.9 De-plied 12-inch radius of curvature specimen with interface location shown

[0/90/+45/-45/0/90/+45/-45 … -45/+45/90/0/-45/+45/90/0/-45/+45/90/0/-45/+45/90/0]

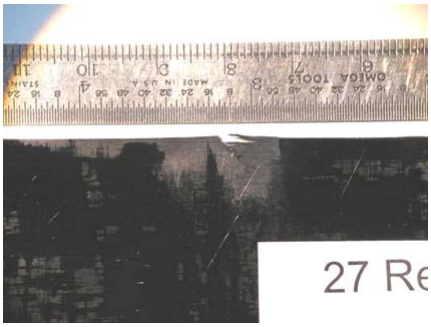

Figure 5.10 De-plied 12-inch radius of curvature specimen with interface location shown

[0/90/+45/-45/0/90/+45/-45 … -45/+45/90/0/-45/+45/90/0/-45/+45/90/0/-45/+45/90/0]

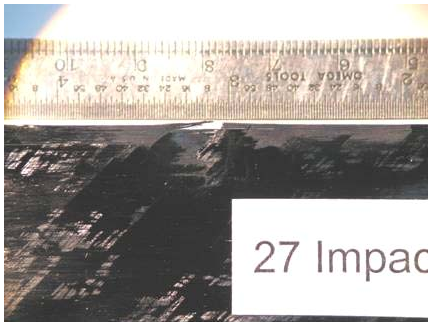

Figure 5.11 De-plied 12-inch radius of curvature specimen with interface location shown

[0/90/+45/-45/0/90/+45/-45 … -45/+45/90/0/-45/+45/90/0/-45/+45/90/0/-45/+45/90/0]

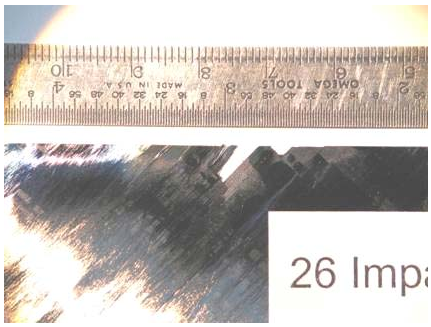

Figure 5.12 De-plied 12-inch radius of curvature specimen with interface location shown

[0/90/+45/-45/0/90/+45/-45 … -45/+45/90/0/-45/+45/90/0/-45/+45/90/0/-45/+45/90/0]

Figure 5.13 De-plied 12-inch radius of curvature specimen with interface location shown

[0/90/+45/-45/0/90/+45/-45 … -45/+45/90/0/-45/+45/90/0/-45/+45/90/0/-45/+45/90/0]

Figure 5.14 De-plied 12-inch radius of curvature specimen with interface location shown

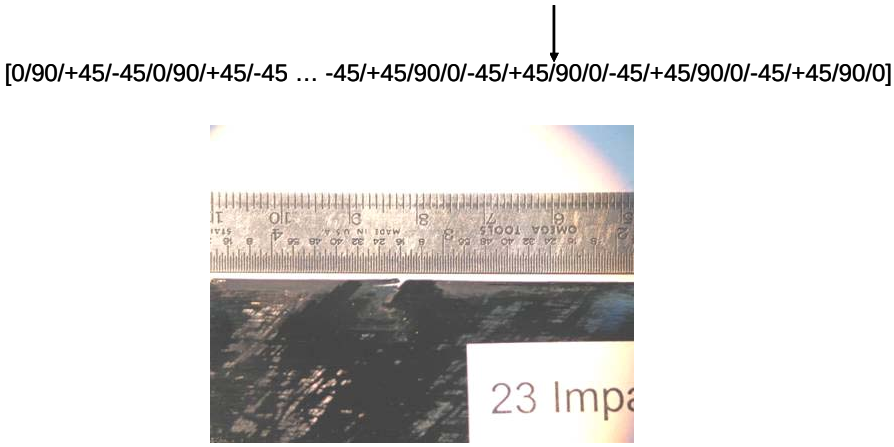

Figure 5.15 De-plied 12-inch radius of curvature specimen with interface location shown

A careful examination of the delaminated surfaces at each interface indicated that the delamination was peanut-shaped and always extended along the fiber direction of the ply furthest away from the impact site. These results are similar to those reported by numerous other researchers [Gaffari, Joshi, Liu] for ballistic impact of flat composite panels and indicate that there are no significant differences in the distribution of through-the-thickness damage between curved and flat composite panels. Consequently, the destructive de-ply technique was not applied to all of the impacted composite panels. Instead, the destructive ply-by-ply examination was used as a validation tool for the C-scan results.

Photographs of the de-plied specimen were imported into digital editing software with the goal of reconstructing the cumulative damage area depicted in the non-destructive C-scans. The delaminated areas from each of the de-ply photographs (Figures 5.6-5.15) were extracted and digitally layered, as seen in Figure 5.16, for comparison to the non-destructive results. Due to the sectioning of the sample for penetrant injection, the reconstructed delamination only

represents half of the damaged area. The reconstructed image was therefore copied and mirrored for easier comparison to the original C-scan image as shown in Figure 5.17. Good agreement was found between the multi-layer reconstruction and the C-scan. Measurements along the width, length, and diagonal were within 15% of each other as tabulated in Table 5.1.

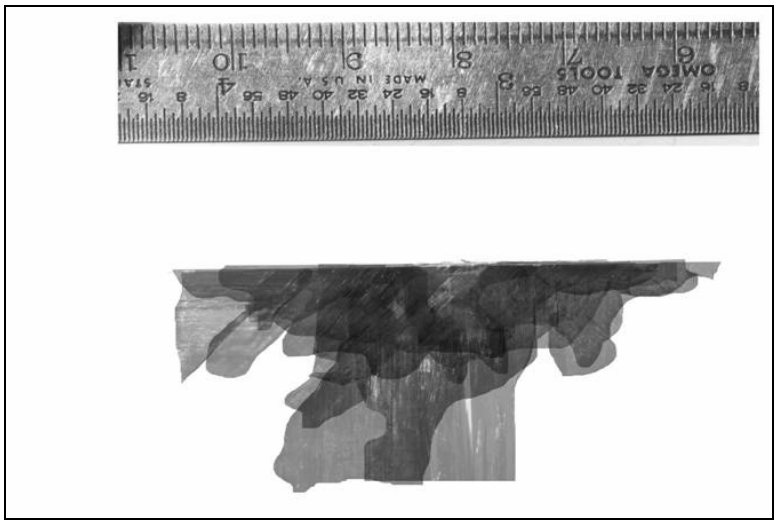

Figure 5.16 Layered reconstruction of the damage zone for a de-plied specimen

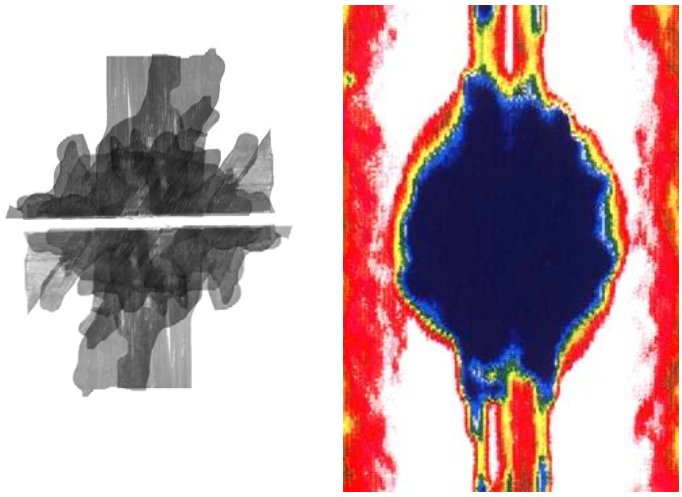

Figure 5.17 Comparison of the reconstructed de-plied images to the original C-scan result

Table 5.1 Comparison of dimensions for damage zones from reconstructed de-ply and the original C-scan for a 12-inch radius of curvature composite panel

	Reconstructed De-Ply	Original C-Scan	Percent Difference
Length (inches)	1.92	1.85	4%
Width (inches)	2.08	2.38	13%
Diagonal (inches)	2.16	2.28	5%

5.4 Post-Impact Evaluation of Curved Aluminum Panels

In this section, the observations of damage in aluminum panels subjected to ballistic impact at various impact velocities will be described. Flat and curved aluminum panels were investigated to identify any potential effect of panel curvature on the impact damage generated.

Four sets of aluminum panels with varying amounts of curvature were impacted with steel spheres at various impact velocities and the ballistic impact results were presented in Chapter 2. The four radii of curvature investigated were infinite (flat), 12-inch, 8-inch, and 4.4-inch. Post-impact photographs of the panels (from the exit side) showing the resulting impact damage are presented in Figures 5.18-5.21. The bright ring of light, seen in some of the photographs, is a reflection from the light source.

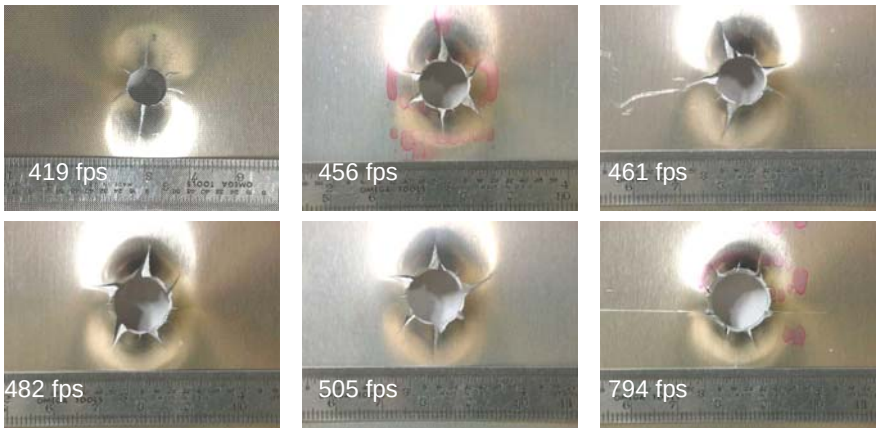

Figure 5.18 Post-impact, exit-side, images of infinite radius of curvature (flat) aluminum panels impacted at various velocities

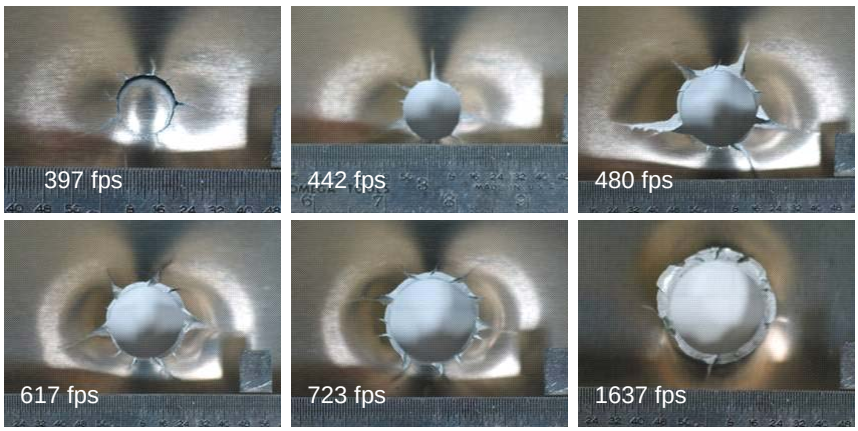

Figure 5.19 Post-impact, exit-side, images of 12-inch radius of curvature aluminum panels impacted at various velocities

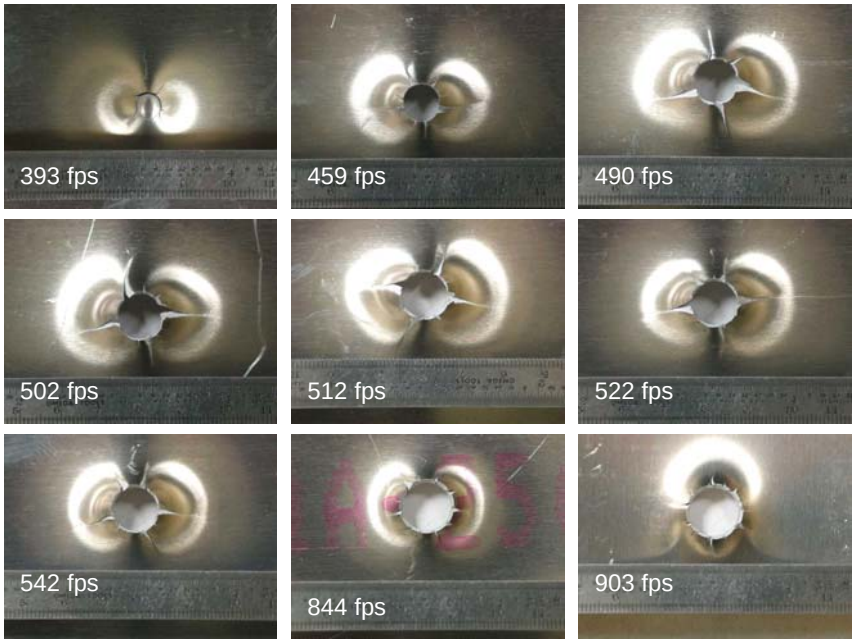

Figure 5.20 Post-impact, exit-side, images of 8-in radius of curvature aluminum panels impacted at various velocities

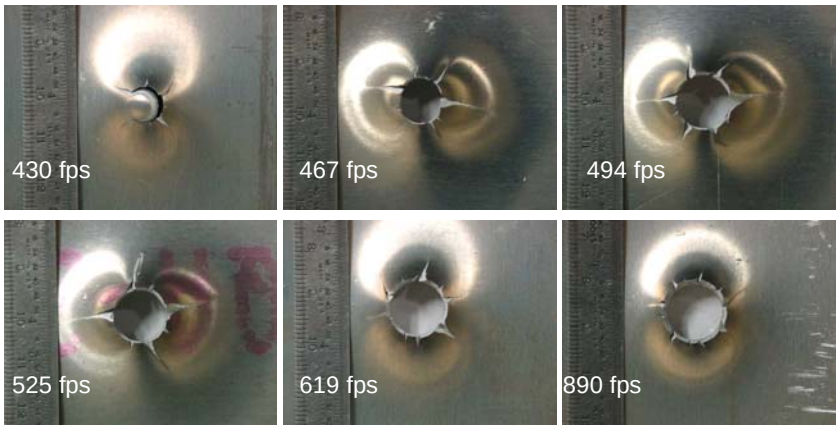

Figure 5.21 Post-impact, exit-side, images of 4.4-inch radius of curvature aluminum panels impacted at various velocities

By comparing numerous post-impact still photographs from panels impacted at varying velocities, a pseudo-dynamic progression of damage can be

envisioned. Neglecting plastic deformation, the first damage appears as a circumferential crack accompanied by the bulging of a small amount of aluminum that is in contact with the projectile, as shown in the first image of Figure 5.19. As the impact velocity is increased, a plug is extruded from the panel and radial cracks begin to form. The next stage consists of a larger plug extrusion, extension of the radial cracks, and petaling of the aluminum material. Petaling, sometimes referred to as ductile hole formation, is a process in which the projectile plastically deforms the cantilever-like 'petals' of material that have been created by the radial cracking [Wilkens (1978), Zukas (1990)].

Further increases in impact velocity result in more extensive radial cracking and petaling, until the material has deformed to the point where the projectile can pass through the opening. This combined process of plug formation, radial cracking, and petaling continues until the impact velocity becomes high enough that the material experiences a change in failure mechanism. When this threshold is reached, the projectile begins to perforate the material in a punch-press manner. During this stage, plug formation is still present but the material does not develop extensive radial cracks. Instead, the perforation process is accompanied by a multitude of short radial cracks as seen in the last images of Figures 5.18-5.21.

Measurements were made of the exit-hole size for each of the aluminum plates and the results are presented in Figure 5.22. It is interesting to note that, in all cases, and more importantly in cases involving complete penetration, the measured exit-hole size was always less than the projected area (0.196 in^2) of the

½-inch diameter spherical projectile. In contrast, the composite laminate results (Figures 5.1-5.5) all show damage zones that are an order of magnitude (or more) larger than the projected area of the impacting projectile.

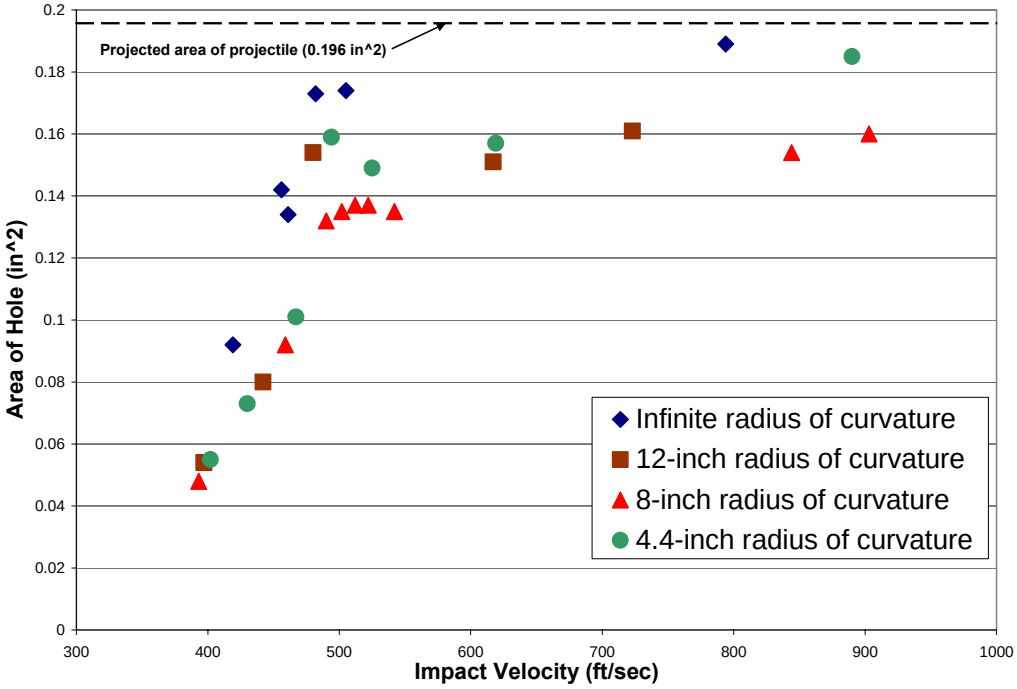

Figure 5.22 Exit-hole size as a function of impact velocity for aluminum panels with varying amounts of curvature. Dashed line represents the projected area of the ½-inch diameter projectile

These results show that, for all of the panel curvatures investigated, the exit-hole size increases as the impact velocity is increased. Two distinct regions, possibly associated with a change in failure mechanism, exist regardless of panel curvature. In the first region, the size of the exit-hole increases rapidly, in a linear manner, up to a certain point. In the second region, the exit-hole size continues to increase as the impact velocity is increased, but it does so at a slower rate. While it cannot be conclusively stated to be the case, the data in this second region appear to asymptotically approach a limiting value. Additional examination of

the data suggests that this limiting value may also vary with panel curvature. For the tests conducted, comparisons of exit-hole sizes for similar impact velocities showed that the infinite radius of curvature (flat) aluminum panel had the largest exit-hole size followed by the 4.4-inch radius of curvature aluminum panel, the 12-inch radius of curvature aluminum panel, and the 8-inch radius of curvature aluminum panel. Interestingly, the relationship between exit-hole size and panel curvature appears to be qualitatively similar to the non-monotonic relationship between the ballistic limit and the panel curvature, in that the panel configuration with the highest ballistic limit (an 8-inch radius of curvature) had the smallest exit-hole sizes and the panel configurations with the lower ballistic limits (an infinite radius of curvature and a 4.4-inch radius of curvature) had larger exit-hole sizes.

5.5 Chapter Summary

In this chapter, a preliminary study of the impact-induced damage in both composite and aluminum panels has been reported. Non-destructive and destructive evaluation methods were employed to identify qualitative trends in the damage induced by the ballistic impact. For the composite panels, these trends showed a decrease in the damage area (as measured by C-scan) as the impact velocity increased. This finding was consistent with other findings that have been reported in the literature. It was also observed that the more highly-curved composite panels (4.4-inch radius of curvature) had a generally larger damage area than panels with less curvature (12-inch radius of curvature) for comparable

impact velocities. In all cases, the damage area was significantly larger than the projected area of the impacting projectile, even for ballistic impacts where the projectile completely penetrated the panel and exited with a significant residual velocity.

The impact-induced trends observed for the aluminum panels appear to be the opposite of those observed for the composite panels. As the impact velocity was increased, the exit-hole size (as measured from the rear of the panel) increased with increasing velocity for the aluminum panels. It was also observed that all of the exit-holes were smaller than the projected area of the ½-inch projectile.

The next chapter, Chapter 6, is the concluding chapter of this dissertation. Concluding remarks will be presented, along with a summary and re-statements of some of the key findings from this research. Recommendations for future work that can build on this foundation will also be presented.

Chapter 6 Concluding Remarks

6.1 Overview

A hybrid experimental and numerical investigation was conducted to investigate the relationship, if any, between the curvature of an impacted panel and the ballistic impact response. Results from experiments and numerical modeling of both aluminum and composite panels with varying amounts of cylindrical curvature have been presented, interpreted, and discussed. Dynamic deformation measurements and strain-gage-instrumented impact tests were used to do the following: (1) answer important questions about the material properties that should be specified when numerically simulating the ballistic impact response of composite laminates; and (2) validate some of the key assumptions that were made in the interest of efficiently and economically modeling the ballistic impact event, an important objective of this effort. A preliminary study was also conducted, and has been described, wherein the physical damage induced in the composite panels was assessed by using both non-destructive (C-scan) and destructive (ply-by-ply separation) techniques.

The most significant findings from this research effort have been summarized in this chapter. Previously presented key figures, showing summary data supportive of those findings, have been repeated in this chapter for completeness and ease of reference. The chapter, and this dissertation, concludes with some recommendations on future work that may provide fruitful avenues of investigation for researchers who wish to build on the foundations that have been laid here.

6.2 Summary of the Most Significant Findings from this Research

The initial experimental investigation into the effects of panel curvature on the ballistic impact response of graphite epoxy composite panels suggested (see Figure 6.1) that the ballistic limit increased monotonically as the curvature of the panel was increased. Further exploration of the relationship between the curvature of an impacted panel and the associated ballistic limit through numerical modeling of the ballistic impact response of curved aluminum panels revealed that the relationship was non-monotonic, was actually parabolic in nature, and that there was an optimal panel curvature with respect to maximizing the ballistic limit. This can be seen clearly in Figure 6.2.

Experimental ballistic testing of curved aluminum panels, conducted to validate the numerical modeling results, reaffirmed both the non-monotonic, parabolic relationship between the curvature of a panel and the associated ballistic limit, and the existence of an optimal panel curvature for maximizing the ballistic limit. This information is shown in Figure 6.3.

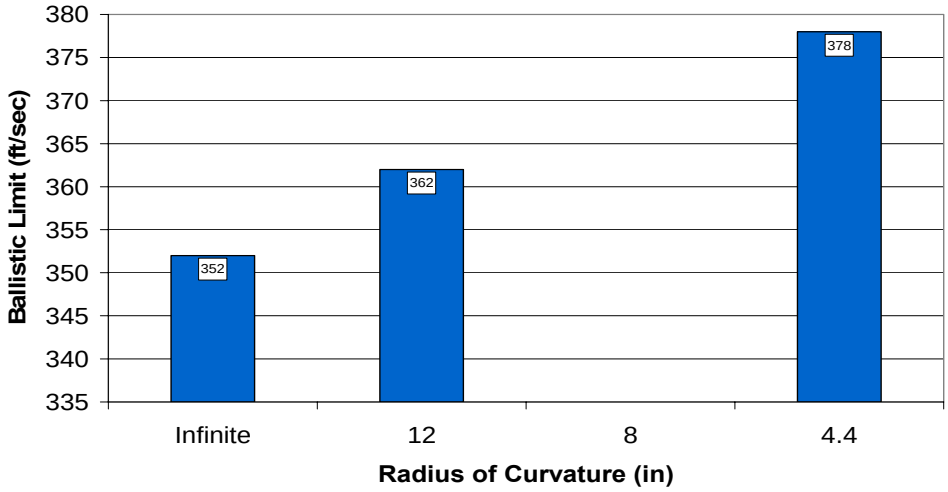

Figure 6.1 Experimentally-determined ballistic limits for composite panels with three different radii of curvature

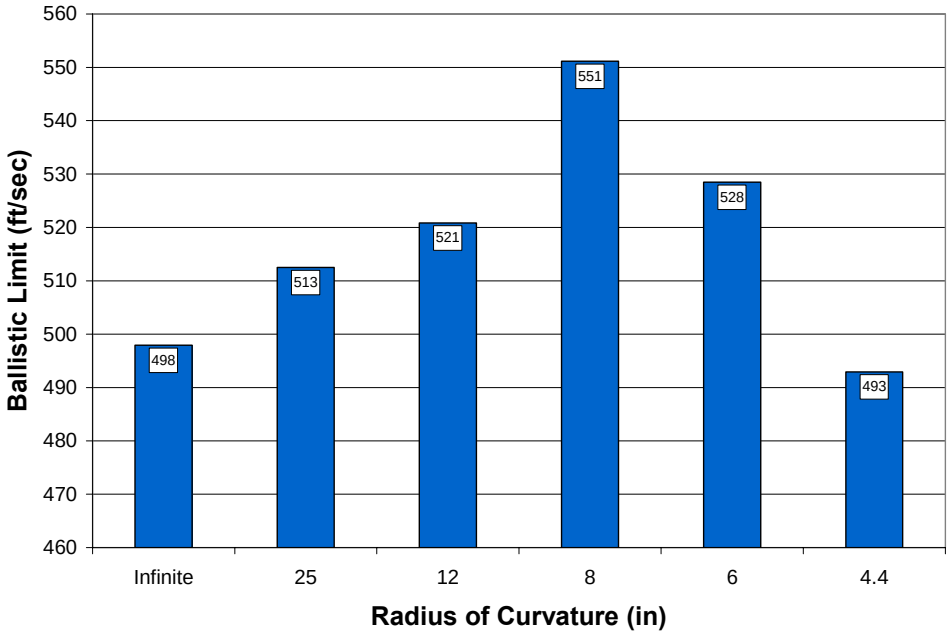

Figure 6.2 Numerically-determined ballistic limits for aluminum panels with six different radii of curvature

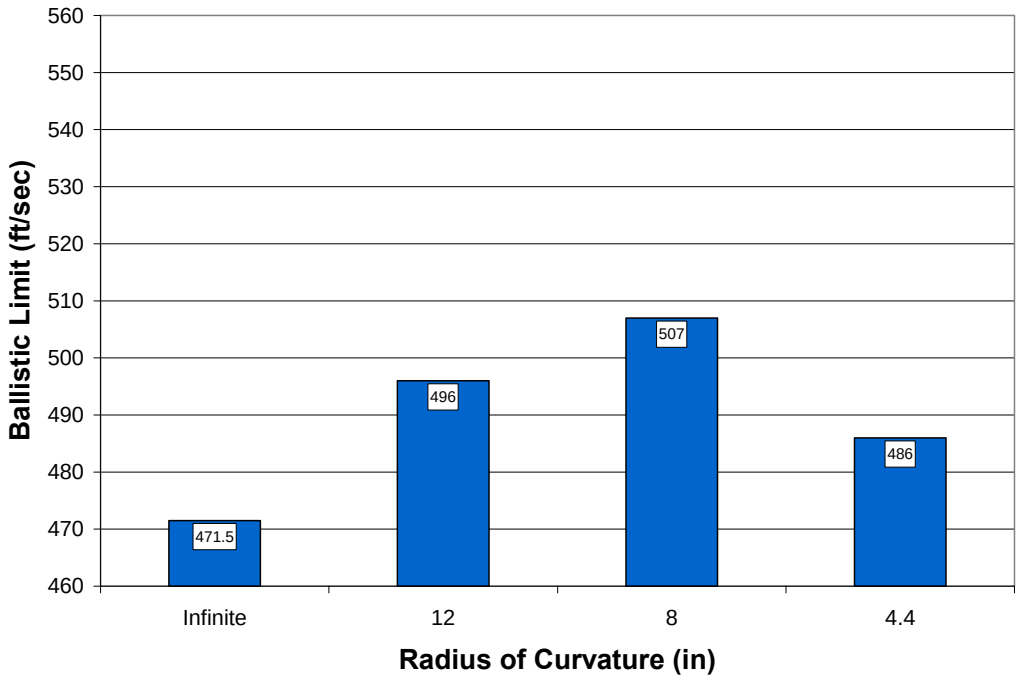

Figure 6.3 Experimentally-determined ballistic limits for aluminum panels with four different radii of curvature

For the aluminum material, the experimentally-validated numerical models consistently and reliably modeled the post-impact residual velocity of the projectile, the threshold (ballistic limit) separating penetrating and non-penetrating impact events, and the panel response (out-of-plane deformation) to ballistic impact. This was achieved by specifying the standard material properties for 2024-T3 aluminum alloy (used to fabricate the experimentally-tested panels) together with a single additional parameter, the failure strain that determined when an element should be deleted from the finite element mesh used to represent the panel undergoing ballistic impact.

It should be pointed out that the opportunity to specify a failure strain was not used as a means of doing model fitting for the different curvatures examined.

Rather, the most appropriate value for this parameter was established during the early stages of the modeling process, and its magnitude was then held constant throughout all of the subsequent numerical simulations for aluminum panels of varying curvature subjected to ballistic impacts over a wide range of initial projectile velocities. A comparison of the experimental and numerically-obtained ballistic curves for the four different radii of curvature tested is shown in Figure 6.4.

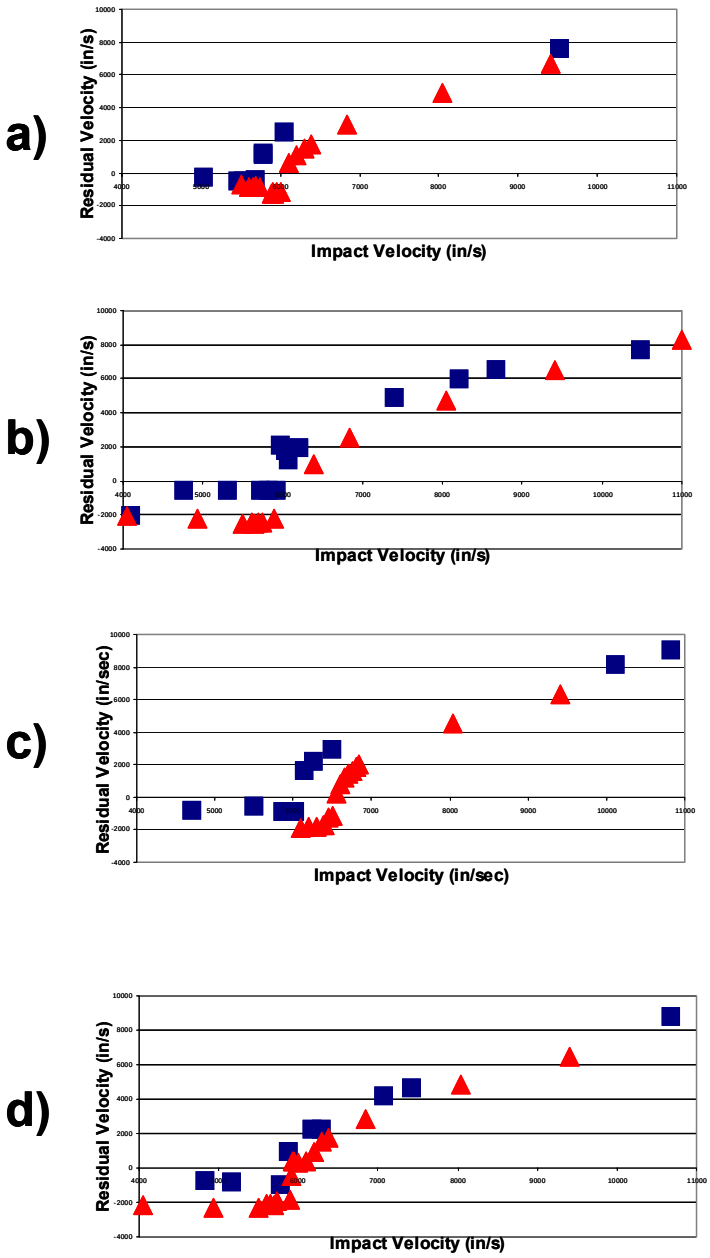

Figure 6.4 Comparison of numerical (depicted by triangles) and experimental (depicted by squares) ballistic curves for aluminum panels with: (a) an infinite radius of curvature, (b) a 12-inch radius of curvature, (c) an 8-inch radius of curvature, and (d) a 4.4-inch radius of curvature

The preliminary numerical modeling effort for the ballistic impact response of curved composite panels did not show very good agreement with the experimental data. In this case also, a failure strain value was specified for the composite laminate based on the fitting of numerical modeling results to experimental data. However, in specifying material properties for the laminate, an effective elastic modulus value also had to be specified and was initially derived using the "rule-of-mixtures." Experimental data from impact studies on strain-gage-instrumented composite panels showed that a flexural-wave-based effective modulus value derived from the experimentally-determined wave propagation characteristics of the laminate was more appropriate for modeling the ballistic event in composite panels.

Incorporation of this flexural-wave-based effective elastic modulus into the numerical model restored the good correlation with experimental results, as shown in Figure 6.5. The numerical modeling also provided information about an intermediate panel curvature that had not been evaluated experimentally for the composite panels. The combined experimental-numerical results showed that an optimal radius of curvature, as had been observed previously for the aluminum panels, also exists for the composite panels. This is evident from Figure 6.6.

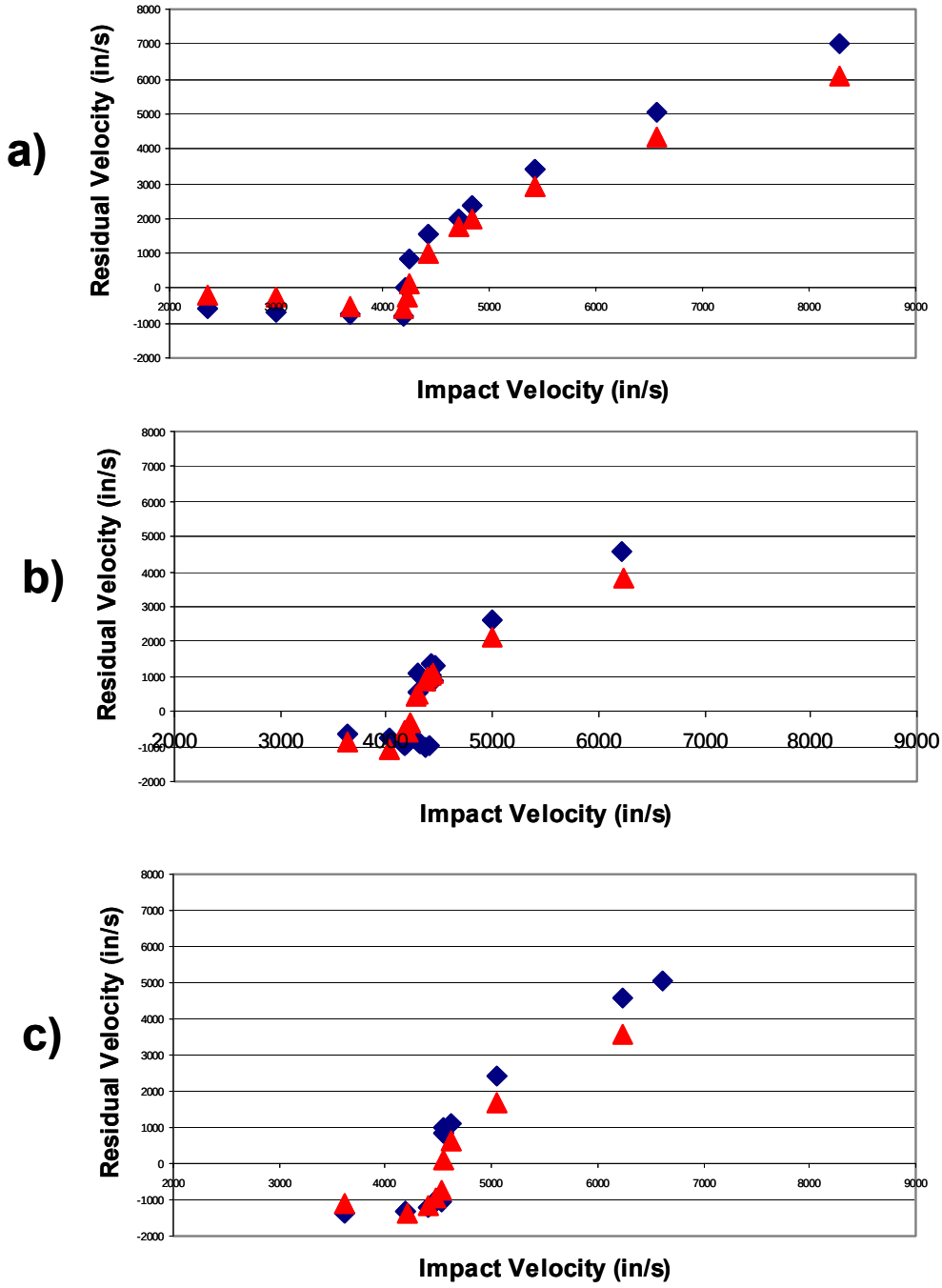

Figure 6.5 Comparison of numerical (depicted by triangles) and experimental (depicted by diamonds) ballistic curves for composite panels with: (a) an infinite radius of curvature (b) a 12-inch radius of curvature, and (c) a 4.4-inch radius of curvature

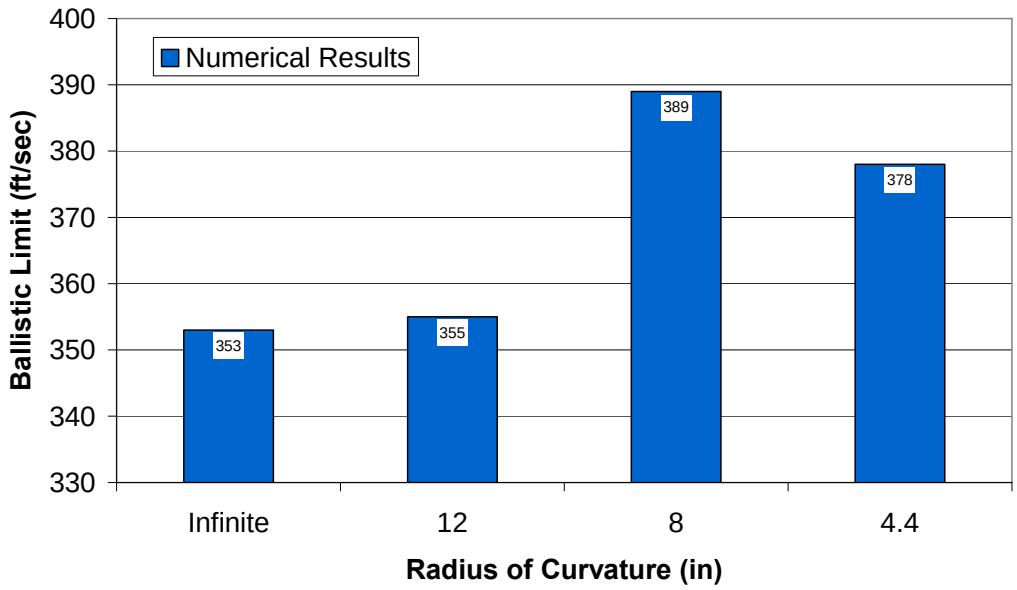

Figure 6.6 Numerical ballistic limits for curved composite panels showing a numerically predicted optimal curvature

The overall results from the numerical modeling for both the aluminum and the composite panels showed that the ballistic impact event can be consistently and reliably modeled for both flat and curved panels, provided that a key parameter, the specified elastic modulus correctly captures the characteristics of the wave propagation behavior for the panel being modeled.

Non-destructive, post-impact, C-scan evaluations of the composite panels indicated that the severity of impact damage may also vary with panel curvature. Measurements of the damage zone area in the impacted composite panels, shown in Figure 6.7, indicated that the 4.4-inch radius of curvature panels generally exhibited a larger damaged area than did the 12-inch radius of curvature panels.

Measurements were also made of the exit-hole size in the impacted aluminum panels. As shown in Figure 6.8, the flat (infinite radius of curvature) panels had the largest exit-hole sizes for comparable impact velocities, while the

8-inch radius of curvature aluminum panels had the smallest exit-hole sizes, again for comparable impact velocities. For the aluminum panels, the relationship between exit-hole size and panel curvature was found to be qualitatively similar to the non-monotonic relationship between the ballistic limit and the panel curvature, in that the panel configuration with the highest ballistic limit (an 8-inch radius of curvature) had the smallest exit-hole sizes and the panel configurations with the lower ballistic limits (an infinite radius of curvature and a 4.4-inch radius of curvature) had larger exit-hole sizes.

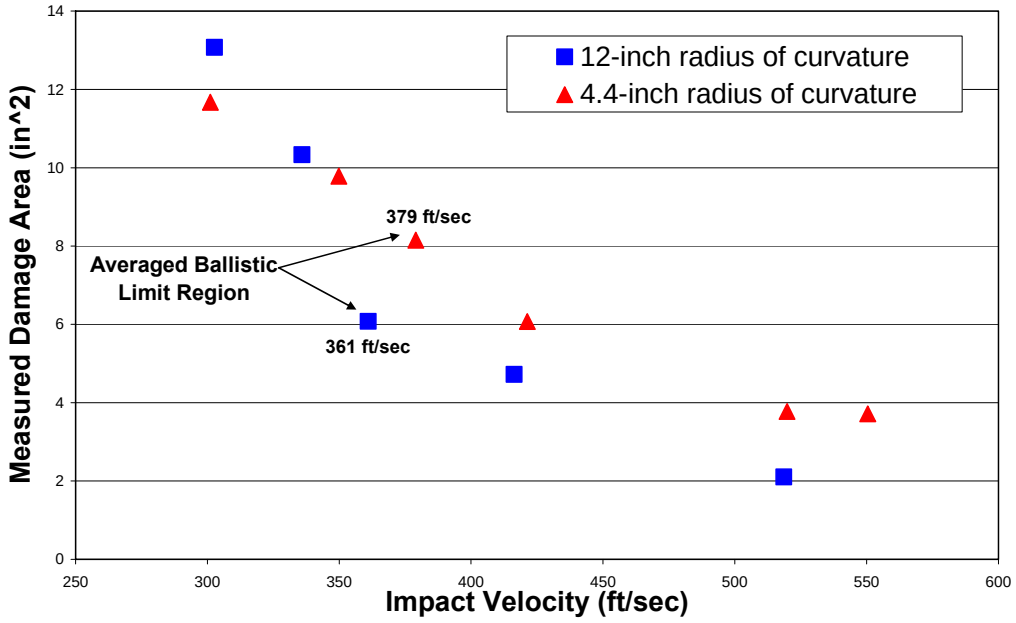

Figure 6.7 Damage area measured from C-scans for 12-inch and 4.4-inch radius of curvature composite panels. Measurements within ±15 fps of the ballistic limit have been averaged and plotted at the ballistic limit to clarify the figure.

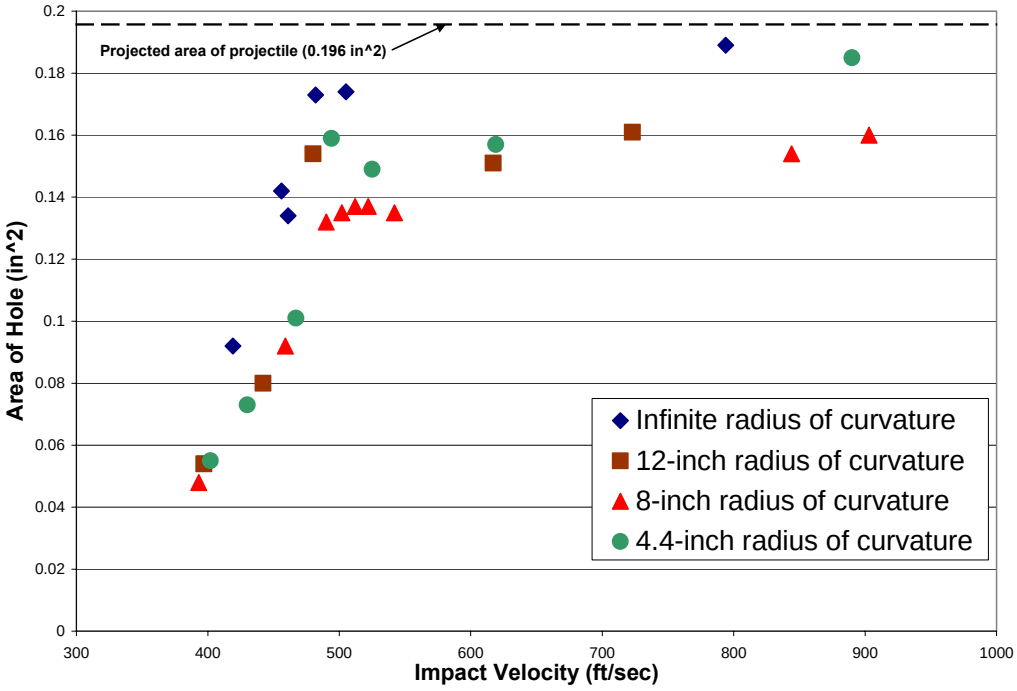

Figure 6.8 Exit-hole size as a function of impact velocity for aluminum panels with varying amounts of curvature. Dashed line represents the projected area of the ½-inch diameter projectile

6.3 Suggestions for Future Work

The numerical simulations performed as part of this research accurately captured the ballistic impact response (residual projectile velocities) and the dynamic panel deformation for both aluminum and composite laminate panels. However, no attempt was made to model the details of the impact damage (particularly in the composite material) as part of the simulation process. Incorporation of a damage model into the simulation would be a significant improvement. Additionally, the need to use a flexural-wave-based elastic modulus when modeling the response of composite panels was demonstrated specifically for a 'quasi-isotropic' laminate configuration. The ability of this

flexural-wave-based elastic modulus concept to model more generic, anisotropic, composite configurations would also be of interest for follow-on investigations.

The results from use of the flexural-wave-based elastic modulus suggest that, at least for the case of the quasi-isotropic laminates, the material properties of the matrix material control the wave propagation characteristics, and hence the ballistic impact response of the composite panels. Experimental ballistic impact testing of purely matrix material panels and fiber-reinforced matrix material with varying degrees of reinforcement could provide additional insights into the role of the fiber material in determining an effective or "bulk" ballistic impact response.

Strain-gage measurements of the flexural wave speed were conducted for flat composite panels and used to infer the effective elastic modulus that should be specified in the numerical simulations of the composite panel response. A more detailed experimental program that examines the effect of panel curvature on the flexural wave speed may be warranted. Differences in the flexural wave speed, as measured parallel and perpendicular to the curvature direction, could also be investigated.

Finally, this research was limited to a specific panel thickness for both the aluminum and composite panels. Additional research incorporating expanded dimensional analyses in order to generalize the results presented in this dissertation could prove beneficial.

Appendix A: High Speed Videos of Ballistic Impact

Representative high speed video files are included on the CD-ROM. An index is included here for reference to the content of the files. Please note that some of the video files should be manually brightened for better viewing

File Name	Narrative Description
12_al_52psi	This video shows a ½-inch diameter projectile impacting an aluminum panel with a 12-inch radius of curvature. The impact velocity is 341 ft/sec. This is a rebound event but no measurement was made for the residual velocity of the projectile. The camera framing rate was 8300 frames/sec. A large field of view has been selected so that the boundary supports are in view during the impact event. This video shows movement of the supports during the impact event and provides visual evidence that the supports were not completely fixed.
12_al_68psi	This video shows a ½-inch diameter projectile impacting an aluminum panel with a 12-inch radius of curvature. The impact velocity is 397 ft/sec. This is a rebound event and the residual velocity of the projectile is -48.3 ft/sec. The camera framing rate was 60,000 frames/sec. Cross-marks on the panel were used for making dynamic displacement measurements during the impact event. This video (along with a second view) was used to generate the data presented in Section 4.3.7 of the text.
12_al_81psi	This video shows a ½-inch diameter projectile impacting an aluminum panel with a 12-inch radius of curvature. The impact velocity is 442 ft/sec. This is a rebound event and the residual velocity of the projectile is -49.6 ft/sec. The camera framing rate was 15,000 frames/sec. This video is a representative sample of a non-penetration event just below the calculated ballistic limit of the 12-inch radius of curvature panels. The camera trigger wire (trailing the projectile) is visible in the video. This video also provides a good view of the ejected plug hole.
12_al_95psi	This video shows a ½-inch diameter projectile impacting an aluminum panel with a 12-inch radius of curvature. The impact velocity is 480 ft/sec. This is a penetration event but no measurement was made for the residual velocity of the projectile. The camera framing rate was 60,000 frames/sec. This video is a representative sample of a penetration event just above the calculated ballistic limit of the 12-inch radius of curvature panels.

12_comp_37psi	This video shows a ½-inch diameter projectile impacting a composite panel with a 12-inch radius of curvature. The impact velocity is 277 ft/sec. This is a rebound event and the residual velocity of the projectile is -43.2 ft/sec. The camera framing rate was 60,000 frames/sec. This video illustrates the localized damage in the vicinity of the impact area. The video shows the small area surrounding the impact event experiencing larger gross movement than the surrounding material. This difference is assumed to be caused by localized damage mechanisms such as delamination and matrix cracking.
flat_comp_48psi	This video shows a ½-inch diameter projectile impacting a composite panel with an infinite radius of curvature (flat panel). The impact velocity is 322 ft/sec. This is a rebound event and the residual velocity of the projectile is -52.2 ft/sec. The camera framing rate was 60,000 frames/sec. This video is a representative sample of a non-penetration event for the flat composite panels. Comparison to the video of the representative penetration event provides a qualitative comparison for the magnitudes of out-of-plane displacements. The non-penetrating event results in a larger magnitude of out-of-plane displacement.
flat_comp_85psi	This video shows a ½-inch diameter projectile impacting a composite panel with an infinite radius of curvature (flat panel). The impact velocity is 452 ft/sec. This is a penetration event and the residual velocity of the projectile is 280 ft/sec. The camera framing rate was 60,000 frames/sec. This video is a representative sample of a penetration event for the flat composite panels. Comparison to the video of the representative non-penetration event provides a qualitative comparison for the magnitudes of out-of-plane displacements. The penetrating event results in a lower magnitude of out-of-plane displacement. This video also shows that a small amount of composite-spall material is ejected on the impact side of the composite panel.
12_comp_rearview	This video shows the rearview of a ½-inch diameter projectile impacting a composite panel with a 12-inch radius of curvature. The camera framing rate was 120,000 frames/sec. The video shows the initial bulge of the projectile, the splitting of the rear laminate, fiber breakage, spall ejection, the penetrating projectile, and the closing of the exit hole.

4_al_double_impact	This is a video of a LS-DYNA simulation showing the side view of a ½-inch diameter projectile impacting an aluminum panel with a 4.4-inch radius of curvature. In the video, the projectile can be seen penetrating the panel. Immediately after exiting the panel, the projectile comes into contact with the rear of the vibrating panel and the residual velocity of the projectile is increased as a result.
flat_al_double_impact	This is a video of a LS-DYNA simulation showing the side view of a ½-inch diameter projectile impacting an aluminum panel with an infinite radius of curvature. This is a rebound event illustrating another example of the projectile coming back into contact with the vibrating plate. As a result of the double impact, the residual velocity of the projectile is increased. This video is included to document the ability of the finite element model to accurately model the panel response during ballistic impact. Observations of double impact events in experimental testing have been reported in the literature.

Appendix B: Non-destructive C-Scan Evaluations

The non-destructive evaluation reference files are included on the CD-ROM. An index is included here for reference to the content of the files.

File Name	Radius of Curvature (inches)	Impact Velocity (ft/sec)	Residual Velocity (ft/sec)
C1	4.4	550	422
C2	4.4	520	380
C3	4.4	301	-114
C4	4.4	421	200
C5	4.4	350	-111
C6	4.4	385	91.6
C7	4.4	367	-103
C8	4.4	379	81.6
C9	4.4	370	0
C10	4.4	373	-86.6
C11	4.4	372	0
C12	4.4	379	70.4
C14	4.4	376	0
C15	4.4	377	-75.6
C16	4.4	377	-85.7
D1	12	519	380
D2	12	303	-55.3
D3	12	416	216
D4	12	336	-60.7
D6	12	364	-83.2
D7	12	366	-79.0
D8	12	370	74.3
D10	12	371	111
D11	12	368	116
D12	12	368	89.1
D14	12	358	47.7
D15	12	358	91.2
D16	12	348	-80.3
D17	12	352	-68.4
D18	12	350	-76.1
D19	12	346	-75.0
D20	12	363	71.7
D21	12	359	-75.5
D22	12	358	-71.7
D5	12	356	No measurement
D9	12	371	No measurement
D13	12	366	No measurement
C13	4.4	376	No measurement

References

Ambur, D.R., Jaunky, N., Lawson, R.E., and Knight N.F., "Numerical simulations for high-energy impact of thin plates," *International Journal of Impact Engineering*, Vol. 25, Issue 7, August 2001, pp. 683-702

Belytschko, T.B. and C.S. Tsay, "Explicit Algorithms for Nonlinear Dynamics of Shells," *AMD* Vol. 48, ASME, 209-231 (1981)

Borvik, T., Hopperstad, O.S., Berstad, T., and Langseth, M., "Numerical simulation of plugging failure in ballistic penetration," *International Journal of Solids and Structures*, Vol. 38, August 2001, pp. 6241-6264

Christoforou, A.P., and Swanson, S.R., "Analysis of simply-supported orthotropic cylindrical shells subject to lateral impact loads," *Journal of Applied Mechanics*, Vol. 57, 376-382, June 1990

Czarnecki, G.J., "A preliminary investigation of dual mode fracture sustained by graphite/epoxy laminates impacted by high-velocity spherical metallic projectiles," Master's Thesis, University of Dayton, 1992

Dieter, G.E, *Mechanical Metallurgy*, McGraw-Hill, Inc., NY, 1986

Doherty, J.E., *Nondestructive Evaluation*, in *Handbook on Experimental Mechanics (2nd Ed.)*, VCH Publishers, Inc., NY 1993

Gaffari, S., "Impact Damage in Graphite/Epoxy Laminates: Damage Characterization, Acoustic Emission, and Finite Element Simulation," Ph.D. Dissertation, University of Florida, 1989

Greszczuk, L.B., and Chao, H., *USAAMRDL-TR-75-15*, U.S. Army Air Mobility R&D Center, 1975

Joshi, S.P. and Sun, C.T., "Impact Induced Fracture in a Laminated Composite," *Journal of Composite Materials*, Vol. 19, January 1985.

Kistler, L.S., "Low velocity impact on curved laminated composite panels," Ph.D. Dissertation, University of Michigan, 1996

Langhaar, H.L., *Energy Methods in Applied Mechanics*, Wiley, NY 1962

Lee S.-W.R. and Sun, C. T., "Dynamic penetration of graphite/epoxy laminates impacted by a blunt-ended projectile," *Composites Science and Technology*, Volume 49, Issue 4, 1993, Pages 369-380

Lin, H.J. and Lee, Y.J., "Impact-Induced Fracture in Laminated Plates and Shells," *Journal of Composite Materials*, Vol. 24, November 1990, pp. 1179-1199

Liu, D. and Malvern, L.E., "Matrix Cracking in Impacted Glass/Epoxy Plates," *Journal of Composite Materials*, Vol. 21, July 1988.

Livermore Software Technology Corporation (LSTC), *LS-DYNA Theoretical Manual*, 1998

Livermore Software Technology Corporation (LSTC), *LS-DYNA User's Manual*, 2003

Mallick, P.K. Fiber-*Reinforced Composites: Materials, Manufacturing and Design*, 2nd Ed., Marcel Dekker, NY, 1993

Mikhail, E.M., Bethel, J.S., and McGlone, J.C., *Introduction to Modern Photogrammetry*, John Wiley and Sons, NY, 2001

Palazotto, A. and Perry, R., "Impact Response of Graphite/Epoxy Cylindrical Panels," *AIAA Journal*, Vol. 30, July 1992, pp.1827-1832

Ramkumar, R.L., and Thakar, Y.R., "Dynamic Response of Curved Laminated Plates Subjected to Low Velocity Impact," *Journal of Engineering Materials and Technology*, Vol. 109, Jan 1987, pp.67-71.

Recht, R.F., "High Velocity Impact Dynamics: analytical modeling and plate penetration dynamics," in *High Velocity Impact Dynamics*, Wiley-Interscience, NY, 1990

Swanson, S.R., Smith, N.L., and Qian, Y., "Analytical and experimental strain response in impact of composite cylinders," *Composites Structures*, Vol. 18, 95-108, 1991

Sun, C.T. and Li, S., "Three-dimensional effective elastic constants for thick composite laminates," *Journal of Composite Materials*, Vol. 22, 1988, pp. 629-639

Sun, J., "Experimental study of universal phenomena of impact on laminated composite plates by rigid sphere projectiles," Masters Thesis, University of New Orleans, 1996

Swanson, S.R., Smith, N.L., and Qian, Y., "Analytical and Experimental Strain Response in Impact of Composite Cylinders," *Composite Structures*, Vol.18, 1991, pp. 95-108

Ugural, A.C., *Stresses in Plates and Shells*, McGraw-Hill, Inc., NY 1981

Wilkins, M.L., "Mechanics of Penetration and Perforation," *International Journal of Engineering Science*, Vol. 16, 1978, pp. 793-807

Zukas, J.A., Nicholas, T., Swift, H.F., Greszczuk, L.B., and Curran, D.R., *Impact Dynamics*, Wiley-Interscience, NY, 1982.

Zukas, J.A., *High Velocity Impact Dynamics*, Wiley-Interscience, NY, 1990